AD A139866

DTIC FILE COPY

THEORETICAL AND EXPERIMENTAL STUDY OF RADAR BACKSCATTER FROM SEA ICE

APR 6 1984

A

THE UNIVERSITY OF KANSAS CENTER FOR RESEARCH, INC.
2291 Irving Hill Drive—Campus West
Lawrence, Kansas 66045

This document has been approved for public release and sale; its distribution is unlimited.

THEORETICAL AND EXPERIMENTAL STUDY OF RADAR BACKSCATTER FROM SEA ICE

Young-Soo Kim
R.K. Moore
R.G. Onstott

Remote Sensing Laboratory
Center for Research, Inc.
The University of Kansas
Lawrence, Kansas 66045-2969

RSL Technical Report
RSL TR 331-37

January 1984

Supported by:

OFFICE OF NAVAL RESEARCH
Department of the Navy
800 N. Quincy Street
Arlington, Virginia 22217

Contract N00014-76-C-1105

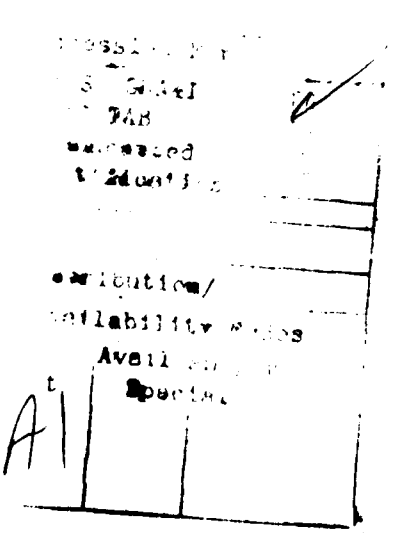

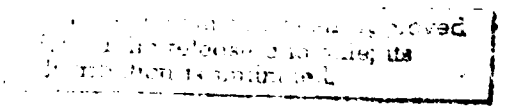

ABSTRACT

Active and passive microwave sensors are known to provide valuable information on the distribution of types of sea ice in the Arctic where darkness and cloud cover prevail. However, the variability of the microwave signatures of sea ice depending on the region, temperature, snow cover, surface roughness, etc. have prevented us from understanding the sea-ice-electromagnetic-wave interactions completely enough to specify optimum sensor parameters and to allow the most reliable interpretation possible. This has led to various expeditions for the last 15 years or so.

Here a model is described for the radar backscatter from first-year and multiyear sea ice, based on simple scattering layers. The physical-optics model using an exponential correlation function is shown able to predict the signatures of first-year ice. The radiative transfer volume-scatter model can describe the backscattering from multiyear ice for frequencies higher than about X-band, while the surface scattering contribution has to be included for lower frequencies. A simple semi-empirical model is shown to be a good approximation to the radiative transfer model in describing the volume scattering contribution of multiyear ice. A parametric study was conducted to determine the possible ranges of σ^0 for multiyear ice and first-year ice using the theoretical models. Within reported ranges of values of physical characteristics of sea ice, the theoretical model behavior confirms the experimental findings that Ku- and X-band frequencies, and incidence angles larger than about 30° to 40°, are better than lower frequencies in discriminating multiyear ice from first-year ice.

TABLE OF CONTENTS

LIST OF FIGURES

LIST OF TABLES

1.0 INTRODUCTION

Remote sensing can have a great impact on a variety of problems associated with sea ice. Sea ice can be viewed either as an operational hazard or as a climate indicator and modifier. Some of the important ice parameters are the extent, concentration, type, drift velocity, internal stress, snow cover, top and bottom ice roughness, etc.

Safe and economical navigation in ice-infested waters requires the ability to distinguish and map ice types and conditions at least on a daily basis over the entire shipping route to permit effective routing of tankers. If near-real-time ice data can be provided, bringing gas and oil from the Canadian Arctic area by tankers alone would be benefitted by some $100 million per year through reduced shipping time, reduced operating and maintenance costs, and reduced insurance costs related to hazards and environmental damage [Raney, 1982].

There are several methods for obtaining information from aircraft and spacecraft about the ice cover and adjacent open sea. The principal methods are: (1) visible light sensor, (2) thermal infrared sensors, (3) radar and laser altimeters, (4) passive microwave radiometers, and (5) active microwave systems. Each of these gives different information about ice, with different errors and difficulties involved [Carsey, 1982]. Darkness or cloud cover in the Arctic region poses the most significant problem to visible-light ice surveillance. Thermal-IR systems reveal warmer areas associated with open water and thin ice, but the presence of a little snow complicates the interpretation. Laser altimetry can be used in ice sheet profiling, but aircraft altitude variation can cause difficulties.

Passive microwave systems use the difference in emissivity for open water and for different ice types, and they have been shown to be quite useful. Their inherently poor resolution limits their use, however.

For active microwave (radar) systems the backscattered power is determined by the surface roughness and by the internal dielectric and physical structures of the ice medium. Therefore they can differentiate ice types because such characteristics differ. The synthetic-aperture radar (SAR) has the greatest potential because it provides a map with very fine resolution. The optimum radar parameters (frequency, angle of incidence, polarization and resolution) have yet to be determined.

There are still problems in the interpretation of both active and passive signatures for different sea ice types and conditions at different frequencies, especially for the summer season and the marginal ice zones.

Sea ice is a very dynamic medium. Many kinds of ice are present and they are continually changing shapes, as well as growing during the cold seasons. Snow cover and surface roughness have variations in all spatial scales. The surrounding water and leads between ice floes change microwave signatures depending on wind speed and directions. No single measurement or theoretical model can characterize the microwave signature of sea ice. Hence, many expeditions have taken place to gather the microwave signatures of sea ice under different conditions in different areas.

The University of Kansas has made a large number of backscattering measurements since 1977 for different ice types, in several geographic areas, for L-, X- and Ku-band frequencies. Recently, a C-band system was added, and valuable measurements were made under summer and fall

conditions in Mould Bay, N.W.T., Canada. The fall expedition results are summarized here.

In addition, a theory was developed to explain the microwave backscattering from sea ice as an aid to understanding the different microwave signatures from different ice types. Multiyear ice (180-360 cm thick) is generally thicker and harder than first-year (30-180 cm thick) ice; it needs to be distinguished because its presence severely impedes navigation. In this research, the two major types of ice are characterized with two different backscattering mechanisms; surface scattering alone for first-year ice, and combined volume and surface scattering for multiyear ice.

Both earlier observations and the newly acquired data set were analyzed to study the applicability of various theoretical models. An extensive literature search was conducted to gather physical and electrical characteristics of sea ice considered to be relevant to microwave remote sensing.

A parametric study was conducted to see the possible ranges of the scattering coefficient σ^0 of multiyear ice and first-year ice after the theoretical models were shown to be able to predict or match the data sets with a reasonable set of model parameters. From the parametric study, the most suitable radar parameters for sea-ice monitoring were selected.

1.1 Background

Since 1962, considerable experimental data on the microwave signatures of sea ice have been collected with both active and passive remote sensors. Scattering theories have been developed to describe the

interaction of electromagnetic waves with nature, assuming that the nature can be described with certain average statistical parameters. Recently, the surface and volume scattering theories have been applied to remotely sensed ground targets, including snow, vegetation, soil, ocean waves, etc.

Only a few attempts have been made to explain theoretically the observations by active and passive electrical characteristics. This is partly due to the lack of ground truth in earlier experiments and also due to the complexities and variabilities of sea ice itself.

Parashar [1974] applied to sea ice the general theory, developed by Fung [1969], of wave scattering by a horizontally weakly inhomogeneous medium. The model includes small-scale roughness of the air-ice interface and also a bilinear mean vertical permittivity profile for sea ice, with anisotropic small random perturbations in the ice volume. The formulation starts with the basic wave equation in each medium, and the solution is obtained using the small-perturbation method and the Fourier-transform technique. The expressions for the first-order normalized backscattering cross-section, σ^0, were obtained in terms of surface and volume correlation lengths and standard deviations for each medium.

Parashar's [1974] solution for the cross-polarized σ^0 is zero, probably due to neglect of higher order terms in the perturbation series. Parashar had some success in predicting the 0.4 GHz and 13 GHz scatterometer data by arbitrarily adjusting the model parameters (necessary because there was no ground truth accompanying the data). The small perturbation method was possibly applicable to thick first-

year and thinner ice types, but not applicable to multiyear ice due to the presence of scattering centers within the ice.

Hallikainen [1980] used the layered model with smooth surface to explain the passive UHF measurements of low-salinity first-year ice as a function of ice thickness. Because of the low scattering loss associated with low frequencies (0.6 and 0.9 GHz), it was possible to neglect any volume-scattering considerations. The brightness temperature was directly related to the small ice thicknesses and the model predicts oscillatory behavior of a half-wavelength dielectric slab correctly. This concept cannot be used directly in the microwave region, but it may be applicable to very thin ice for frequencies at L-band.

Golden and Ackley [1981] noted the reflective anisotropy of the bottom of sea ice associated with 100 MHz impulse-radar soundings. They proposed that the asymmetrical geometry of brine inclusions causes an anisotropy in the penetration of the impinging electric field into the brine layers which are assumed to have a relative dielectric constant of 80 + j 1000. By assuming ellipsoidal brine layers whose axial ratios vary with depth, their model predicts the anisotropic radar return from ice bottom correctly. However, in the microwave region, only the upper portion of sea ice is important because of attenuation, especially for first-year ice; the bottom anisotropy might have some role for the L-band frequencies.

Hallikainen [1982] studied the applicability of the radiative transfer model to predicting the brightness temperature of sea ice and fresh-water ice in the frequency range of 5 to 37 GHz. The fresh-water ice data at 5 GHz could not be fitted with the radiative transfer model,

while at 18 GHz the agreement was reasonable. At 37 GHz, the model prediction agrees fairly well with the experimental sea-ice data. He concluded that the layered model is applicable when the scattering is negligible, and the radiative transfer model is applicable when the scattering dominates over absorption.

Fung and Eom [1982] developed a radiative-transfer theory which combines rough surface and volume scattering effects, and applies to backscatter measurements of snow and sea ice. The surface-scattering effect is accounted for by the Kirchhoff model, and the inhomogeneous layer is modeled by either the Rayleigh phase matrix or a continuous random medium with a cylindrically symmetric correlation function for its permittivity. By assuming several model parameters, the theoretical like- and cross-polarized curves provided satisfactory agreements in level and trend to the measured multiyear ice and first-year ice data at 9 and 13 GHz. Use of the Born phase matrix in place of the Rayleigh phase matrix gave somewhat inferior agreements, and they concluded that the nonspherical or columnar scatterers are not essential for explaining sea ice scattering at the frequencies around X-band. Fung and Eom's model was further studied in this research.

1.2 Organization

This report is organized into 8 sections. Section 2 summarizes the effort to find the dielectric constant of sea ice as a function of frequency, salinity, and temperature. An extensive literature search was conducted to study the available sea ice characteristics considered to be relevant to microwave remote sensing and this section provides the approximate formulas relating the dielectric constant of sea ice to

measured salinity and temperature. Although these formulas are not very satisfactory, their simple forms are suitable for further development of the backscatter model for sea ice.

Section 3 considers the surface scattering model for first-year ice. The surface scattering theories are reviewed first, and then, by assuming that the volume scattering contribution can be neglected, the signatures of first-year ice are tested against the predictions of surface scattering theories. By using the measured surface-height correlation length and standard deviation, it is shown that the physical optics model using an exponential correlation function provides a good fit to measured angular and frequency behaviors of σ^0 of first-year ice.

Section 4 considers the volume-scattering model for multiyear ice. The air bubbles in the recrystallized ice layer in the top portion of multiyear ice are assumed to be the main volume scatterers. In the radiative-transfer approach, the volume scattering layer is characterized by the scattering albedo and the optical depth. Then the effect of varying physical characteristics (air bubble size, density, dielectric constant of background ice, layer depth) of the volume scattering layer is studied using the radiative-transfer model. When the frequency is below about X-band, it is shown that the volume scattering contribution can be smaller than the surface scattering contribution, and the total provides a good general agreement to the measured frequency and angular behavior of σ^0 of multiyear ice.

Section 5 provides semi-empirical formulations. The complicated theoretical solution of the radiative-transfer equation can be reduced to a simple analytical solution if the multiple scattering and the volume-surface interaction can be neglected [Karam and Fung, 1982]. In

this approach, the volume backscattering coefficient is given by the sum of the backscattering coefficients of all the single scatterers. Within the reported ranges of multiyear ice characteristics, the solution using the semi-empirical formulation is shown to be very close to that of the formal radiative-transfer model. Using the simple model, the volume-scattering contribution of first-year ice is calculated and it is shown to be negligible for most cases.

Also in this section, the effect of snow cover on sea ice is studied. The low thermal conductivity of snow compared to that of sea ice effectively raises the temperature of the upper surface of the sea ice. The higher temperature results in higher dielectric constant. The effect of 10 cm snow cover on 3-m-thick ice is to lower the σ^0 of multiyear ice by about 0.3 dB when the air temperature is -20° C. The effect of 10 cm snow cover on first-year ice is less than 0.2 dB. The snow cover on sea ice is also studied using the empirical equations [Ulaby, et al., 1982] describing the effect of snow cover on natural surfaces. It is shown that the effect of snow cover on first-year ice can be severe (5 cm of dry snow cover can raise the σ^0 by 8 dB at 9 GHz), while that on multiyear ice is shown to be smaller. The presence of wet snow cover can block the volume scattering contribution of the multiyear ice. The effect of wet snow cover on first-year ice should be smaller than that of dry snow cover because the σ^0 of wet snow is lower than that of dry snow.

Section 6 describes, to the best of current knowledge, the optimum radar parameters for sea ice classification. The experimental findings are studied first. The theoretical models that seemed able to predict or match the data sets with a reasonable set of model parameters are

selected; then by adjusting the model parameters within reported ranges of values, the possible ranges for σ^0 for multiyear ice and first-year ice are calculated. From these ranges of values, it is seen that the best radar parameters for sea ice monitoring are: higher frequencies than about X-band and incidence angles larger than about 30° to 40°. No specific resonances have been found to select any particular frequency or incidence angle, either in the measurements or in the theoretical model behavior.

Because depolarization is a secondary effect for the surface scattering (first-year ice) while this is not true for volume scattering (multiyear ice), cross-polarization should be better than like-polarization in discriminating multiyear ice from first-year ice.

Section 7 presents the measurement results for sea ice under fall conditions. In late October it is shown that a large contrast exists in σ^0 between multiyear ice and first-year ice or grey ice. However, in early October with warmer temperatures, the thin first-year ice and the multiyear ice can give similar signatures. Also in this section, an attempt was made to fit the data with the theoretical or semi-empirical models presented in Sections 3 through 5. With appropriate choice of model parameters, the model prediction matches the multiyear ice data very well, and the grey ice data to some degree.

Section 8 provides a complete summary of the research, the general conclusions and the recommendations for further research.

2.0 DIELECTRIC CONSTANT OF SEA ICE AS A FUNCTION OF FREQUENCY, SALINITY AND TEMPERATURE

An extensive literature search was conducted to study the available characteristics (physical and electrical) of sea ice considered relevant to microwave remote sensing.

This section provides a brief summary of dielectric behavior of sea ice. Other physical characteristics are mentioned in appropriate sections where they are needed in modeling sea ice.

Although the formulas for calculating dielectric constant of sea ice are approximations, their simple forms are suitable for further development of a backscatter model for sea ice.

One common technique of getting average dielectric constant of sea ice is to assume that it is a mixture of pure ice and brine/air inclusions. By investigating the dielectric behavior of individual items (pure ice and brine), and by measuring or estimating the volume fraction of brine and air inclusions, one can apply various dielectric mixture theories to get the average dielectric behavior of sea ice. Dielectric constant of brine is very high compared to that of pure ice, and therefore it strongly affects the average dielectric constant of sea ice even though the volume fraction of brine is relatively small.

2.1 Frequency Behavior Between 1 and 18 GHz

In general, both ε' and ε'' of sea ice decrease as frequency is increased from 1 GHz to 18 GHz. This occurs because the very high dielectric constant of brine decreases with frequency (see Figure 2.1), although that of pure ice may increase in the frequency range of interest (see Figure 2.2). Vant's measurement [1976] clearly shows a strong decrease for the imaginary part, while the real part also shows

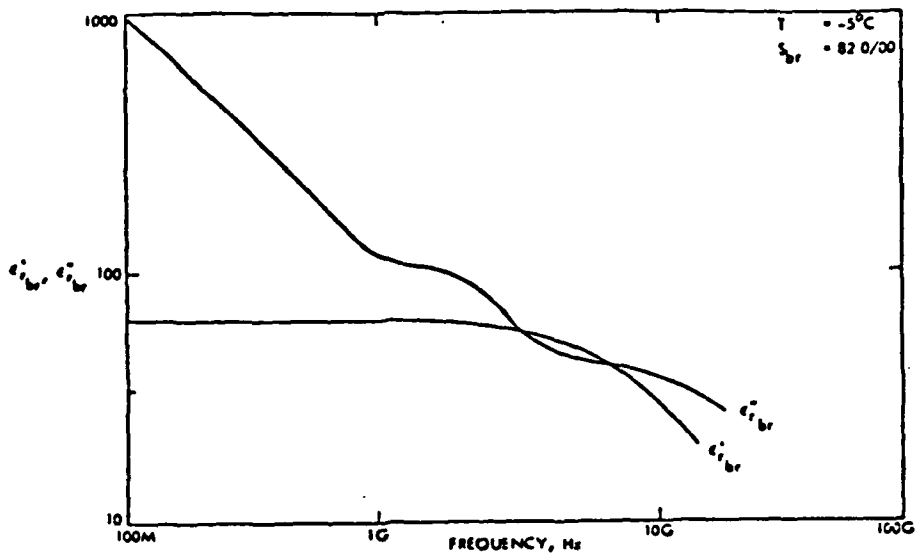

FIGURE 2.1: Real and Imaginary Parts of the Relative Dielectric Constant of Brine (Vant, et al., 1978).

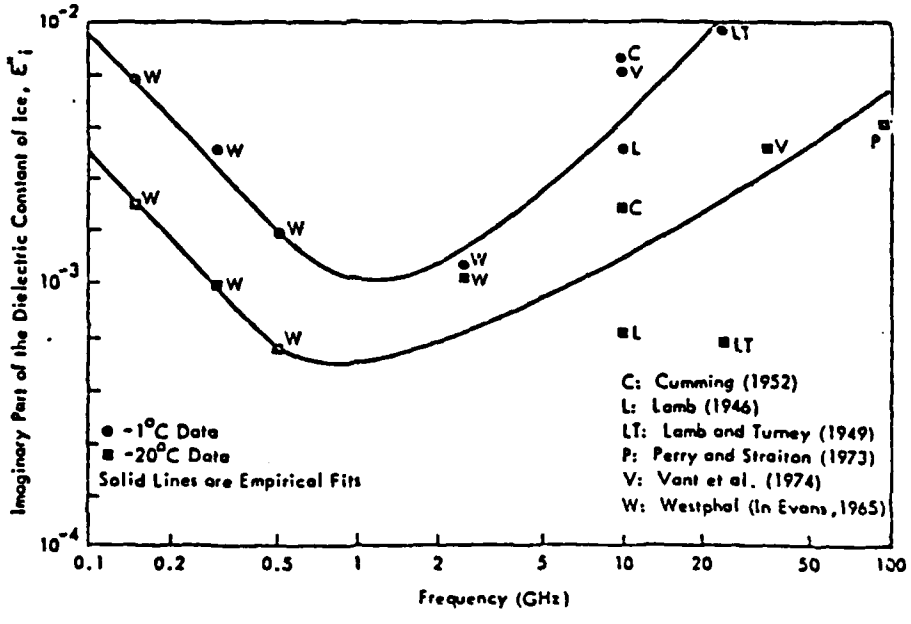

FIGURE 2.2: Imaginary Part of the Relative Dielectric Constant of Pure and Fresh-Water Ice (Ulaby, et al., 1982).

gently decreasing behavior (see Figure 2.3). Hoekstra and Cappillino [1971] showed different frequency behavior with a minimum of ε'' between 4 and 8 GHz, but the values were unreasonably high. Hallikainen [1982] derived a set of empirical constant multipliers for ε' and ε'' at different frequencies relative to the values at 500 MHz. The values in the frequency range of interest are:

$$\varepsilon'(18\ \text{GHz}) = 0.98\ \varepsilon'(5\ \text{GHz}) = 0.93\ \varepsilon'(1\ \text{GHz}) = 0.86\ \varepsilon'(0.5\ \text{GHz}) \quad (2.1)$$

$$\varepsilon''(18\ \text{GHz}) = 0.92\ \varepsilon''(5\ \text{GHz}) = 0.61\ \varepsilon''(1\ \text{GHz}) = 0.46\ \varepsilon''(0.5\ \text{GHz}) \quad (2.2)$$

These scale factors form the basis for a linear variation of ε with frequency over the 1 to 18 GHz region; once the dielectric behavior of sea ice as a function of temperature and salinity is determined, values can be assigned at other frequencies.

2.2 Temperature and Salinity Dependence of Dielectric Constant of Sea Ice

A handful of reported measurements are available on temperature and salinity dependence of ε of sea ice. The only conclusions one can draw are: (1) the dielectric constant of sea ice decreases as temperature is lowered, and (2) it generally increases as salinity increases, although this dependence depends on ice type. These are mainly because the brine volume decreases as temperature is lowered, and because higher salinity means larger brine volume. Several reported measurements and the values used in theoretical models are shown in Figure 2.4(a) and 2.4(b), respectively.

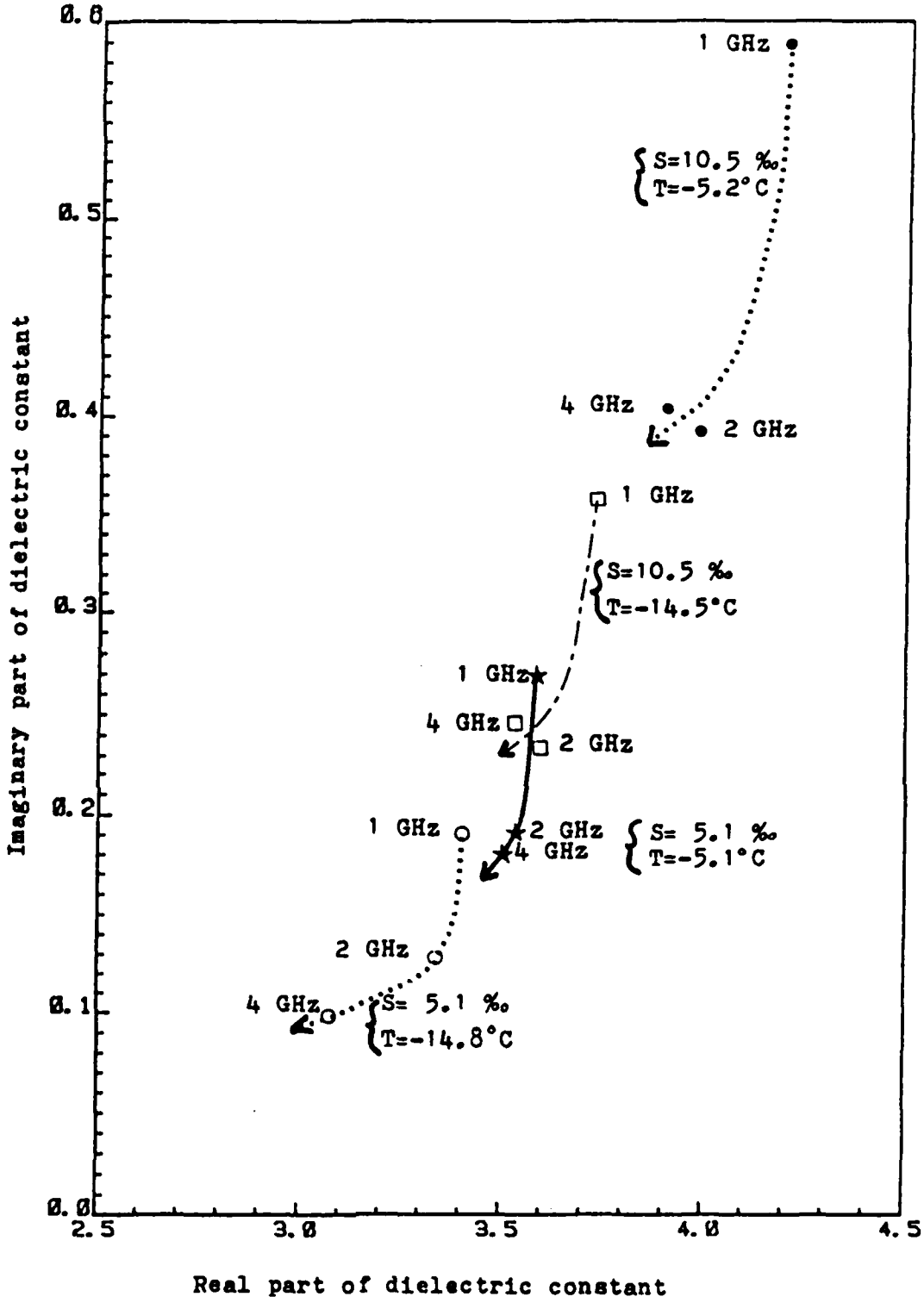

FIGURE 2.3: Frequency Behavior of Measured Values of Dielectric Constant of Sea Ice (Vant, 1976).

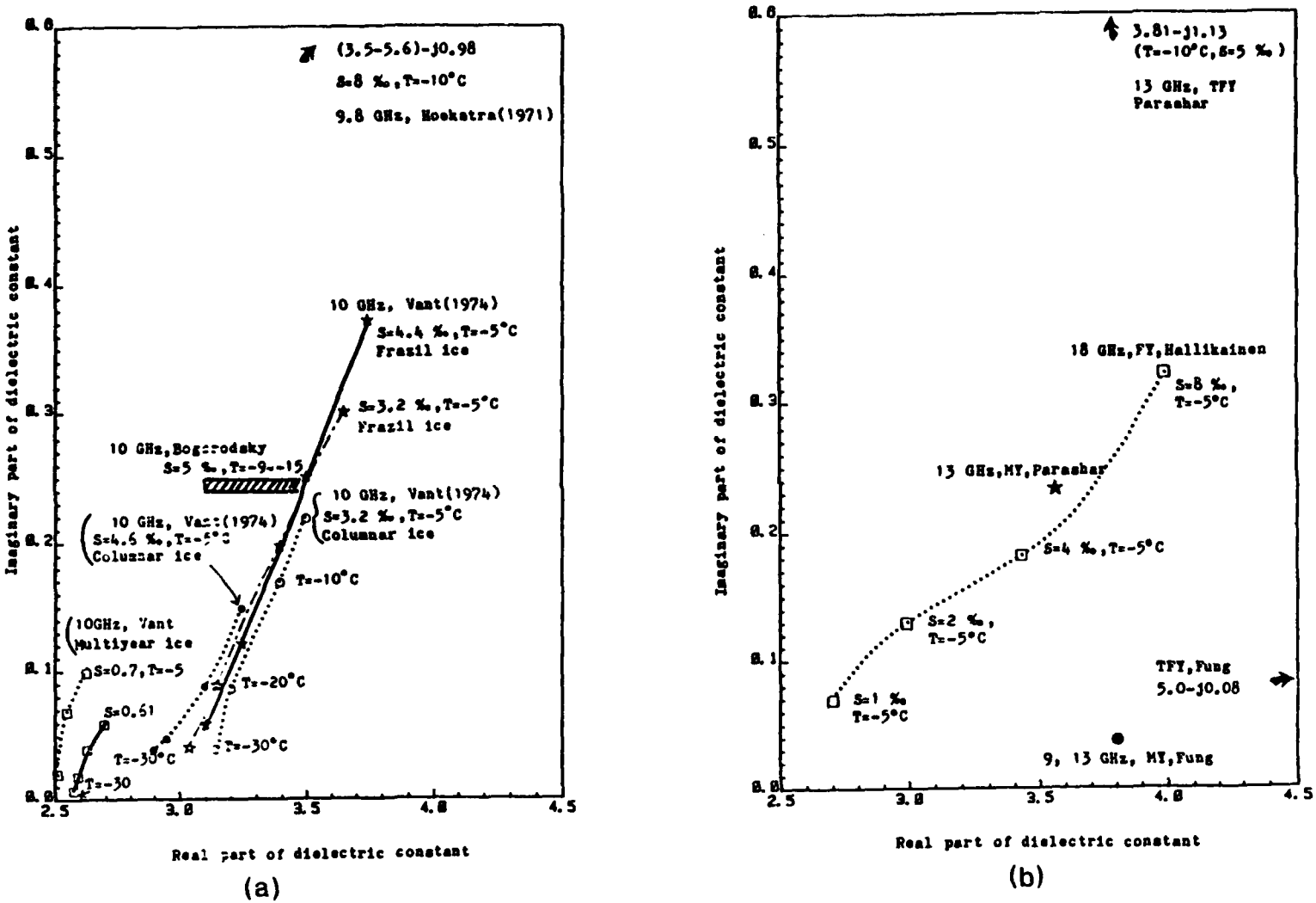

FIGURE 2.4: Dielectric Constant of Sea Ice. (a) Measured values; (b) The values used in several theoretical sea ice models.

It is certain that the dielectric constant of sea ice is a very sensitive function of temperature near the melting point, although the melting point also depends on the salinity of sea water. Even far below the melting point (e.g., -20° C) Vant's [1974] measurement at 10 GHz showed clear dependence of dielectric constant (especially the imaginary part) on the temperature (see Figure 2.5). Hallikainen's result does not seem to show much variation when the ice salinity is less than $4^{o}/oo$ once the temperature reaches -5° C (see Figure 2.6).

Clearly all of these uncertain variations depend on the ice types and even on the specific sampling technique and on the measurement method used. When one also considers the natural variability of sea ice, use of a complicated mixing formula does not seem to be justified because one has to assume various parameters like brine pocket shape, orientation, air bubble shape, etc.; yet we need some kind of formula that relates the dielectric constant of sea ice to salinity and temperature because these two parameters are easy to measure and accompany most of the backscatter data. If one could estimate the dielectric constant from the measured salinity and temperature, the radar backscatter mechanisms could better be understood.

Simple empirical equations relating the dielectric constant of sea ice to the brine volume that have been tested by Vant [1974, 1978] were reasonably good. These simple empirical equations seemed to be suited for the study of radar backscatter from sea ice (at least for the temperature below -5° C). The equations have the form $\varepsilon' = a+b\ V_{br}$ and $\varepsilon'' = c+d\ V_{br}$, where a, b, c, and d are constants depending on ice type. The brine volume V_{br}, can be estimated as a function of measured

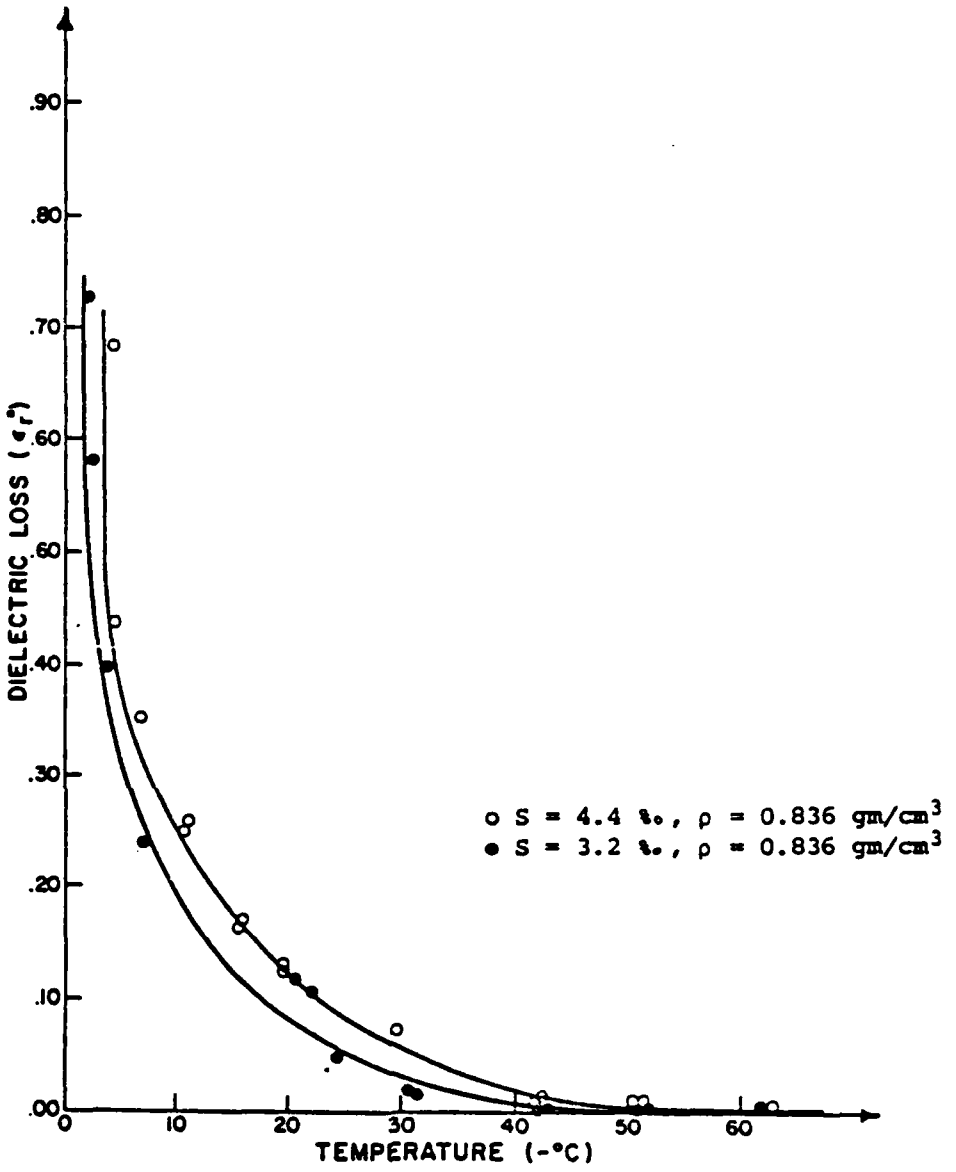

FIGURE 2.5: Variation of Imaginary Part Dielectric Constant (ϵ_r'') of Brazil Sea Ice with Temperature at 10 GHz (Vant, 1976).

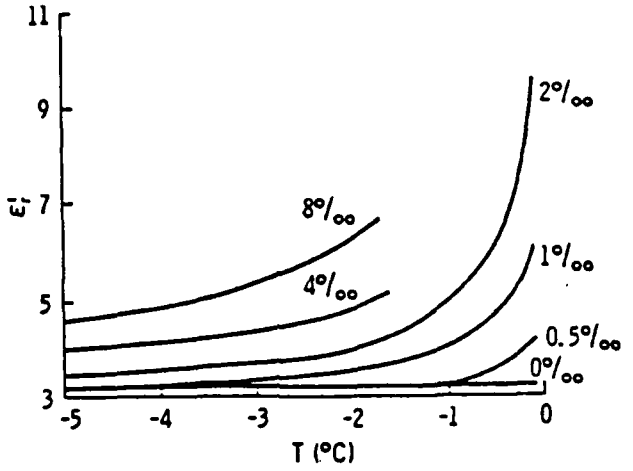

(a) Real Part

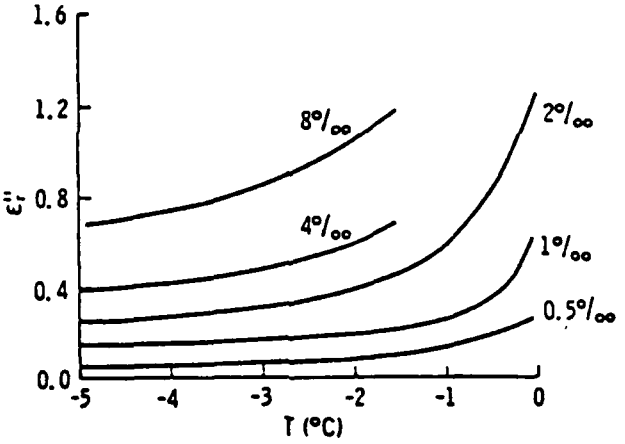

(b) Imaginary Part

FIGURE 2.6: Dielectric Constant of Sea Ice for Various Salinities at 0.5 GHz (Hallikainen, 1982).

salinity and temperature using the equation given by Frankenstein and Garner [1967].

$$V_{br} = S(-\frac{49.185}{T} + 0.532), \text{ in parts per thousand} \qquad (2.3)$$

The empirical equations given by Vant are:

$$\varepsilon' = 3.05 + 7.2\ V_{br}/1000, \text{ for first-year ice at 4 GHz} \qquad (2.4)$$

$$\varepsilon'' = 0.024 + 3.3\ V_{br}/1000, \text{ for first-year ice at 4 GHz} \qquad (2.5)$$

$$\varepsilon' = 2.46 + 22.4\ V_{br}/1000, \text{ for multiyear ice at 10 GHz} \qquad (2.6)$$

$$\varepsilon'' = 0.006 + 10.0\ V_{br}/1000, \text{ for multiyear ice at 10 GHz} \qquad (2.7)$$

Once the dielectric constant at a given frequency is estimated for measured values of salinity and temperature, the values of ε' and ε'' at other frequencies can be estimated using the frequency behavior given by equations (2.1) and (2.2).

Equations (2.4) and (2.5) for first-year ice are compared with the measured values by Vant [1974] in Table 2.1. The results are not very encouraging. The estimates at 4 GHz seem to be lower than the 10 GHz measurements, especially for the ε''. This does not agree with the trend expected by the decreasing frequency behavior, but usually the frazil ice (formed from supercooled turbulent water) is believed to have higher dielectric constant while the model given by equations (2.4) and (2.5) was derived for general first-year ice categories. The estimated values of the dielectric constant vary when the salinity and temperature are varied, as shown in Table 2.2. In a plot of ε' vs ε'' (see Figure 2.7) these points all lie in a straight line. The dielectric constant varies

from 3.14-j 0.06 at T = -20° C, S = 4°/oo to 3.95-j 0.43 at T = -5° C, S = 12°/oo.

These varying dielectric constants affect the reflection coefficients involved in surface scattering and, for multiyear ice, they also affect the volume scattering. Equations (2.6) and (2.7) for multiyear ice are compared with the measured values by Vant in Table 2.3 and the estimated values are shown in Figure 2.7. The empirical estimates seem to give a too large value for ε'' when the temperature is below -10° C.

TABLE 2.1
ESTIMATED AND MEASURED DIELECTRIC CONSTANTS OF FIRST-YEAR ICE

	S = 4.4°/oo		S = 3.2°/oo	
	Estimated (f = 4 GHz)	Measured, Frazil Ice (f = 10 GHz)	Estimated (f = 4 GHz)	Measured, Frazil Ice (f = 10 GHz)
T = - 5°C	3.38 - j0.17	3.75 - j0.37	3.29 - j0.13	3.65 - j0.3
-10	3.22 - j0.10	3.5 - j0.25	3.18 - j0.08	3.4 - j0.2
-20	3.14 - j0.07	3.25 - j0.12	3.12 - j0.06	3.15 - j0.09
-30	3.12 - j0.06	3.1 - j0.06	3.10 - j0.05	3.05 - j0.04

TABLE 2.2
ESTIMATED DIELECTRIC CONSTANT OF FIRST-YEAR ICE AT 4 GHz

	S=12°/oo	10°/oo	8°/oo	4°/oo	0.6°/oo
T = -5°C	3.95-j0.43	3.8 -j0.37	3.65-j0.3	3.35-j0.16	3.09-j0.04
-10	3.52-j0.25	3.44-j0.2	3.36-j0.17	3.21-j0.1	3.07-j0.03
-15	3.38-j0.17	3.32-j0.15	3.27-j0.12	3.16-j0.07	3.07-j0.03
-20	3.31-j0.14	3.27-j0.12	3.22-j0.1	3.14-j0.06	3.06-j0.03
-30	3.24-j0.11	3.21-j0.10	3.18-j0.08	3.11-j0.05	3.06-j0.03
-40	3.20-j0.09	3.18-j0.08	3.15-j0.07	3.10-j0.05	3.06-j0.03

TABLE 2.3
ESTIMATED AND MEASURED DIELECTRIC CONSTANT OF MULTIYEAR ICE AT 10 GHz

	S = 0.6°/oo		S = 0.7°/oo	
	Estimated	Measured	Estimated	Measured
T = - 5°C	2.6 - j0.07	2.7 - j0.06	2.62 - j0.08	2.63 - j0.1
-10	2.53 - j0.04	2.63 - j0.04	2.55 - j0.04	2.55 - j0.07
-20	2.50 - j0.02	2.6 - j0.02	2.51 - j0.03	2.5 - j0.02
-30	2.49 - j0.02	2.57 - j0.01	2.49 - j0.02	2.47 - j0.01

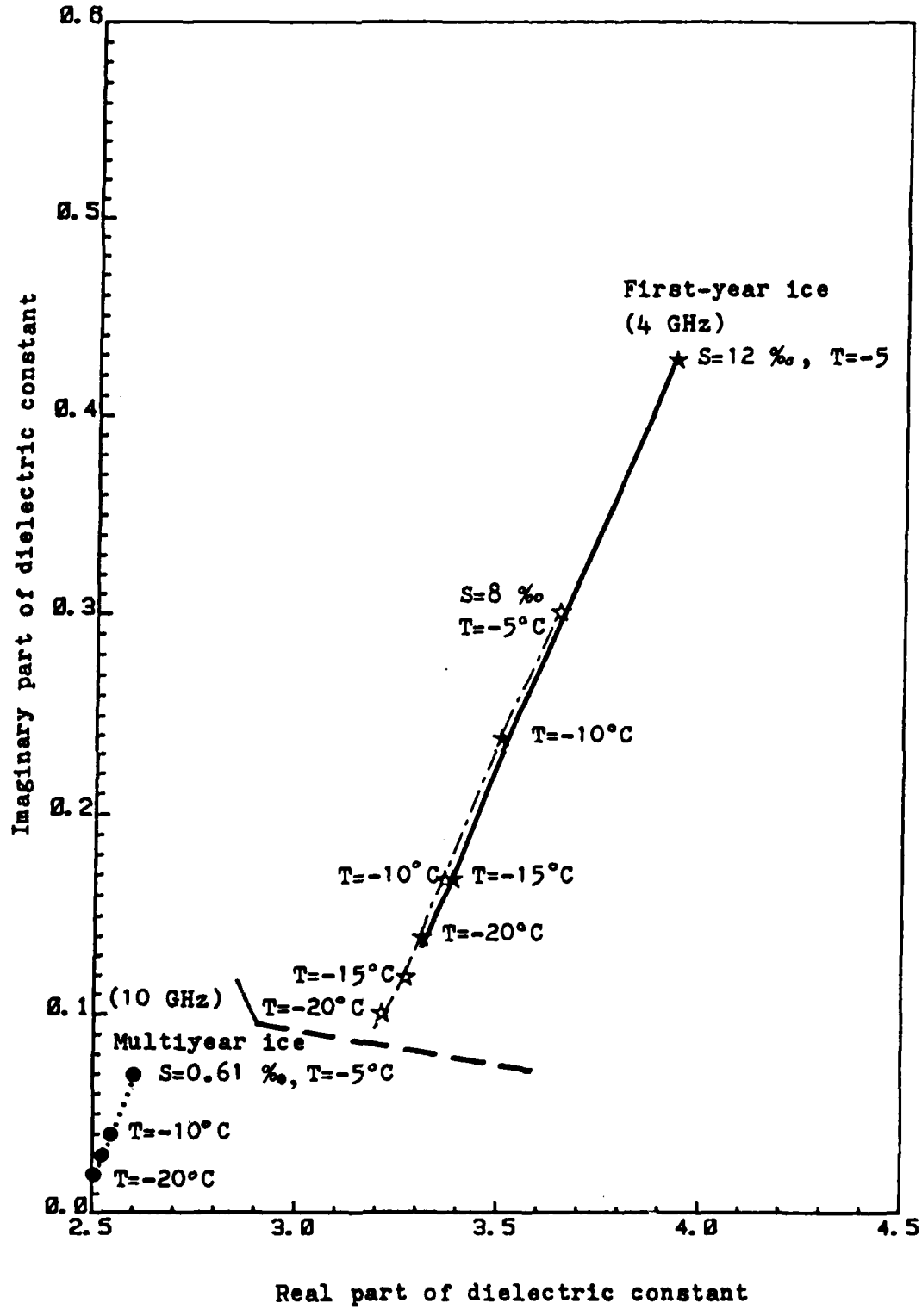

FIGURE 2.7: Estimated Dielectric Constant of First-Year Ice (4 GHz) and Multiyear Ice (10 GHz)

3.0 SURFACE SCATTERING

Physical parameters, like salinity and temperature, affect the dielectric properties of sea ice, which in turn determine the scattering behavior of sea ice in combination with other parameters like surface roughness, size of scatterers inside the ice, etc.

In general, the magnitude of the real part of the dielectric constant of sea ice is far greater than that of the imaginary part. Therefore ε' largely determines the Fresnel reflection coefficient at the ice surface, while ε'' largely determines the penetration (attenuation) into the ice, as well as the scattering contribution due to the inclusions inside the ice medium.

Due to high loss and very small inclusions, surface scattering can be assumed to be the dominant scattering mechanism for summer ice or very thin ice, or even very lossy snow-free first-year ice. In this section, the surface scattering theories are reviewed, and then the signatures of first-year ice are tested against the predictions of surface scattering theories.

3.1 Effect of Surface Roughness

Surface scattering is usually described by the Kirchhoff method for surfaces with a large radius of curvature (compared to wavelength), and by the small perturbation method for surfaces with small scales of roughness. Also, two-scale surface theory has been successfully applied to ocean waves which can be modeled to have both large and small scales of roughnesses.

The Kirchhoff model assumes that the horizontal scale of roughness, or correlation length ℓ, is large compared to wavelength while the

vertical scale of roughness, expressed as the standard deviation σ of surface height is small enough to maintain the average radius of curvature large compared to the wavelength. When the surface height variation is large compared to the wavelength, the Kirchhoff surface integral is simplified using a stationary phase approximation (geometrical-optics model) and when the surface is smoother, it can be simplified using scalar approximation (physical-optics model). Mathematically, the requirements of the Kirchhoff model are written as:

$$\text{correlation length } \ell > \lambda, \text{ or } k\ell > 6 \tag{3.1}$$

$$\text{average radius of curvature } r_c > \lambda. \text{ or } \ell^2 > 2.76\,\sigma\lambda \tag{3.2}$$

$$\text{surface height standard deviation } \sigma > \lambda/4\cos\theta \text{ or } k\sigma > 1.6/\cos\theta \tag{3.3}$$

$$\text{rms slope of the surface } m < 0.25 \tag{3.4}$$

Equations (3.1) and (3.2) are the basic assumptions for the Kirchhoff model, equation (3.3) is for the stationary phase approximation, and equation (3.4) is for the scalar approximation. The backscattering cross-section for the Kirchhoff surface is derived in Ulaby et al. [1982], and the effect of varying model parameters or choosing different correlation functions can be found in Eom [1982].

For relatively rough surfaces whose backscattering cross-sections show a slowly varying angular behavior near nadir, the geometrical optics model seems to be able to predict the backscattering behavior at small incidence angles. Figure 3.1 shows the effect of varying the surface rms slope with this model.

For smoother surfaces, the physical-optics model seems better suited. This model usually exhibits faster angular drop-off than the

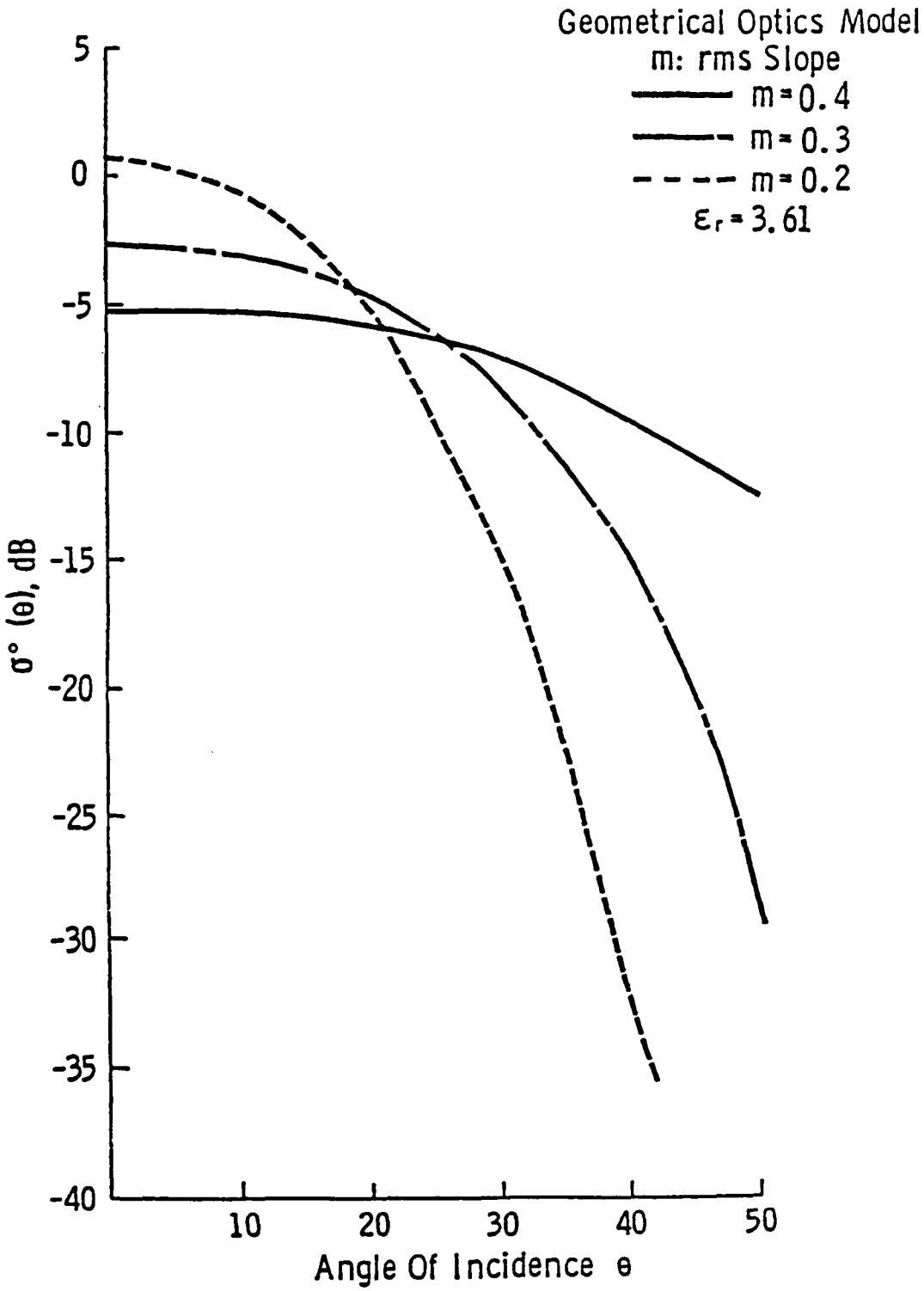

FIGURE 3.1: Geometrical-Optics Model Angular Behavior

geometrical-optics model for small incidence angles. For larger incidence angles, the rate of decay depends on the choice of surface correlation function. The Gaussian correlation function shows a fast angular drop-off, while the exponential correlation function shows large tails. Figure 3.2 shows scattering behavior for the physical-optics model with the Gaussian correlation function. Larger σ or smaller ℓ correspond to a rougher surface, and therefore show a slower angular drop-off. The effect of varying the real part of the dielectric constant is also shown.

Figures 3.3 and 3.4 show frequency responses from 4 to 16 GHz using this model. It is assumed that the surface can be characterized with single values of parameters, σ and ℓ for all the frequencies in question. The question one faces, however, is: are the surface parameters like σ and ℓ frequency-independentπ If the answer is "no", Figures 3.3 and 3.4 do not mean very much. It may be possible that different scales of roughness are responsible for the backscattering at different wavelengths. For many natural surfaces, different correlation lengths or even differnt correlation functions are needed to fit the backscatter data at different frequencies.

3.2 Effect of Salinity and Temperatures

The effect of higher salinity or temperature is to raise the dielectric constant of sea ice, and therefore effectively raise the backscattered power.

Using the result derived in Section 2.0, the maximum variation of ε' for first-year ice due to changes in temperature or salinity is from 3 to 5. This would change the Fresnel reflection coefficient from 0.27

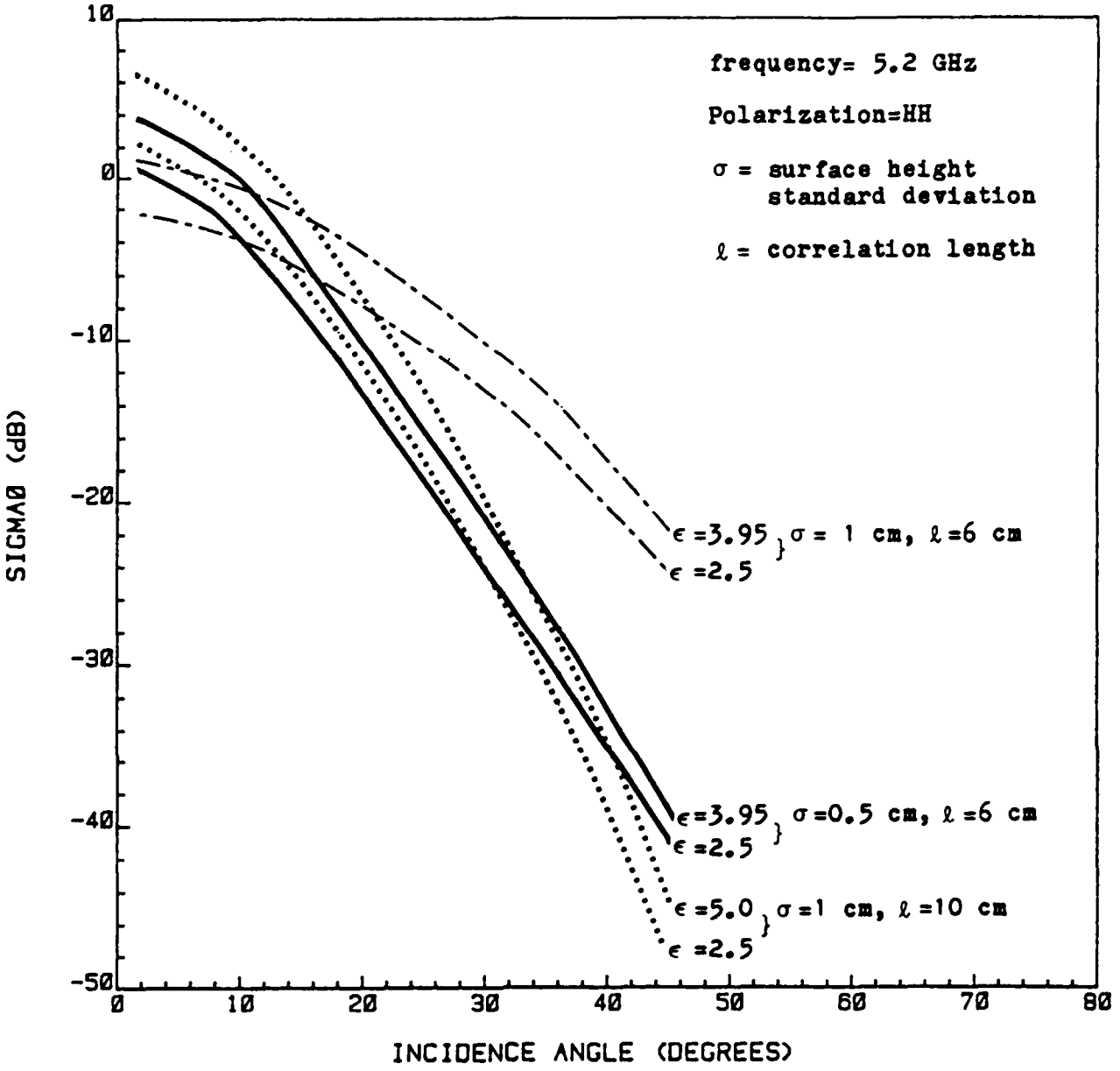

FIGURE 3.2: The Physical-Optics Model Behavior Using A Gaussian Correlation Function. The effect of changing surface parameters together with the effect of variation of dielectric constant are shown.

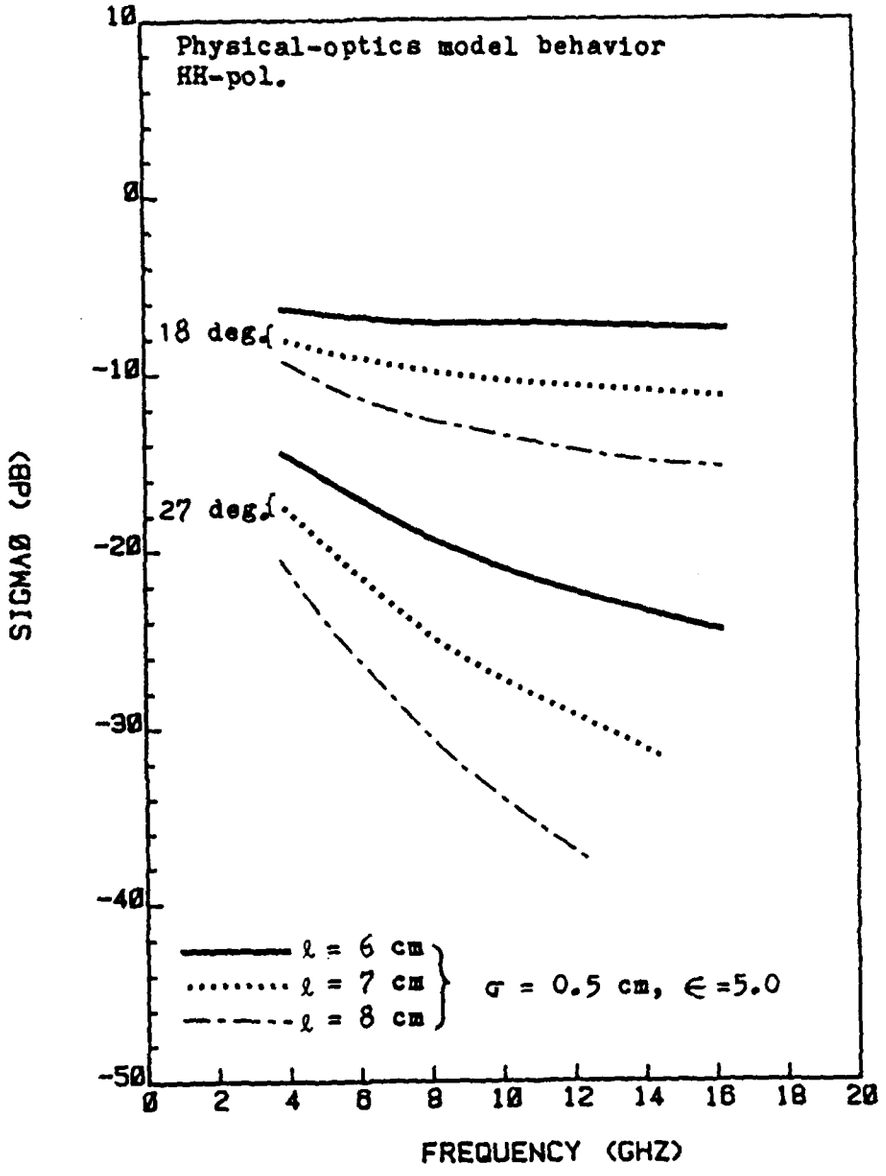

FIGURE 3.3: Theoretical Frequency Behavior of σ^0 Using the Physical-Optics Model with a Gaussian Correlation Function. The effect of surface height correlation length is shown.

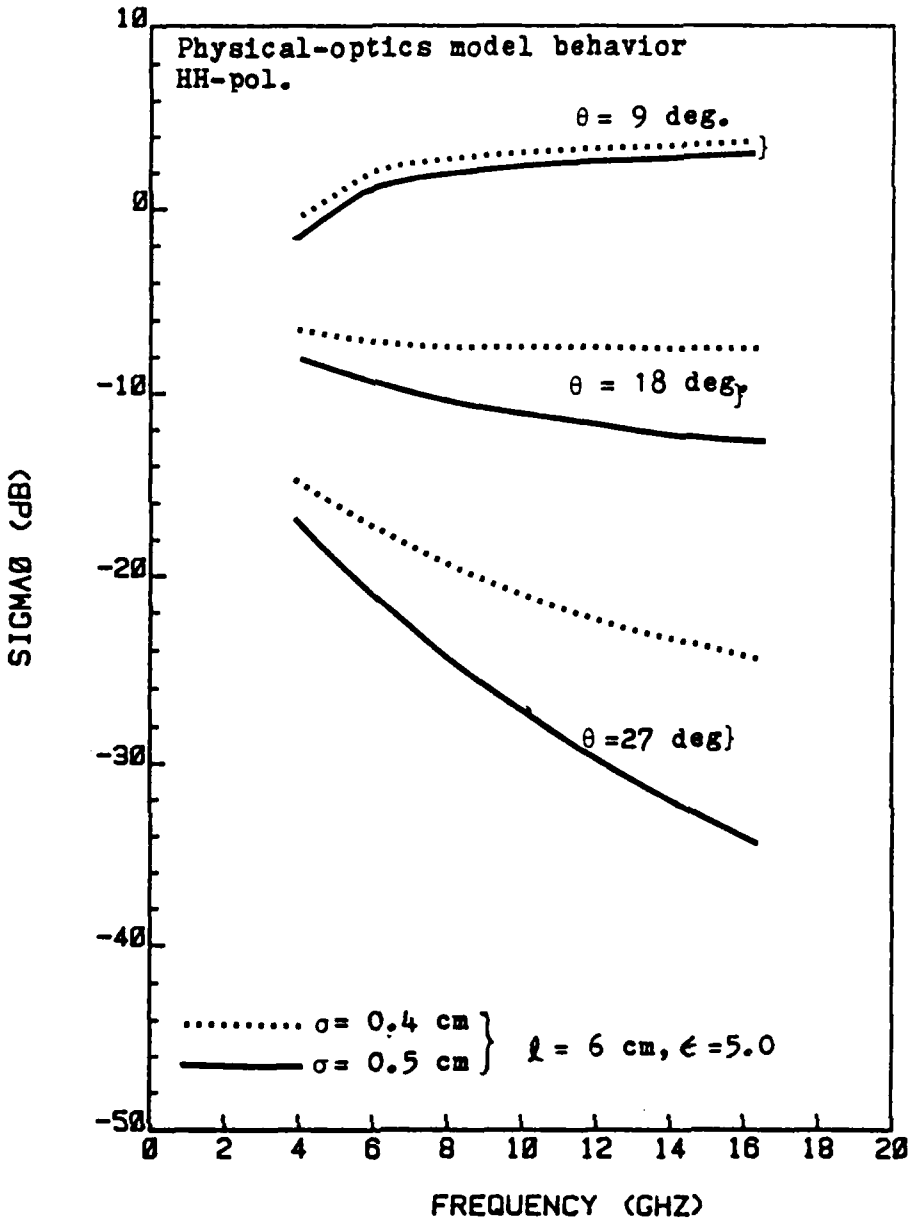

FIGURE 3.4: Theoretical Frequency Behavior of σ^0 Using the Physical-Optics Model. The effect of surface height std. deviation on surface scattering is shown.

to 0.38 for vertical incidence and from 0.38 to 0.5 for incidence angle of 45° with horizontal polarization.

The effect of changes in the Fresnel reflection coefficient to the backscattered power depends on the surface roughness. With the Kirchhoff surface model, the effect due to the maximum possible change in the values of ε' is at most 3 dB (see Figures 3.2 and 3.3), and for the ranges of values shown in Figure 2.7 (ε' = 3 to 4 for first-year ice) the effect is less than 1.7 dB. This effect is independent of specific choice of surface correlation function.

The small variation of ε' with frequency as illustrated in equation (2.1) seems to have a small effect on surface scattering; ε' will be assumed to be constant in the frequency range between 1 and 18 GHz for this study.

3.3 Sea-Ice Surface Scatter Model

3.3.1 Angular Behavior

The power backscattered from sea ice contains contributions from both surface scattering and volume scattering, which might come from snow cover (if any) or from inside the ice (if there are big enough inclusions). To ease the problem, surface scattering will be considered first. It is dominant for summer conditions when the ice surface is wet, or even for the snow-free first-year ice during winter because of its very high loss.

Figure 3.5(a) shows typical backscattering cross-sections measured during the melting season for multiyear ice and first-year ice. The surface scattering can be considered to be dominant here. From the slow angular dropoffs, one can suspect that the geometric optics model with

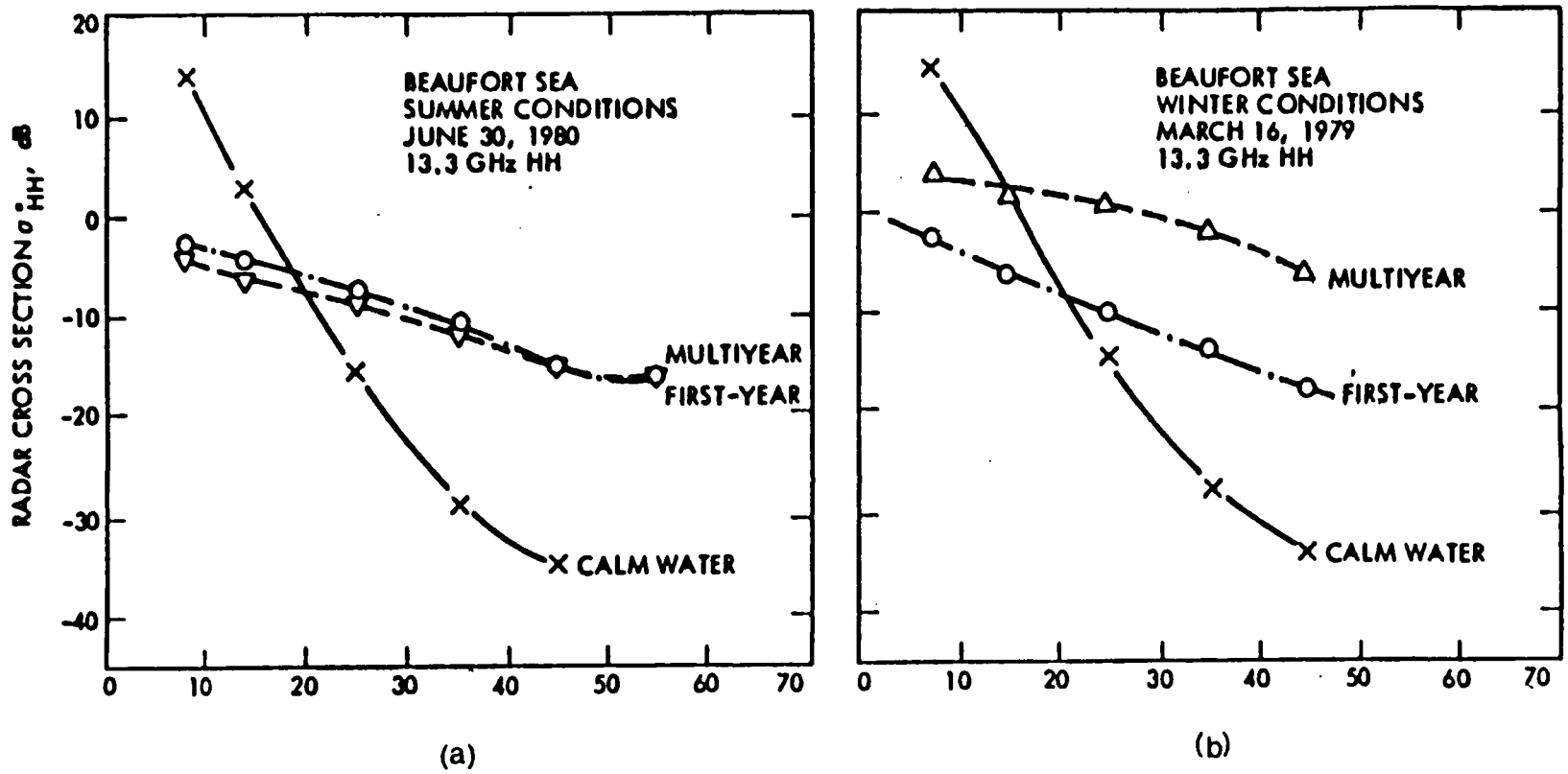

FIGURE 3.5: Measured Backscattering Cross-Sections of Sea Ice and Water. (a) Summer condition; (b) Winter condition. (Gray, et al., 1982).

very large rms slope or the physical optics model with exponential correlation function might work.

Recently Onstott [1983] reported measuring ice surface characteristics during summer, including surface-height correlation length and standard deviation. Table 3.1 is a summary of results for 3 smooth ice profiles and 3 rough ice profiles, along with corresponding values of $k\sigma$ and $k\ell$ at 13.3 GHz. The calculated correlation functions indeed showed the exponentially decaying behavior.

TABLE 3.1
SUMMER ICE SURFACE CHARACTERISTICS

	Sample	1	2	3		1	2	3
Smooth Ice	correlation length, ℓ	6.1	8.9	23	$k\ell$	17	24.8	64.1
	height std. dev. σ	0.21	0.15	0.11	$k\sigma$	0.58	0.42	0.31
Rough Ice	ℓ	7.7	8.2	35.5	$k\ell$	21.4	22.8	98.9
	σ	0.72	0.81	0.49	$k\sigma$	2.0	2.3	1.4
			(cm)			(f=13.3 GHz, $k=2\pi/\lambda$)		

Figure 3.6 shows theoretical angular behavior of σ^0 using an exponential correlation function in the physical optics model. The summer data shown in Figure 3.5(a) are redrawn in Figure 3.6(a) and one can see that the data can very much be predicted using the single-surface scattering model. The surface parameters for the smooth ice (see Table 3.1) gives faster angular dropoff (see Figure 3.6(b)), and

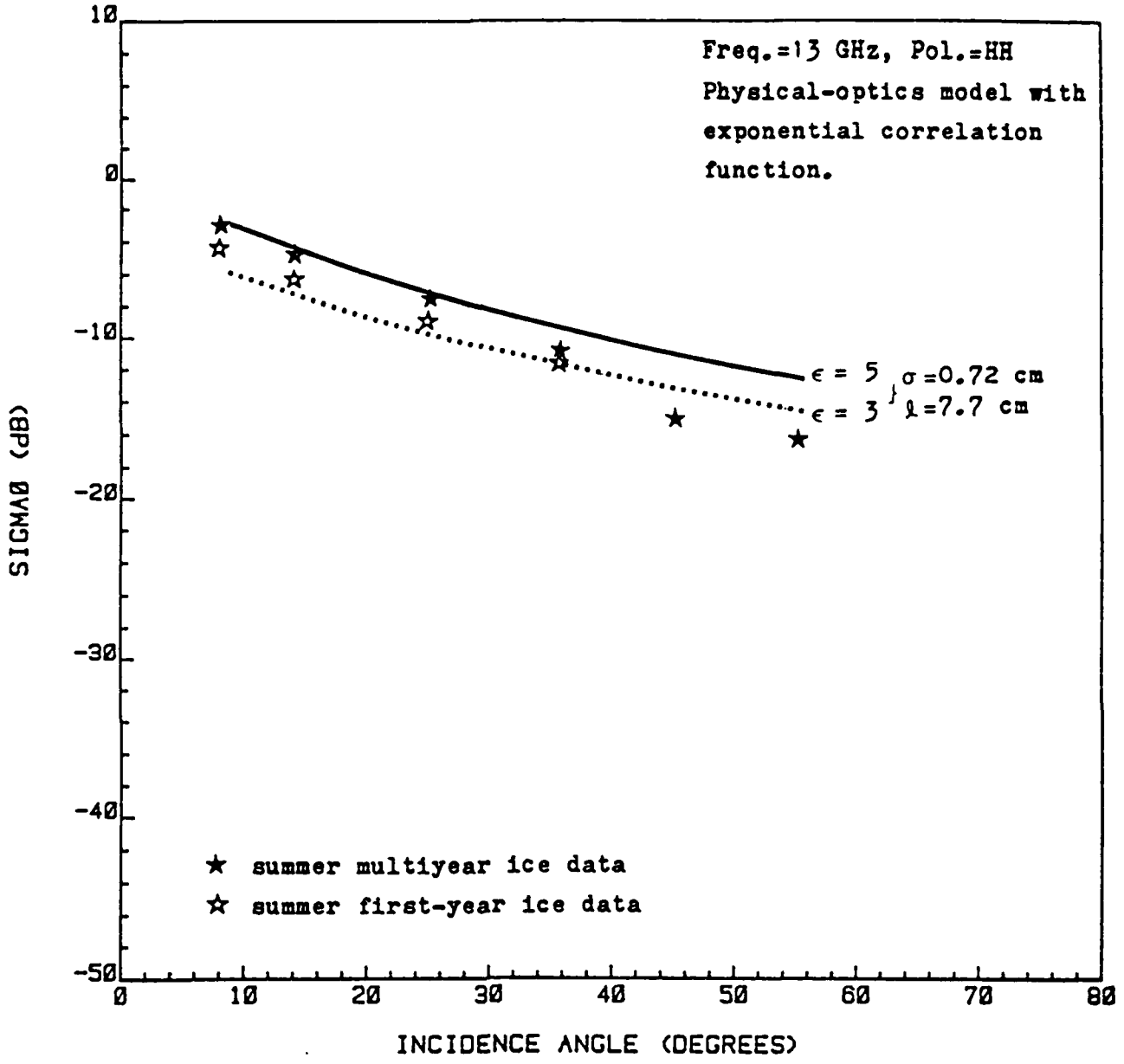

FIGURE 3.6(a): Theoretical (Physical-Optics Model) Angular Behavior of σ°. Also shown is the early summer data when the ice was covered with wet snow (Gray et al., 1982). The surface roughness parameters are real ice data. Taken nearly at the same time of the year (June).

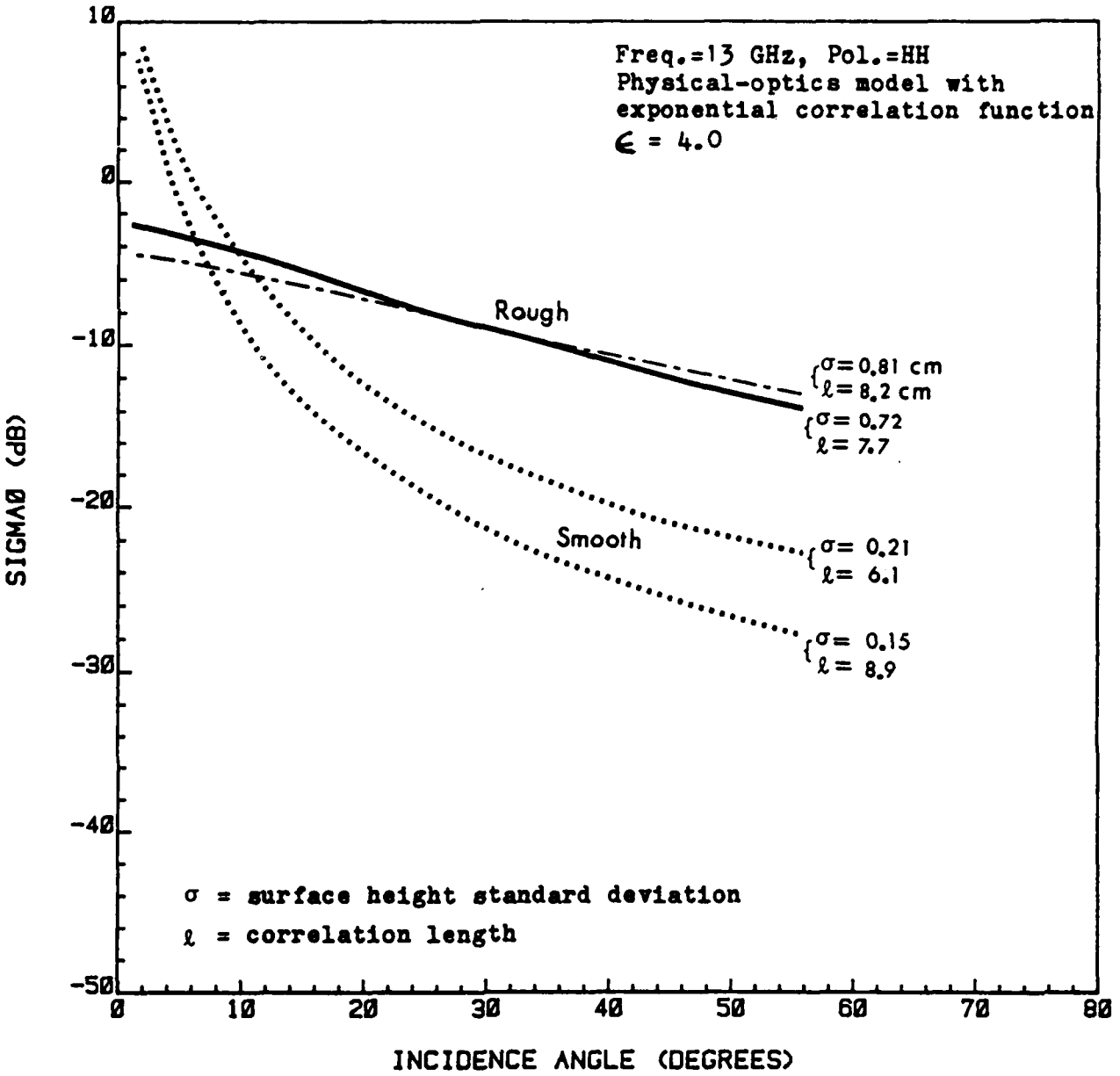

FIGURE 3.6(b): Theoretical Angular Behavior of σ° for smooth and Rough Ice.

the first-year ice during winter shown in Figure 3.5(b) might have had a slightly smoother surface than the summer ice.

This result is encouraging because the single-surface scattering model might explain σ^0 for first-year ice during the whole year, without any help from a small-perturbation or Bragg-resonance type model for large incidence angles. In another sense, the result is discouraging because the surface roughness can make as much as 15 dB difference in the backscattering cross-sections at large incidence angles (see Figure 3.6(b)). If one adds the 2-3 dB variation due to the difference in the dielectric constant, the same ice categories with different surface roughness can give up to 18 dB variation with different temperatures or salinities. This large fluctuation would severely limit the system capability to discriminate different ice types (unless the surface roughness of one type of ice is always different from that of the other type of ice, or different ice types have different scattering mechanisms).

Under summer conditions, the surface scattering can be considered to be dominant for both the multiyear ice and the first-year ice. The macro-scale roughness and snow cover differences between first-year and multiyear ice may result in different σ^0s, even though small-scale roughness for both ice types may be similar. During winter the surface scattering may also be dominant for first-year ice, but volume scattering might be dominant for multiyear ice and these two are distinguishable. The volume scattering will be considered in the next section.

3.3.2 Frequency Behavior

Figure 3.7 shows the theoretical frequency behavior of σ^0 using the same surface parameters for all the frequencies. As one can expect, the smooth ice σ^0 varies more than that for the rough ice and σ^0 for smooth ice increases with frequency for all the incidence angles, while this is not true for rough ice for small incidence angles.

σ^0 decreases with frequency for the Gaussian surface correlation (see Figures 3.2 and 3.3), but the measurements (Figure 3.8) show gently increasing frequency behavior for most of the incidence angles. Therefore the exponential correlation function seems to be more able than the Gaussian correlation function to predict both the angular and the frequency behavior of σ^0 for sea ice.

3.3.3 Polarization Considerations

Figure 3.9 shows the polarization dependence of the backscattering cross-sections of first-year ice. Air bubbles inside the multiyear ice usually are believed to be the main source of volume scattering as well as the depolarized scattering and the effect increases as the frequency is increased. In this section the application of surface scattering theories to scattering from first-year ice is discussed.

The geometrical-optics model neglects the multiple scattering [Fung and Eom, 1979], and therefore predicts that the depolarized backscattering coefficient is zero. Moreover, there is no distinction in this model between vertical and horizontal polarization, since the Fresnel reflection coefficient is evaluated at normal incidence.

For the physical-optics model, use of HH polarization results in a higher scattering cross-section than use of VV polarization at all

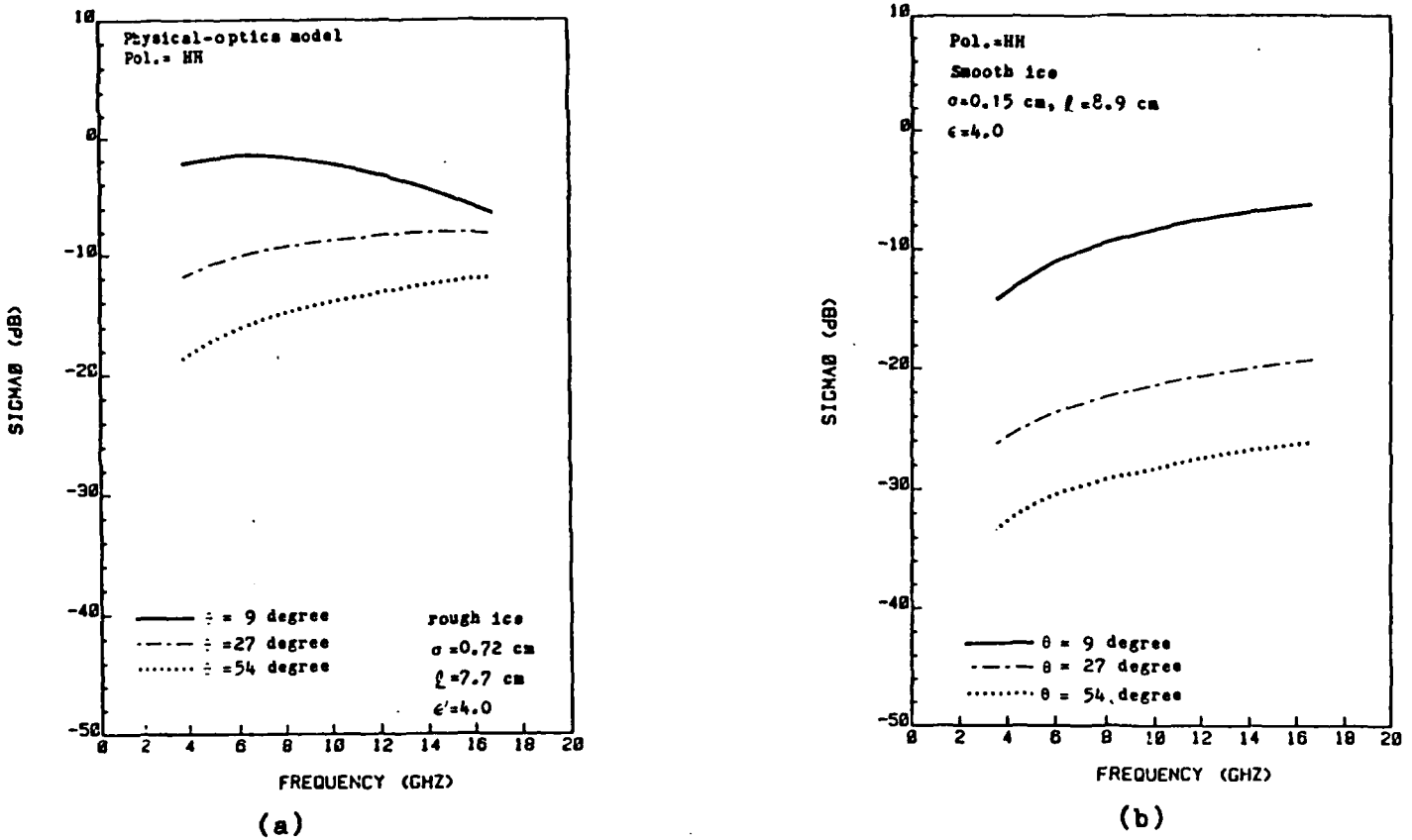

FIGURE 3.7: Theoretical Frequency Behavior of σ^0 of First-Year Ice with HH-Polarization. Physical-optics model using an exponential correlation function. (a) Rough ice; (b) Smooth ice.

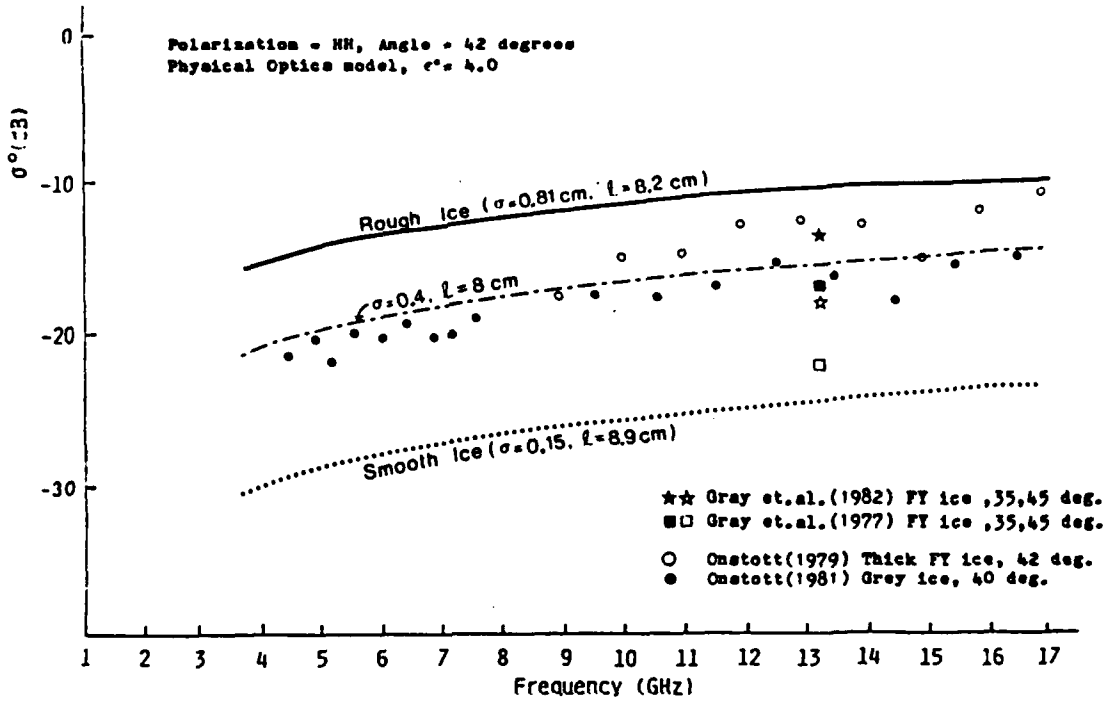

FIGURE 3.8: Physical-Optics Model Frequency Behavior. Also shown are several reported measurements. With proper choice of surface parameters, the model can fit the data very well.

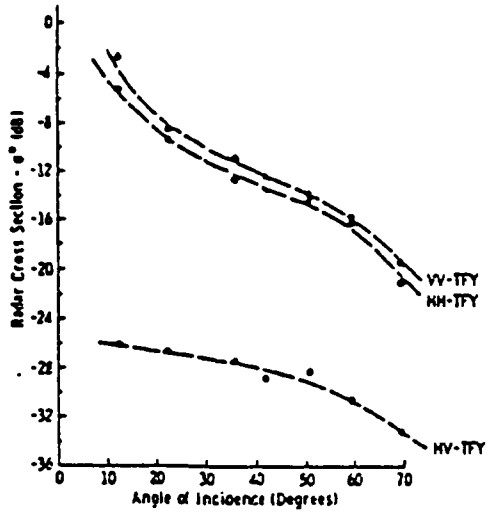

(a) Onstott, et al., 1979

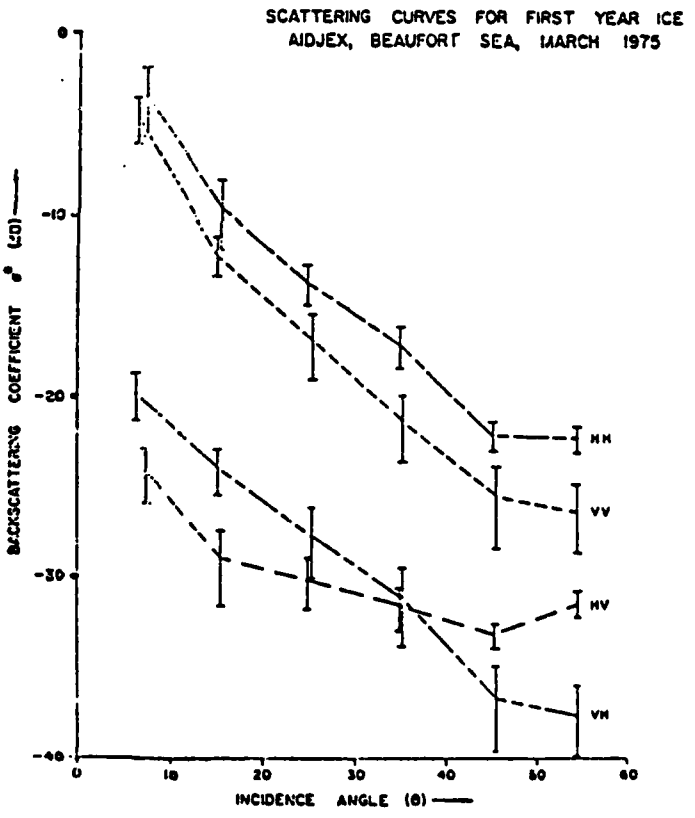

(b) Gray, et al., 1977

FIGURE 3.9: Polarization Dependence of the Backscattering Cross-Section of First-Year Ice at 13 GHz.

angles except vertical incidence, mainly due to the Brewster angle effect. The depolarized backscattering coefficient is also zero, unless multiple scattering is included [Fung and Eom, 1981].

For the small-perturbation model, VV polarization results in slower angular dropoff than HH polarization and therefore σ^0_{VV} is higher than σ^0_{HH} except at nadir. When the wave equation is solved to second order, the cross-polarized term is not zero [Fung, 1968].

From the discussions given in Section 3.3.1, the physical-optics model might be able to be applied to the snow-free first-year ice. The observations by Gray, et al. [1977, Figure 3.9(b)] agree with the model in the sense that σ^0_{HH} is higher than σ^0_{VV}. The difference between the results with VH- and HV-polarization, however, suggests a calibration problem. Onstott's result [1979, Figure 3.9(a)] shows higher σ^0_{VV} than σ^0_{HH} although the difference is small. Parashar [1974] only had VV data at 13.3 GHz, but his theoretical model predicted faster angular dropoff for HH polarization mainly because the small-perturbation method was used.

These confusing results can partly be due to system calibration inaccuracies, but all of them may be true because the ice surface characteristics can have large variations from place to place or from time to time.

3.3.4 Empirical Surface Model

Close to vertical, σ^0 usually varies rapidly with angle and is hard to measure accurately. Also, the measurement may include the coherent, system-dependent (beamwidth-dependent) component [Fung and Eom, 1983] at

small incidence angles. At large incidence angles, beyond about 60°, a different scattering mechanism may take over.

When a measurement is taken over a single target class, and the purpose is to extract dielectric constant (i.e., soil moisture detection), the severe dependence on surface roughness shown in Figure 3.6(b) can be minimized using small incidence angles (7° to 17° for soil-moisture determination) [Ulaby et al., 1981]. On the other hand, when several target classes are present, and they must be discriminated from each other, larger angles of incidence must be used to allow surface-roughness effects to aid in separating the different target classes (see Figure 3.5). Therefore, in this study incidence-angle ranges only between 20° and 60° will be considered.

The backscattering coefficient of first-year sea ice for the angles of incidence between about 15° to 20° and about 50° to 60° can generally be approximated by a straight line on a dB-vs-angle plot; it can be fitted by a model of the form

$$\sigma^o(\theta) = A\, e^{-\theta/\theta_o} \tag{3.5}$$

or

$$\sigma^o(\theta) \text{ in dB} = 10 \log A - \left(\frac{4.34}{\theta_o}\right) \theta \tag{3.5a}$$

where the constant A determines the absolute level of the curve while the constant θ_o shows the rate of decay of the curve. This type of model has been used to describe the backscatter from ocean and various

land targets, and Onstott [1980] tested this type of model for the sea ice data.

The coefficient A is determined by the surface roughness and by the Fresnel reflection coefficient which for sea ice is determined mainly by the real part of the dielectric constant. Here the surface roughness is considered to be the dominant factor as discussed in Section 3.3.1, while the differences in the salinity and the temperature change (below about -5° C) cause a minor variation (2 to 3 dB maximum) between data sets.

The coefficient θ_0 is determined primarily by the surface roughness.

The theoretical scattering coefficients calculated using the physical-optics formulation with the surface parameters shown in Figure 3.6(b) seem to fit a straight line for angles greater than about 20°. The values of coefficients A and θ_0 are shown in Table 3.2. The e-folding angle, θ_0 is about 14° for the smooth-ice categories and is more than 23° for rough ice. The magnitude coefficient, A, ranges from 0.08 to 0.21 for smooth ice and from 0.39 to 0.48 for rough ice. In Table 3.3, the coefficients for several reported measurements are shown. The e-folding angle varies from 10.9° to 19° while the amplitude A varies from 0.18 to 1.0; the relative system calibration might have played an important role in the absolute level variations.

The measurements reported above and the theoretical model predictions are plotted in Figure 3.10 for incidence angles beetween 20° and 60°. Using the measured ice-surface parameters for rough ice and smooth ice, the theoretical model bounds all the measurements considered above, and the physical-optics model seems to be suited to explain the

TABLE 3.2
PHYSICAL-OPTICS MODEL BEHAVIOR BETWEEN 20° AND 60°

	Rough Ice		Smooth Ice	
	σ = 0.72 cm ℓ = 7.7 cm	σ = 0.81 cm ℓ = 8.2 cm	σ = 0.21 cm ℓ = 6.1 cm	σ = 0.15 cm ℓ = 8.9 cm
$\sigma^o = Ae^{-\theta/\theta_o}$	$0.48e^{-\theta/23.3°}$	$0.39e^{-\theta/28°}$	$0.21e^{-\theta/14°}$	$0.08e^{-\theta/13.9°}$
σ^o(dB)	$-3.2-0.186\theta$	$-4.0-0.155\theta$	$-6.7-0.307\theta$	$-11.0-0.313\theta$
pol = HH, f = 13 GHz, ε' = 4.0				

TABLE 3.3
EMPIRICAL MODEL COEFFICIENTS FOR THICK FY ICE, 13 GHz

Source	σ^o	σ^o(dB)	POL	System
Onstott (1977)	$0.53e^{-\theta/19°}$	$-2.8-0.228\theta$	HH	TRAMAS
	$0.78e^{-\theta/17.2°}$	$-1.1-0.252\theta$	VV	TRAMAS
Delker (1979)	$0.44e^{-\theta/15°}$	$-3.6-0.29\ \theta$	VV	TRAMAS
	$0.39e^{-\theta/15.5°}$	$-4.1-0.28\ \theta$	VV	HELOSCAT
Gray (1977)	$0.31e^{-\theta/12.8°}$	$-5.1-0.34\ \theta$	HH	Scatterometer
	$0.18e^{-\theta/11.7°}$	$-7.4-0.37\ \theta$	VV	Scatterometer
Gray (1982)	$0.64e^{-\theta/15.3°}$	$-1.9-0.284\theta$	HH	Scatterometer, Summer
	$1.0\ e^{-\theta/10.9°}$	$0.0-0.397\theta$	HH	Scatterometer, Winter

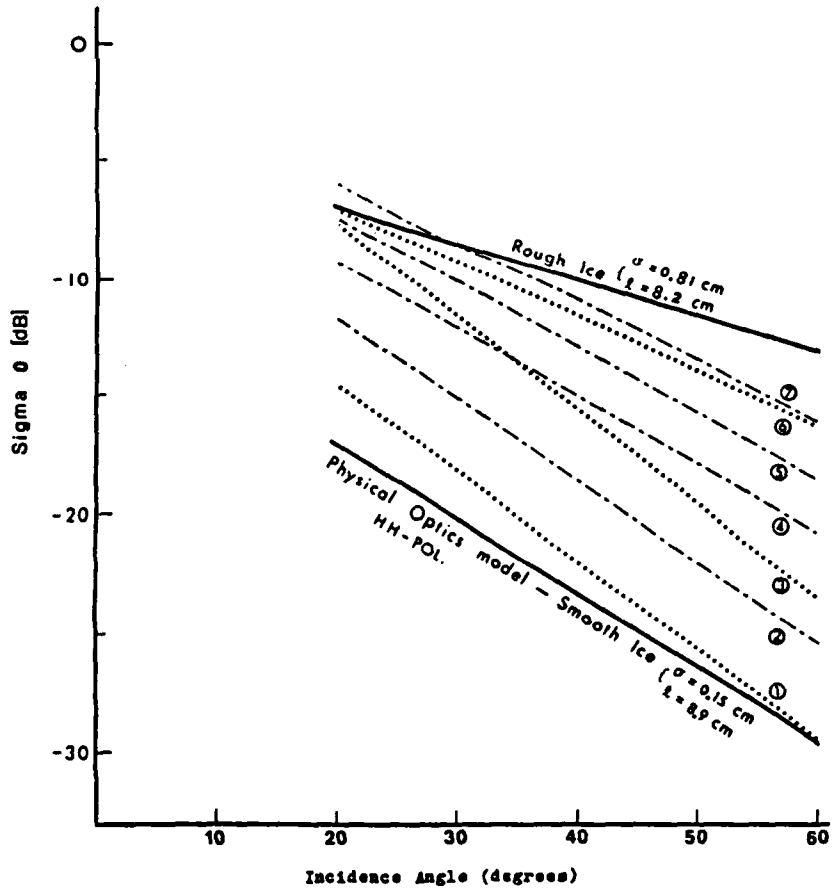

FIGURE 3.10: Reported Measurements of First-Year Ice at 13 GHz; 1=Gray, VV (1977); 2=Gray, HH (1977); 3=Gray, HH winter (1982); 4=Delker, VV (1979); 5=Gray, HH summer; 6=Onstott, HH; 7= Onstott, VV (1977). Physical-optics model behaviors are also shown for a rough ice and a smooth ice.

first-year ice data when proper surface parameters are available or chosen.

The e-folding angle seems to vary from about 10° up to about 20° depending on the surface roughness, and the dynamic range of σ^0 of the first-year ice can be about 10 dB at the incidence angle of 20° and as much as 17 dB at 60°, at 13 GHz.

The empirical model given by the form $\sigma^0 = A \exp(-\theta/\theta_0)$, has the advantage of simplicity. However, this type of model lacks the capability to fit multifrequency data, unless the model parameters, A and θ_0 are given for every frequency. Figure 3.11 shows the frequency behavior of the empirical model constants, e-folding angle and the 40° intercept. Also shown are the model constants of the data between 18° and 54° incidence angle calculated using the physical optics model under two surface roughnesses.

Under the physical-optics model, the e-folding angle of the smooth surface experiences little frequency dependence while that of the rough surface does increase with frequency. The scatter of measured values is too large to see a definite pattern of frequency behavior. However, they may be divided into two sub-groups; one is the relatively smooth group with the e-folding angle of 10° - 15°, another is the relatively rough group with the e-folding angle of 20° to 30°. The measurement of the grey ice [Onstott et al., 1981] between 4 and 17 GHz shows an interesting pattern (see Figure 3.11(a)). With C-band frequencies, the surface may have been smooth while with X-Ku-band frequencies the surface may have been rough. It is hard to draw any conclusion with this small data set. The 40° intercept shows relatively smooth

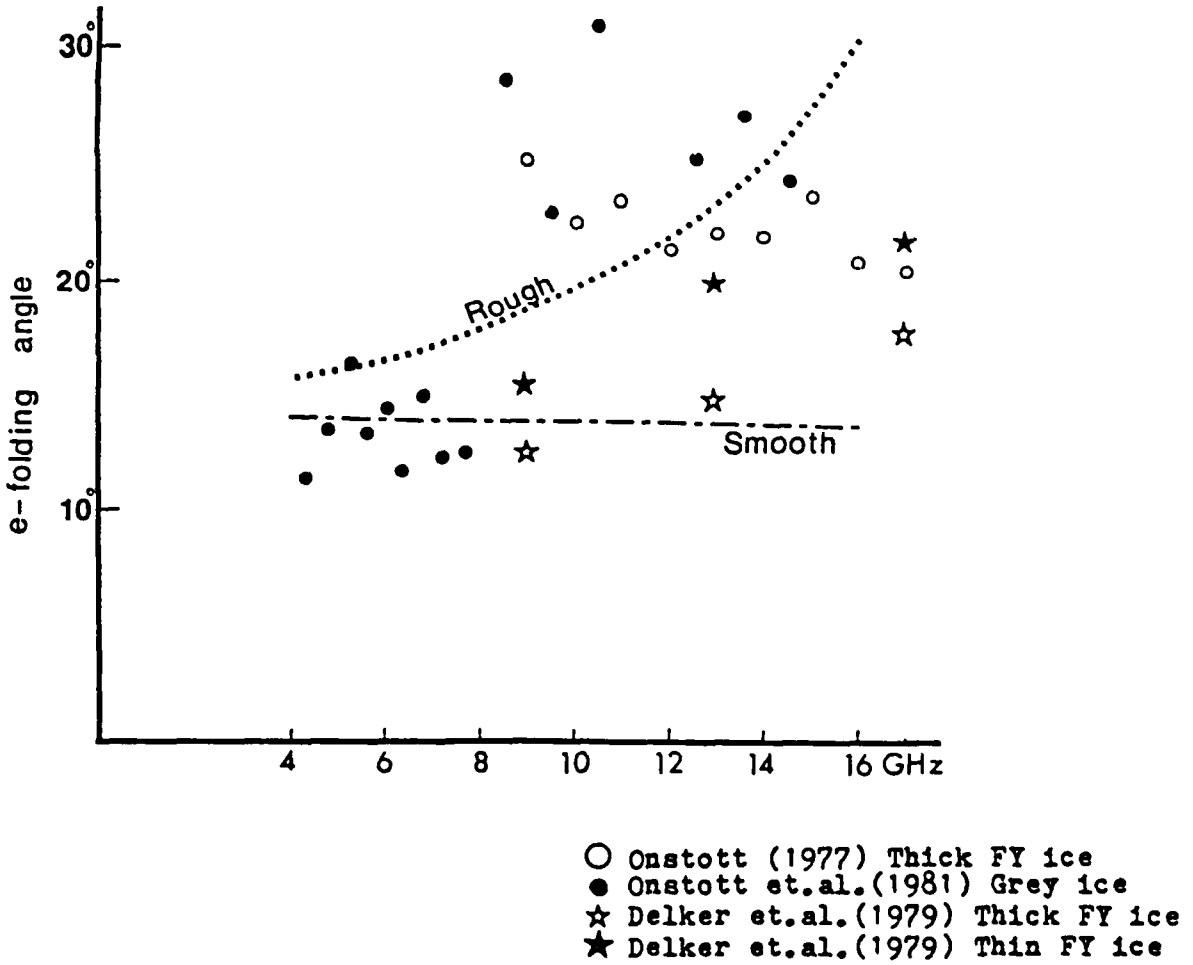

(a)

FIGURE 3.11: Frequency Behavior of Empirical Model Constants. The lines are the straight line fit of the physical optics model prediction between 18° and 54°.

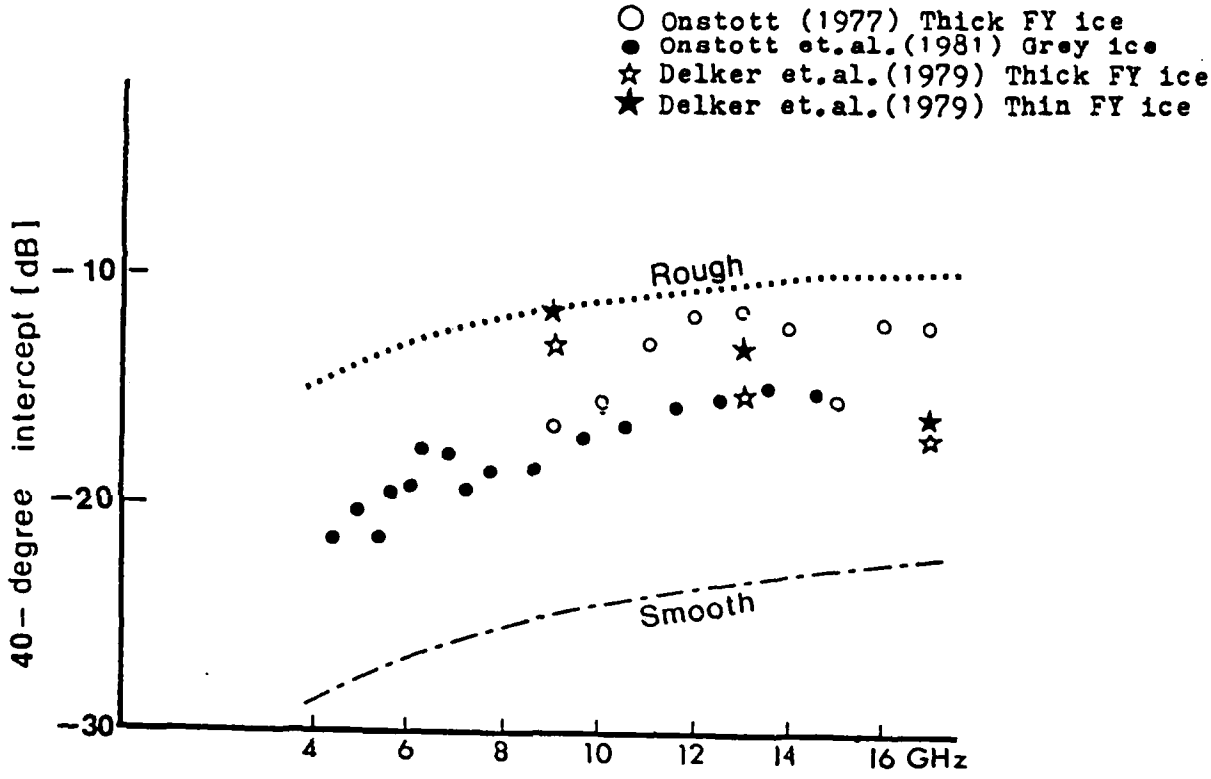

(b)

FIGURE 3.11: Frequency Behavior of Empirical Model Constants. The lines are the straight line fit of the physical optics model prediction between 18° and 54°.

frequency behavior both in the data and the physical-optics model prediction.

The discussion above considered only the surface scattering. This would be the primary effect for a snow-free, very-lossy first-year ice which does not have any big enough air bubbles inside the ice to cause significant volume scatter. Snow cover on sea ice will contribute to backscattering by itself and will modify the ice surface scattering as well as the ice-volume scattering by changing the temperature of the ice surface, which in turn will change the imaginary part of the dielectric constant significantly and, as a result, change the scattering albedo of any inclusions inside the ice. These factors will be considered in the next sections.

4.0 VOLUME SCATTERING

Volume scattering may take place in the snow cover on ice or in the inclusions inside the ice medium. Large air bubbles inside multiyear ice are likely to be a major source of volume scattering. In this section, several volume scattering theories are reviewed, and then the signatures of multiyear ice are tested against the predictions of volume scattering theories.

4.1 Introduction

Two basic approaches are used in theoretical explanations of volume scattering. One is the field approach, which starts with wave equations and includes all the multiple scattering and interference. This approach is very complicated mathematically; in consequence, a number of simplifying assumptions or approximations are required to solve actual problems. Therefore, when this approach is applied to a specific target, the applicability of each assumption has to be studied carefully.

Another approach, which is often called "the radiative transfer theory", assumes that the effect of phase interference or correlation between different field quantities is negligible, thereby allowing power addition. This theory deals with intensities rather than fields and is based on Boltzmann's equation of transfer. In this study, the radiative transfer approach will be adapted. There are two popular methods in radiative transfer theory: the matrix doubling method and the differential and integral equation method.

The matrix doubling method starts with a sufficiently thin layer of optical depth $\Delta\tau$ in which it is assumed that no multiple scattering

occurs. A combination of two such layers results in multiple scattering and can be traced in terms of total effective backward and forward scattering matrices. This process is continued until the desired thickness is built. A detailed method of solution can be found in Eom [1982].. This approach has the advantage of fast computational speed for a single-layer problem; there is no restriction on the amplitude of dielectric fluctuations, and the method can be extended to the problems where the characteristics of the embedded scatterers vary with depth. However, for multi-layer problems the differential-integral-equation method might be better suited [Eom, 1980] and will be discussed further.

4.1.1 Linear Differential- and Integral Equation Method

In this formulation, the medium is characterized by the phase function and the scattering albedo. The equations of transfer for the upward and downward intensities inside the inhomogeneous medium are [Karam and Fung, 1982]

$$\frac{dI^{+}(z)}{dz} = -K^{+} I^{+}(z) + F^{+}(z) \tag{4.1}$$

$$\frac{dI^{-}(z)}{dz} = -K^{-} I^{-}(z) + F^{-}(z) \tag{4.2}$$

where + and - signs represent upward and downward directions, respectively. K^{+} and K^{-} are the extinction coefficient matrices, and F^{+} and F^{-} are the source functions having the form

$$F^{+}(z) = \sec\theta \int_0^{2\pi} d\phi' \int_0^{\pi/2} \sin\theta' d\theta' \left[P(\theta,\phi;\theta',\phi')\, I^{+} + P(\theta,\phi;\pi-\theta',\phi')\, I^{-}\right] \tag{4.3}$$

$$F^-(z) = \sec\theta \int_0^{2\pi} d\phi' \int_0^{\pi/2} \sin\theta' d\theta' \left[P(\pi-\theta,\phi;\theta',\phi')\ I^+\ P(\pi-\theta,\phi;\pi-\theta',\phi')\ I^-\right] \tag{4.4}$$

where $P(\theta,\phi;\theta',\phi')$ is the phase matrix describing the scattering properties of the medium from direction (θ,ϕ) to direction (θ',ϕ'). Several types of phase functions have been studied, including Rayleigh phase function, Mie phase function and also the phase functions for a continuous random medium [Tsang and Kong, 1977]. The pair of transfer equations is usually solved numerically after converting them into a set of linear first-order differential equations.

The boundary conditions for the intensities (I^+ and I^-) at the interface call for transmission and reflection coefficients. For planar interfaces, these coupling coefficients are given by Tsang and Kong [1978] and Shin and Kong [1981]. For rough interfaces the coupling coefficients were derived by Fung and Eom [1979, 1981] and Lee and Fung [1979], for Kirchhoff-surface and slightly-rough interfaces, respectively. Recently Karam and Fung [1982] generalized the intensity scattering problem for a multi-layered random medium with irregular boundaries.

The main advantage of the linear differential- and integral-equation method lies in its conceptual simplicity, and the scalar representation of equations (4.1) and (4.2) has been used extensively for emission problems for snow and vegetation [Ulaby and Stiles, 1980; Attema and Ulaby, 1975]. Karam and Fung's formulation also permits expressing the volume and surface scattering interaction in a closed form for some simplified vegetation models.

4.2 Snow-Free Multiyear Ice

To simplify the problem, snow-free multiyear ice will be considered first. For this case, the physical model shown in Figure 4.1 is proposed. The first layer is the layer of recrystallized ice which contains large air bubbles. The density of this layer is usually reported to be 0.7 - 0.8 gm/cm^3, although this is highly variable [Campbell et al., 1977]. Figure 4.2 shows density profiles for 3 types of ice. The salinity of the first layer is almost zero for multiyear ice (see Figure 4.3), but a slightly higher value (0.7^o/oo) has been noted by Onstott [1980]. The depth of this layer can be assumed to be about 20-30 cm (low density portion from Figure 4.2, or near-zero salinity portion from Figure 4.3), but this milky layer can be as much as 55 cm [Onstott, 1980].

The second layer shown in Figure 4.1 is the clear ice layer with occasional small air bubbles. This layer can be assumed to be a half-space because microwave frequencies are not expected to reach the ice bottom. This layer has salinity of 1-2^o/oo, with density of 0.8 - 0.9 gm/cm^3. The first approximation will be to neglect the air bubbles in this second layer, considering only the first layer as the volume scattering layer. The final model might have to include scattering by the small air bubbles in this second layer.

In view of the radiative transfer approach discussed in Section 4.1, the volume scattering layer is characterized with the scattering albedo ω and the optical depth τ given by

$$\omega = K_s/(K_s + K_a) \qquad (4.5)$$

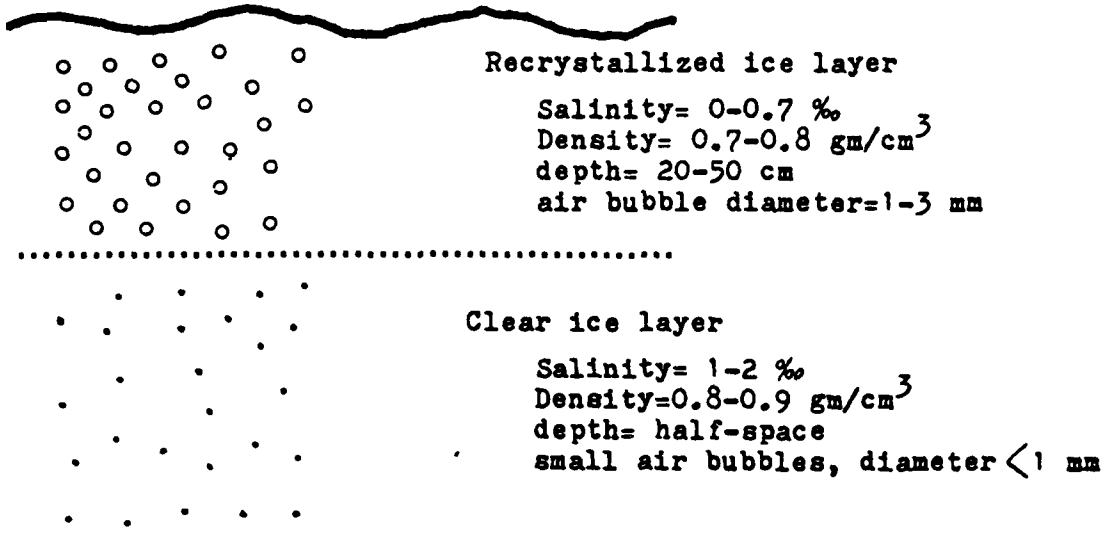

FIGURE 4.1: Snow-Free Multiyear Ice Model

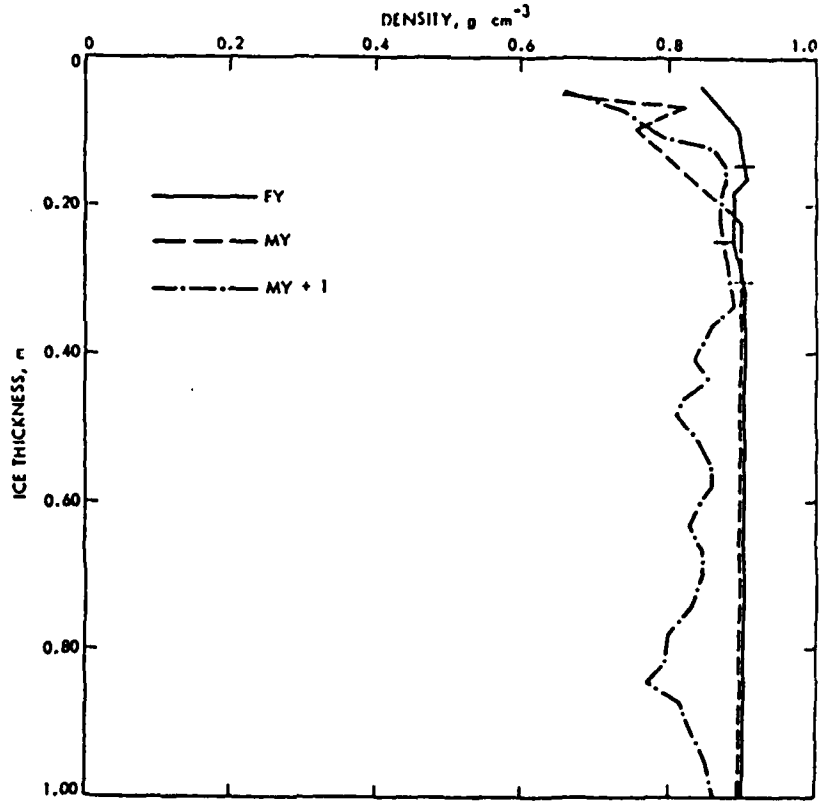

FIGURE 4.2: Density as a Function of Depth Below Surface of Ice Observed in FY and MY Ice. The MY + 1 was measured in the fall when its freeboard tends to be above the MY ice. (Campbell et al., 1978)

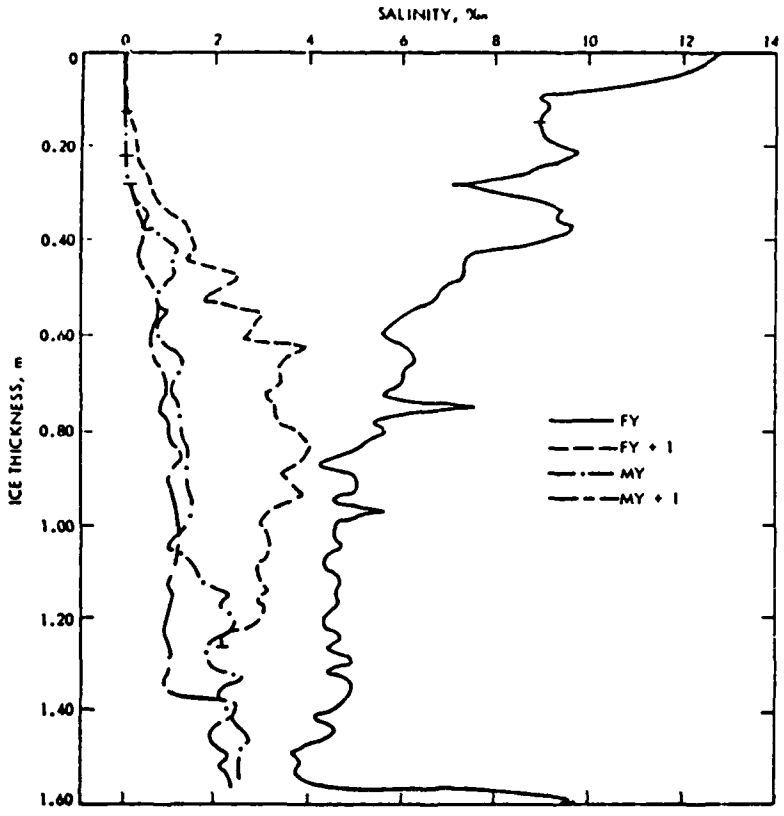

FIGURE 4.3: Salinity as a Function of Depth Below Surface of Ice Observed in (a) First-Year Ice (FY); (b) First-Year Plus 1 Year (FY + 1); (c) Multiyear Ice (MY); and (d) Multiyear Plus 1 Year (MY + 1). Only for curves FY and FY + 1 has the total thickness been shown, whereas the other curves would extend to greater depths. FB designates the respected freeboard for each curve. (Campbell et al., 1978).

$$\tau = (K_a + K_s)d = K_e d \tag{4.6}$$

where K_s is the volume scattering coefficient and K_a is the volume absorption coefficient. Here, the extinction coefficient, K_e, is assumed to be constant in the layer of depth d.

4.2.1 Scattering Albedo

For air bubbles in the ice medium, the absorption will be due to ice only, and the absorption coefficient K_a is

$$K_a = \frac{4\pi}{\lambda_o} \sqrt{\frac{\epsilon_b'}{2}} \left(\sqrt{1 + \tan^2\delta} - 1\right) (1 - f) \tag{4.7}$$

where ϵ_b' is the real part of the dielectric constant of the background ice and f is the volume fraction of the air bubbles inside the ice. The f is usually estimated from the measured density ρ of the ice using the relation [Vant, 1978]

$$f = 1 - \rho/0.926 \tag{4.8}$$

The scattering coefficient K_s is determined by the size of the scatterers relative to the wavelength, number of scatterers per unit volume, and the dielectric constants of the background and scatterers. The air bubbles inside the ice medium can be assumed to be Rayleigh scatterers when the following relation holds [van de Hulst, 1957]

$$(2\pi/\lambda_o)\, r < 0.5 \tag{4.9}$$

where λ_o is the free space wavelength and r is the radius of the scatterer. This relation implies that in the microwave region (up to 18 GHz), the air bubbles can be approximated as Rayleigh scatterers if the diameter is less than 2.7 mm. For larger air bubbles, the simple Rayleigh approximation cannot be used and more complicated equations have to be used to calculate the backscattering cross-section. Although air bubbles larger than this have been observed occasionally, the Rayleigh approximation is used in this study without much loss of generality.

If all of the particles have the same effective radius r, and there are N particles per unit volume, then the volume scattering cross-section K_s is given by [van de Hulst, 1957]

$$K_s = N Q_s \tag{4.10}$$

where

$$N = f/(\tfrac{4}{3}\pi r^3) \tag{4.11}$$

$$Q_s = \frac{8}{3}\pi r^6 \varepsilon_b'^2 k_o^4 \left| \frac{n^2 - 1}{n^2 + 2} \right|^2 \tag{4.12}$$

= scattering cross-section of one scatterer

k_o = free space wave number

n = index of refraction.

In summary, the scattering albedo ω is determined and affected by (1) wavelength (frequency), (2) air bubble size, (3) dielectric constant of background ice (a function of ice salinity and temperature and of

measured frequency) (see Section 2.0), and (4) the density of ice, from which one can estimate the volume fraction of air bubbles. These factors are all variables. Using the range of values illusstrated in Figure 4.1, the scattering albedo is calculated for the frequency range between 1 and 18 GHz.

Figure 4.4(a) illustrates the effect of dielectric constant (effect of salinity and temperature) and density of the ice on scattering albedo in the frequency range between 1 and 18 GHz. Here, the diameter of air bubbles was assumed to be 2 mm. The real part of the dielectric constant of the background ice was taken to be 3.15, which is the value for the fresh water ice. The imaginary part was varied from 0.001 to 0.1. The measured value of ε'' of pure ice ($S = 0^{o}/oo$) ranges from about 0.001 to 0.01 in this frequency range, and it may be temperature- and frequency-dependent [Ulaby et al, 1982]. The behavior, however, is not very well established. When the background ice is saline (up to $0.7^{o}/oo$), the ε'' at 10 GHz can change from 0.01 to 0.1, depending on temperature, as treated in Section 2.0. The value may also be slightly frequency-dependent, but this effect was not included in the calculations. As one can see from the figure, the salinity and temperature of the ice medium can play a major role in determining the scattering albedo. At 10 GHz, the scattering albedo can change from 0.08 to 0.9 when the ε'' of background ice changes from 0.1 to 0.001 as either salinity or temperature changes.

The effect of change in the density of ice is not very severe, as can be seen in the figure. The effect of the size of air bubbles on scattering albedo can be seen in Figure 4.4(b). This also seems to be a significant factor because at 10 GHz, the scattering albedo can change

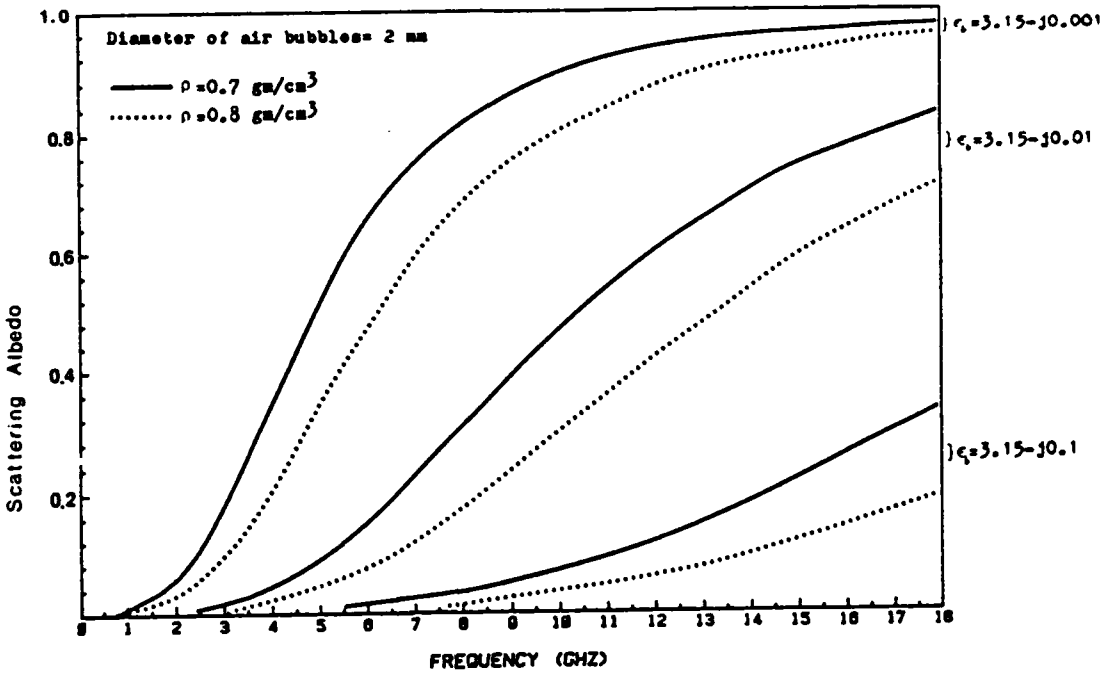

FIGURE 4.4(a) Scattering Albedo as a Function of Frequency for the Air Bubbles Inside the Ice Medium. The effect of change in the dielectric constant of background ice, and also the effect of different densities are shown.

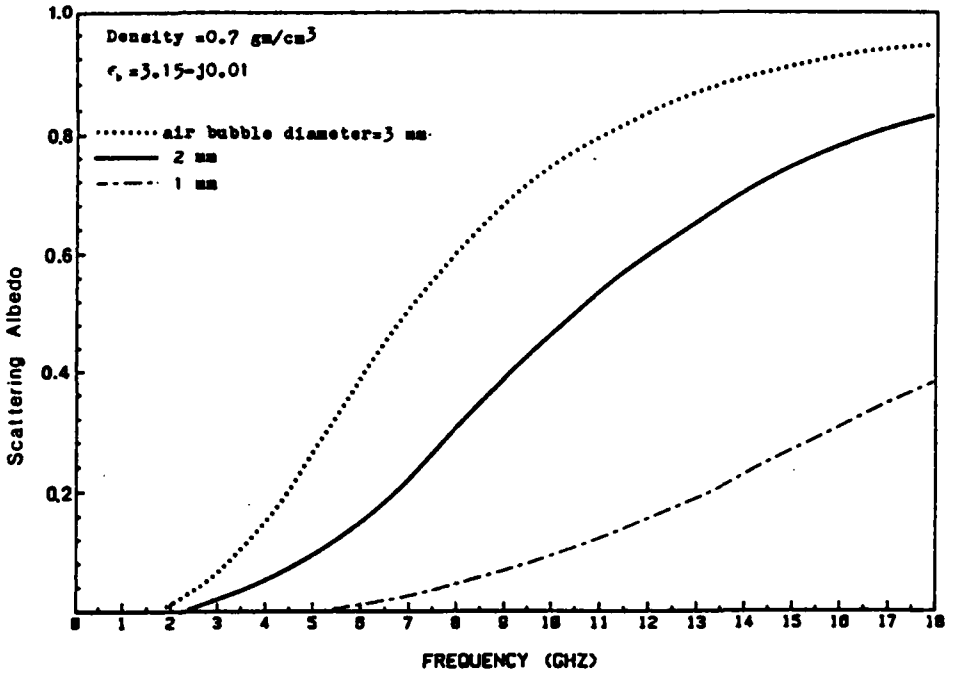

FIGURE 4.4(b): Effect of Air Bubble Size on Scattering Albedo

from 0.1 to about 0.76 when the diameter of the air bubbles changes from 1 mm to 3 mm. Equations (4.10) to (4.12) show that the scattering cross-section K_s changes as r^3.

4.2.2 Optical Depth

The optical depth of a layer changes with all the factors listed in the previous section, and also with the physical depth of the layer. Figure 4.5(a) shows the effect of ε'' on volume extinction coefficient and optical depth. At 10 GHz, the optical depth of a 20 cm layer with 2 mm air bubbles can change from 0.1 to 1.9 when the dielectric constant of background ice changes from 3.15-j 0.001 to 3.15-j 0.1. Figure 4.5(b) shows the effect of the size of the air bubbles when ε_v = 3.15-j 0.01. Here, a large change in optical depth due to the change in the size of air bubbles is noted for the frequencies higher than X-band.

Also, in the solution of the radiative transfer equation, the boundary conditions call for the average dielectric constant of the volume scattering layer. This will be the value including all the air bubbles. Several measured values of the dielectric constant of the multiyear ice can be found in Section 2.2.

4.2.3 Volume Scattering Coefficient of Multiyear Ice

Using the layer characteristics discussed in the previous sections, the backscattering coefficient σ^0 is calculated for the volume scattering layer (air bubbles embedded in the multiyear ice, see Figure 4.1). The method follows that of Eom [1982] for this Rayleigh layer. Figures 4.6 to 4.8 show the theoretical backscattering cross-section for the volume scattering layer at 13 GHz with HH polarization. The volume

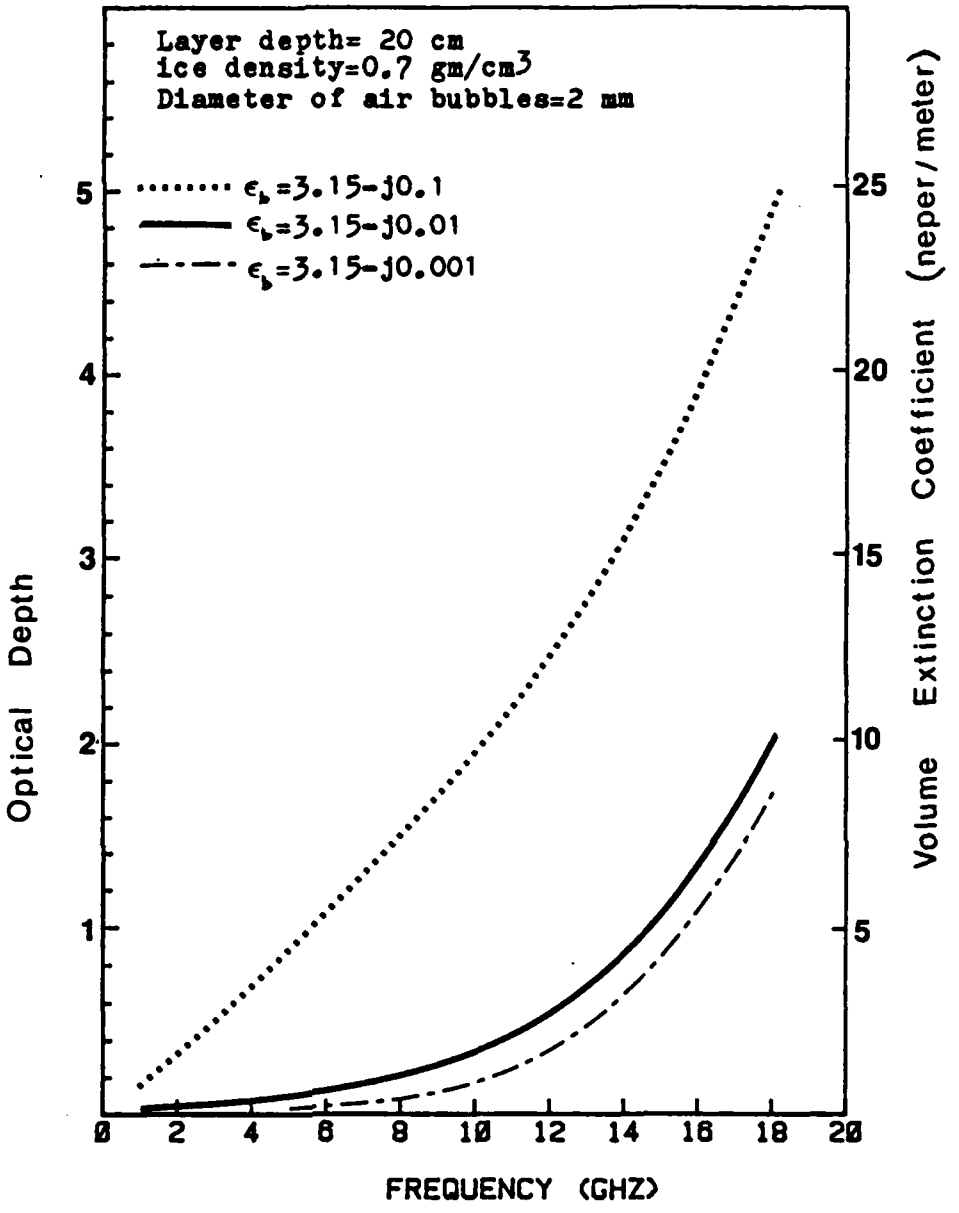

FIGURE 4.5(a): Effect of Dielectric Constant of Background Ice to Optical Depth and the Volume Extinction Coefficient

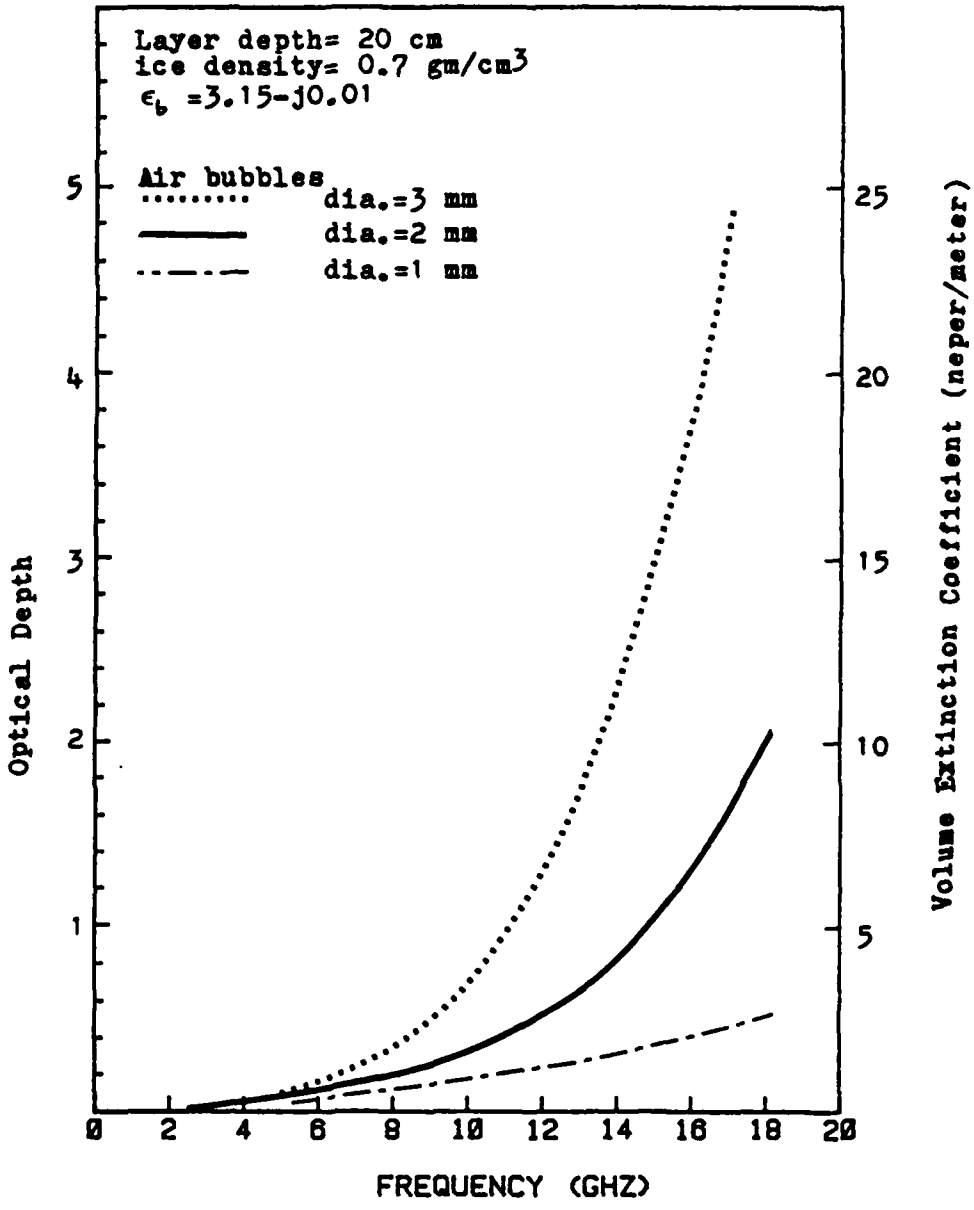

FIGURE 4.5(b): Effect of Air Bubble Size on Optical Depth and Volume Extinction Coefficient

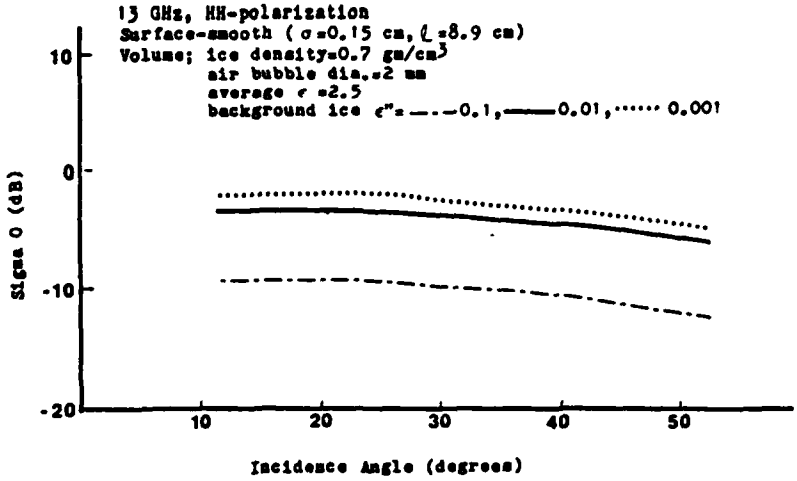

FIGURE 4.6(a): Theoretical Angular Behavior of σ^0 for the Volume Scattering Layer. The 3 curves are for the layers with 3 different albedo and optical depth, which result from the difference in the imaginary part of dielectric constant of ice.

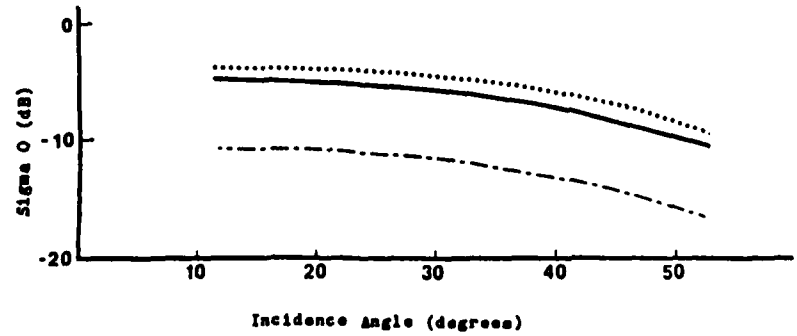

FIGURE 4.6(b): Same as 4.6(a), but with rough surface (σ=0.81 cm, ℓ=8.2 cm).

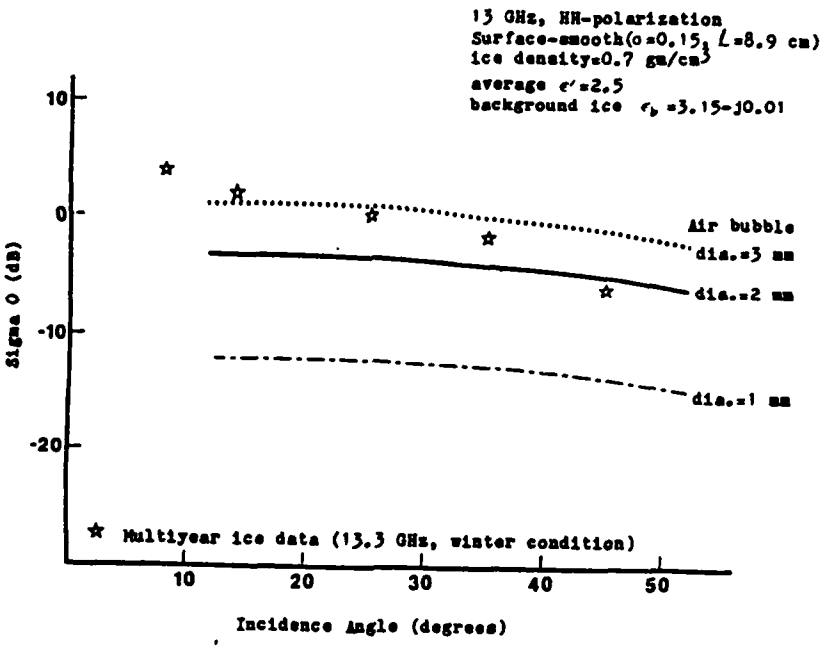

FIGURE 4.7: Theoretical Angular Behavior of σ^0 for the Volume Scattering Layer of Depth = 20 cm. Three curves for the different size air bubbles are shown. Different size air bubbles have different scattering cross-sections, therefore they have different scattering albedo and optical depth. Also shown is the multiyear ice data during winter condition (Gray et al., 1982).

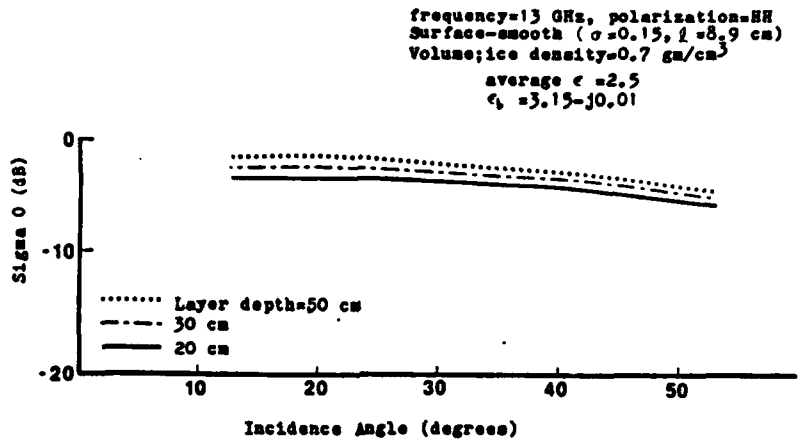

FIGURE 4.8(a): Effect of the Physical Depth of the Volume Scattering Layer. Changing depth of layer increases the optical depth while maintaining the scattering albedo.

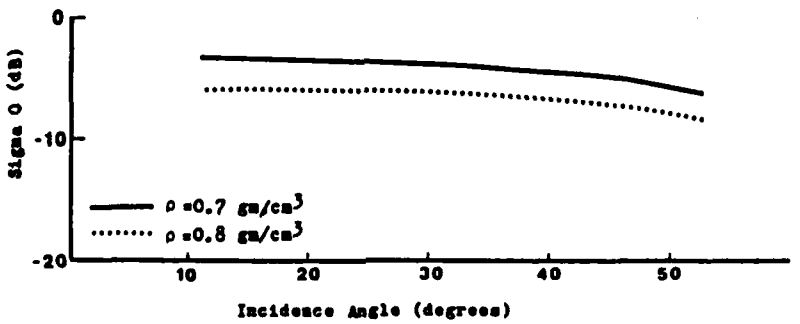

FIGURE 4.8(b): Effect of Density of the Volume Scattering Layer. Increase in density means less volume fraction of the scatterers and smaller volume scattering cross-section, reducing scattering albedo and optical depth.

scattering term interacts with the roughness of the surface to produce the shown. In Figures 4.6(a) and (b), the effects of the imaginary part of the background ice are shown for a smooth surface and a rough surface, respectively. The different values of the dielectric constant are due to the difference in the salinity and temperature of the ice layer, and these modify the scattering albedo and the optical depth as discussed in Sections 4.2.1 and 4.2.2. When the ε'' of the background ice reduces from 0.1 to 0.01, the scattering albedo increases from 0.16 to 0.66 at 13 GHz for the layer with 2 mm air bubbles, and the resultant σ^0 increases about 6 dB for all the incidence angles (see Figure 4.6(a)). A rougher surface reduces the volume scattering contribution to the backscatter direction (less than 2 dB for the surface parameters used in Figures 4.6(a) and (b)).

Figure 4.7 shows the effect of the air bubble size. The layer with larger air bubbles has a larger scattering albedo and optical depth, and the σ^0 increases as much as 9 dB when the average diameter increases from 1 mm to 2 mm. The σ^0 increases further (4 dB) when the diameter of the air bubble increases from 2 to 3 mm. Also shown in the figure are values measured for multiyear ice during winter conditions [Gray, 1982]. Measurements compare reasonably well with theory.

Figure 4.8(a) shows the effect of the physical depth of the layer using the same scattering albedo. When the depth of the layer was changed from 20 cm to 50 cm, the σ^0 increased about 1.5 dB. Figure 4.8(b) shows the effect of the density of the ice layer. Increase in density means less volume fraction of the scatterers and therefore smaller volume-scattering cross-section. When the density was increased from 0.7 gm/cm^3, the σ^0 decreased about 2 to 3 dB.

The effect on σ^0 of the average medium dielectric constant seems to be insignificant in the ranges of values reported ($\varepsilon' = 2.5 - 2.7$). Also the effect of the real part of the dielectric constant of the outside layer (nonscattering layer, $\varepsilon'' = 3.15$ to 4.0) seems to be negligible (less than 0.1 dB).

In summary, the imaginary part of the dielectric constant of the background ice and the size of the air bubbles seem to be the major factors determining the layer scattering characteristic, and the result has been shown accordingly.

In actual measurements the purely surface-scattered term not considered in this section will also be present and will be the dominant factor at small incidence angles. The change of dominance between the surface- and volume-scattering terms occurs at different incidence angles depending on the surface roughness and the frequency.

Figure 4.9 shows the theoretical backscattering coefficients of the multiyear ice at 8 GHz and 13 GHz. Here surface scattering terms and volume scattering terms are shown separately to illustrate the relative contributions. For multiyear ice with a smooth surface, the volume scattering dominates when the incidence angle is greater than about 10° at 8 GHz and about 5° at 13 GHz. For a rough surface, the surface scattering term is higher than the volume term until about 30° incidence angle and remains comparable at larger incidence angles at 8 GHz. At 13 GHz, the volume scattering term is always higher.

Figure 4.10 shows the sum of surface- and volume-scattering terms for multiyear ice with two kinds of surface roughness; also shown are several reported measurements of multiyear ice. The radiative transfer

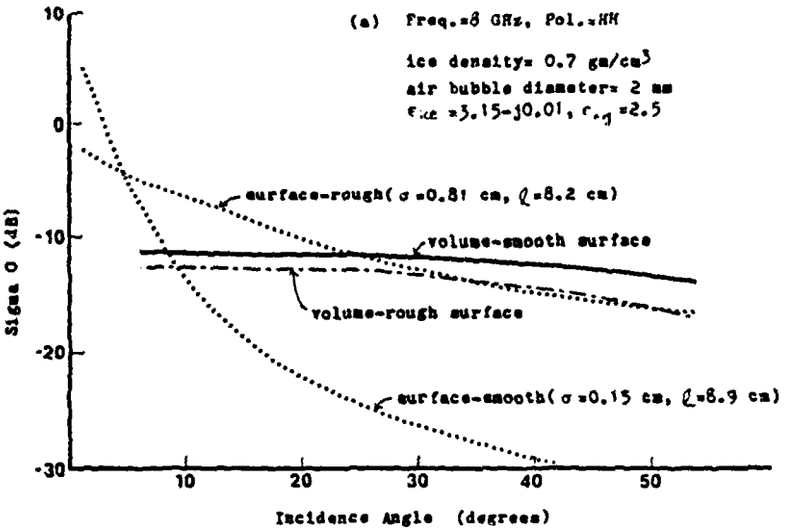

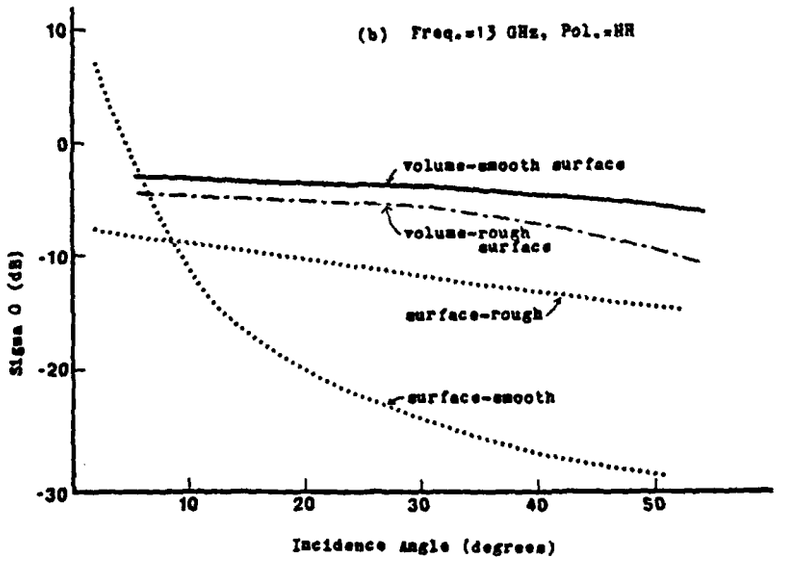

FIGURE 4.9: Theoretical Backscattering Coefficient of Multiyear Ice. Volume scattering terms and surface scattering terms are shown separately.

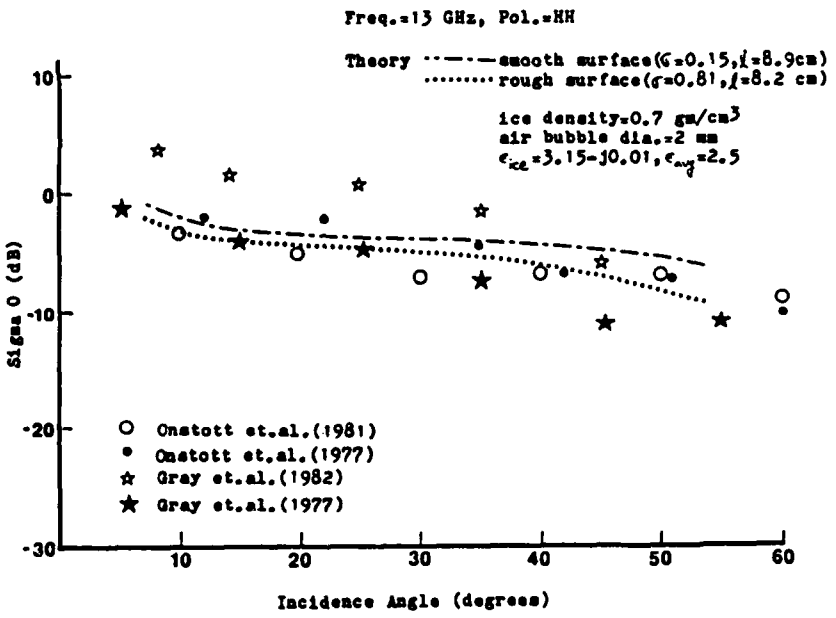

FIGURE 4.10: Comparison of Theoretical Model Behavior with Measurements of Multiyear Ice.

model with a reasonable choice of parameters seems to explain the measurement results.

4.2.4 Theoretical Frequency Response of σ^0 of the Snow-Free Multiyear Ice

When the incident wavelength changes, the corresponding scattering albedo and optical depth of the layer change, as can be seen in Figures 4.4 and 4.5. In the following calculations, a minor frequency dependency of the dielectric constant of sea ice (discussed in Section 2.0) is neglected in the frequency range between 4 and 18 GHz.

Figure 4.11 shows the theoretical volume scattering terms of the backscattering cross-section of the snow-free multiyear ice for the frequencies between 4 and 18 GHz. As can be expected from the frequency behavior of the albedo and the optical depth, the volume scattering term exhibits quite a rapid increase with frequency. Also to be seen in the figure are the effects of ice density and the air bubble size.

In Figure 4.12, purely surface-scattering terms discussed in Section 3.3 are plotted together with the volume-scattering terms. For multiyear ice with a smooth surface, the volume-scattering term dominates over the surface-scattering term for all the frequencies between 4 and 18 GHz. However, when the surface becomes rougher, the surface-scattering term increases drastically while the volume scattering term decreases slightly. Therefore, at low microwave frequencies, the surface-scattering term dominates over the volume-scattering term. For the physical parameters of the multiyear ice shown in the figure, the crossover occurs around 8 GHz (for incidence angle = 31°). The total backscattering cross-section, σ^0, is the sum of the surface- and volume-scattering terms. In Figure 4.13, the total backscattering cross-sections for smooth multiyear ice and rough

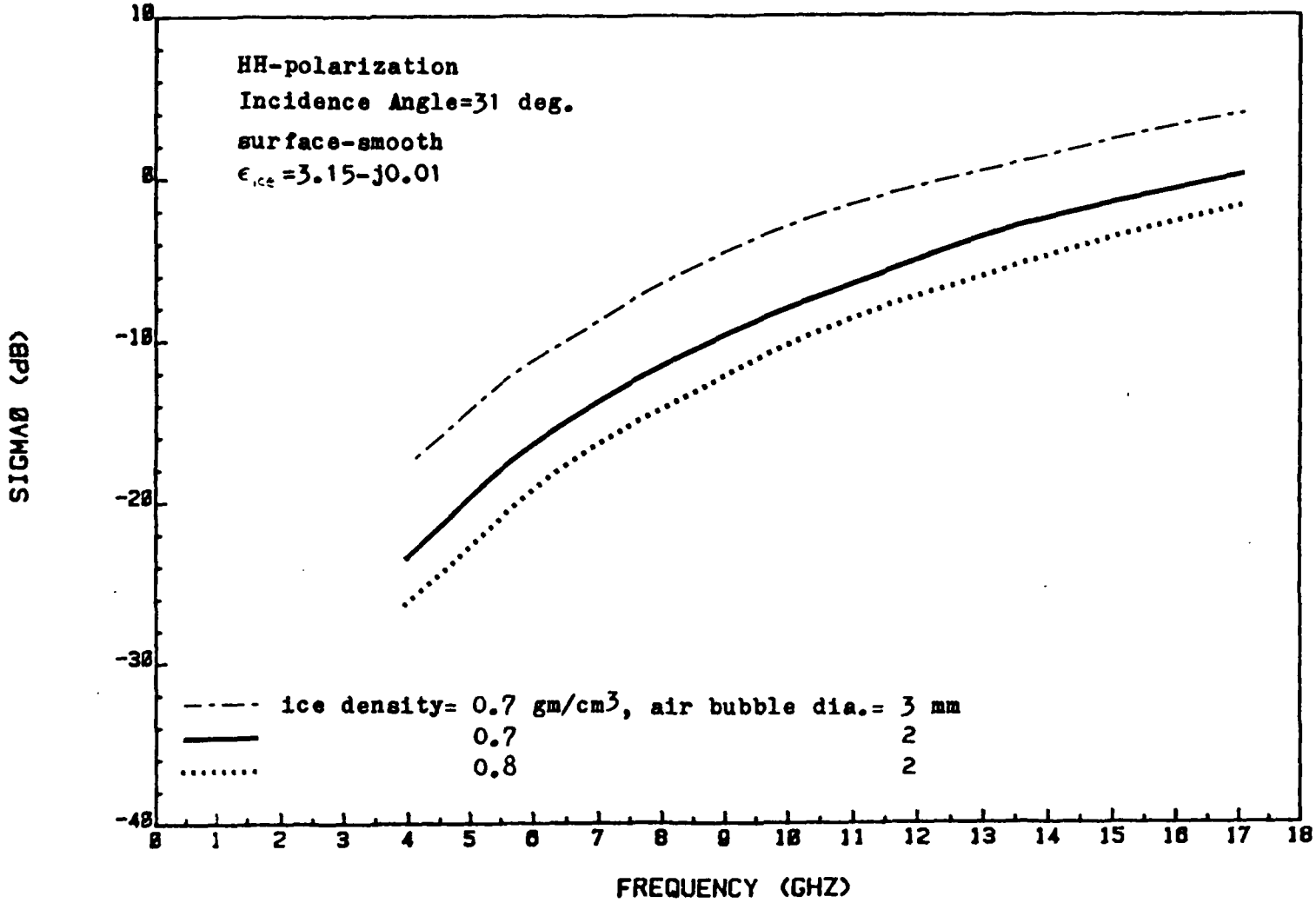

FIGURE 4.11: Theoretical Frequency Behavior of σ^0 (Volume Scattering Term).

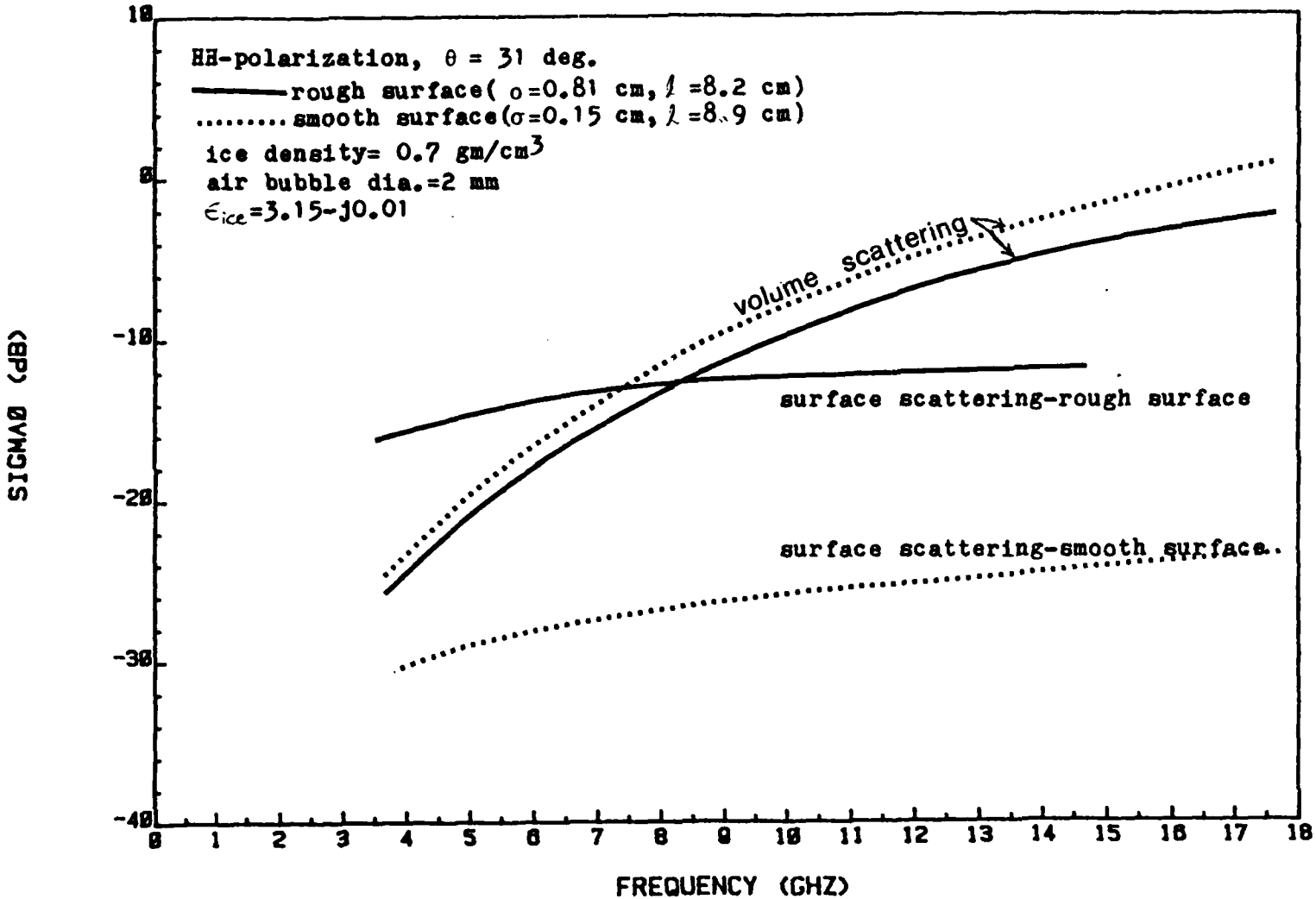

FIGURE 4.12: Theoretical Frequency Behavior of σ^0 . Surface scattering term and volume scattering terms are plotted separately, for two kinds of surface roughness.

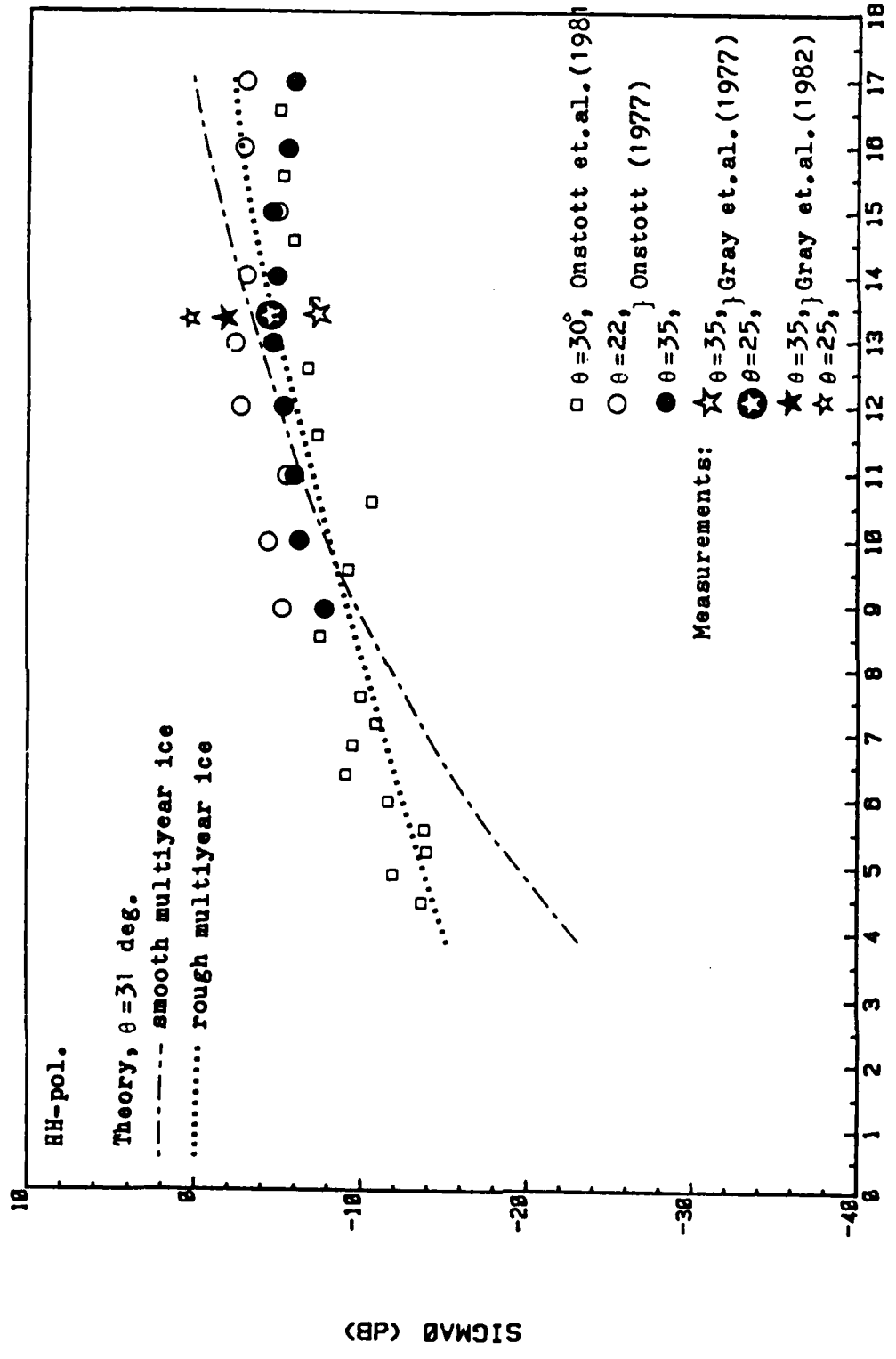

FIGURE 4.13: Theoretical Frequency Response of the Backscattering Coefficient of Multiyear Ice with Smooth Surface and Rough Surface. The model parameters are the same as shown in Figure 4.12. Also shown are several reported measurements.

multiyear ice are plotted. Also shown in the figure are several reported measurements. In general, the radiative transfer model (with proper choice of parameters) predicts the frequency behavior of σ^o satisfactorily, although the model neglected snow layer effect and the targets included up to 10 cm of snow. The effect of snow cover is treated later.

4.2.5 Polarization Considerations

Due to the Brewster angle effect, the power transmitted into the ice medium is larger for the vertically polarized waves than the horizontally polarized waves. Therefore, when the volume scatterers are spherical or do not have any particular anisotropy, one can expect that σ^o_{VV} is generally higher than σ^o_{HH}.

For vegetation with the leaves inclined more horizontally, higher σ^o_{HH} than σ^o_{VV} has been noted [Tsang et al., 1981]. The air bubbles in in sea ice are generally reported to be spherical. Shin and Kong [1981] noted that σ^o_{VV} is higher than σ^o_{HH} for a half-space medium with spherical scatterers; they also noted that (when the volume scattering layer is finite) the effect of bottom interface might cause higher σ^o_{HH} than σ^o_{VV}. This is likely when the dielectric constant of the bottom layer is much larger than that of the upper layer. This effect would have to be considered for a thin snow layer on the ground, but for multiyear ice the bottom interface is arbitrary (see Figure 4.1) and the ice-water boundary is so far below that the microwaves do not reach it.

Figure 4.14 shows several reported measurements of multiyear ice. Onstott's results [1980] always had higher σ^o_{VV} than σ^o_{HH}, while Gray et al., [1977] reported higher σ^o_{HH}, but the difference between these two

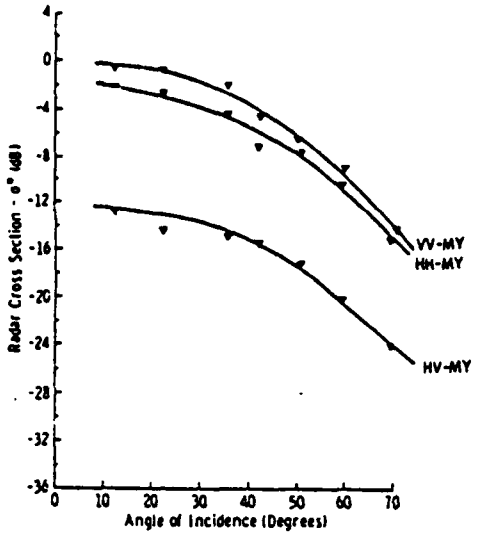

(a) from Onstott et.al.(1979)

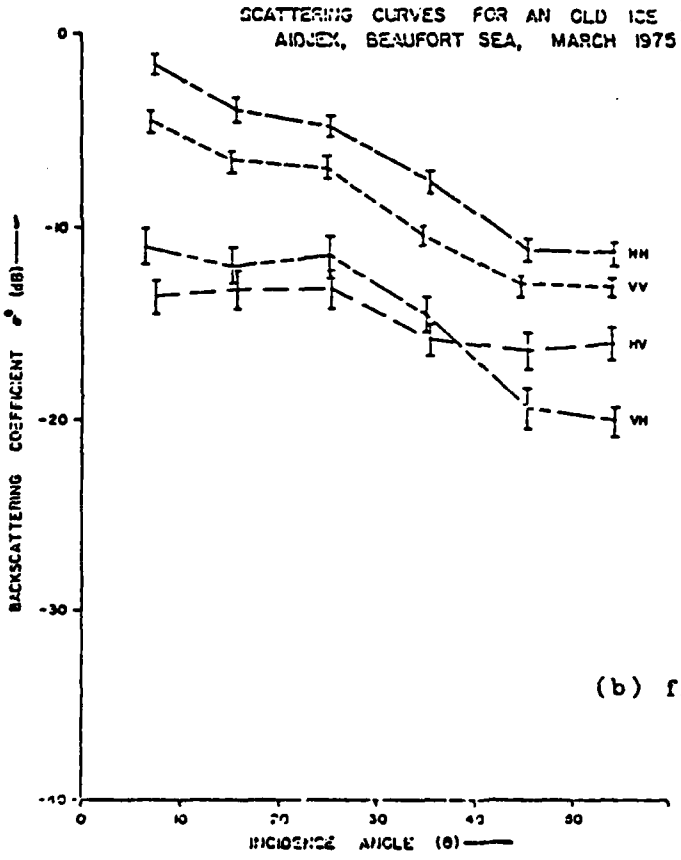

(b) from Gray et.al.(1977)

FIGURE 4.14: Polarization Dependence of σ^0 of Multiyear Ice. Frequency = 13 GHz

like-polarizations is relatively small. Figure 4.15 shows the theoretical volume scattering coefficient as a function of frequency for multiyear ice with HH- and HV-polarizations. VV results are nearly identical to those of HH. Several reported measurements are also plotted together and good agreement with the theoretical model can be seen. The depolarization ratio ($\sigma^o_{HH}/\sigma^o_{HV}$) decreases with frequency. Figure 4.16 shows the theoretical and experimental angular behavior of σ^o_{HH} and σ^o_{HV} at 13 GHz. Again, a good agreement can be seen.

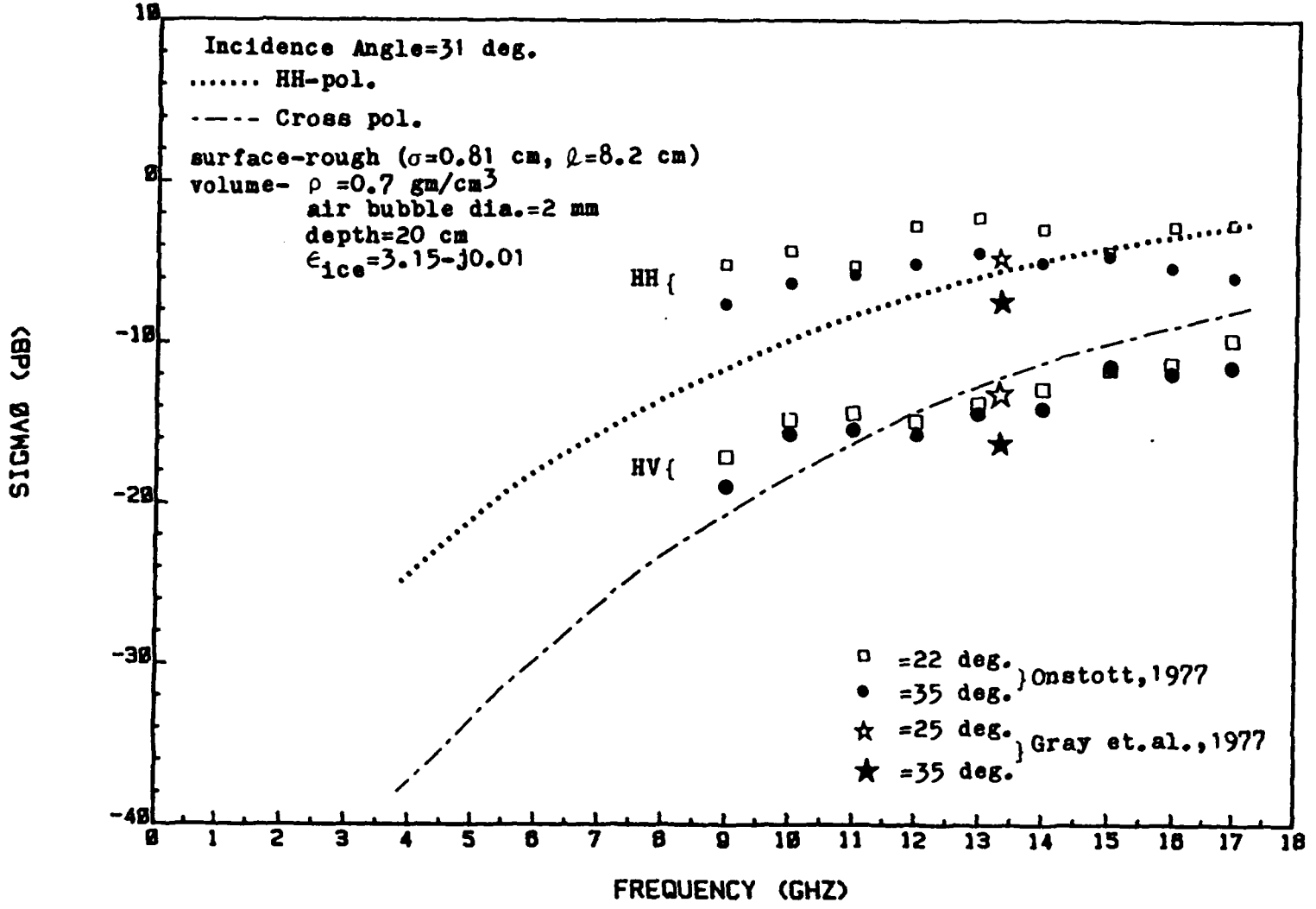

FIGURE 4.15: Theoretical Volume Scattering Backscattering Coefficient of Multiyear Ice with Rough Surface. Like- and cross-polarized cases are calculated and compared with measurements, although the pure surface-scattering term is not included in calculations.

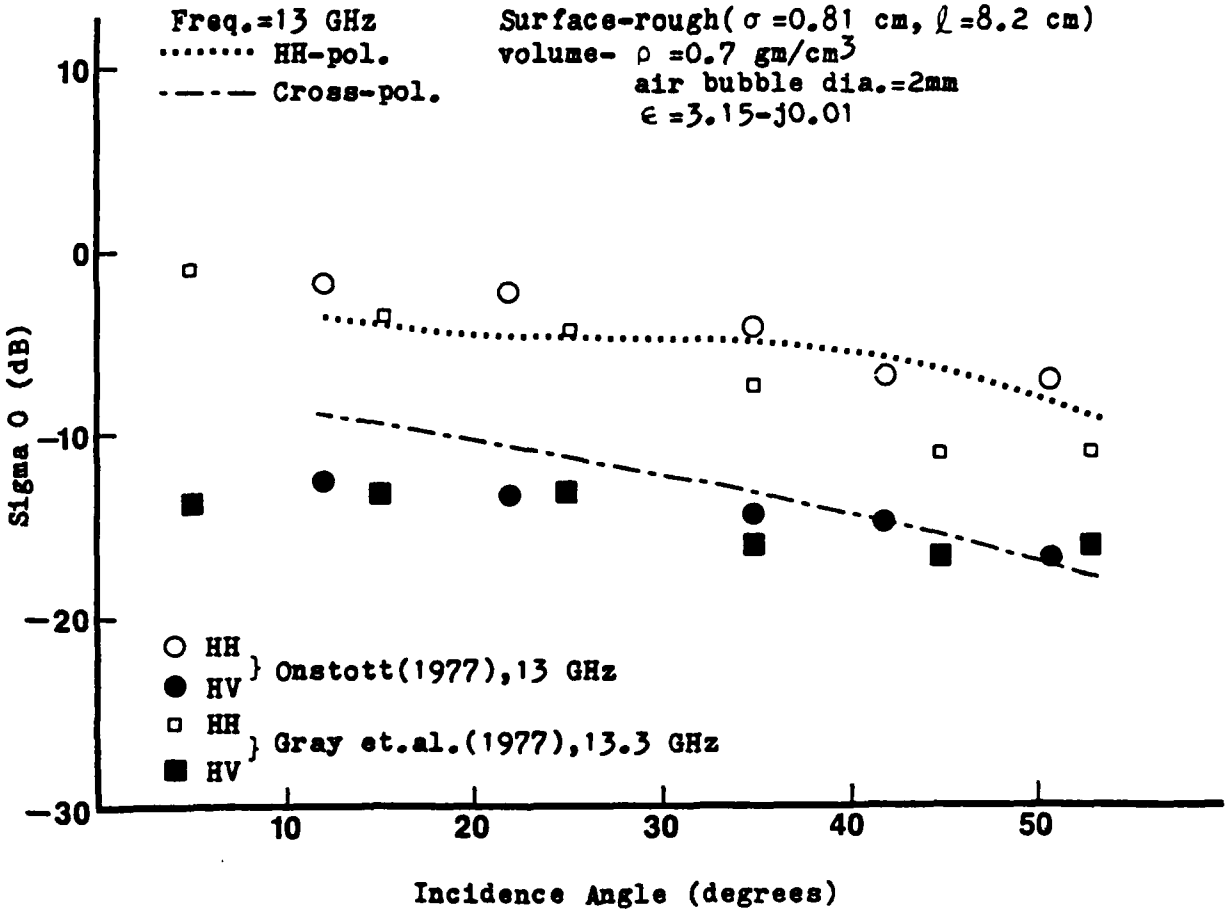

FIGURE 4.16: Theoretical Backscattering Coefficient of Multiyear Ice with Rough Surface. Like- and cross-polarizaed cases are calculated and compared with measurements.

5.0 SEMI-EMPIRICAL FORMULATIONS

5.1 Zeroth-Order Scattering Coefficient σ^o for Snow-Free Multiyear Ice

In view of the simple, single-layer model for multiyear ice shown in Figure 4.1, the scattering coefficient has been modeled with the following semi-empirical equation.

$$\sigma^o(\theta) = \sigma^o_s(\theta) + T^2(\theta)\left[\sigma^o_v(\theta') + \frac{\sigma^o_g(\theta')}{L^2(\theta')}\right] \qquad (5.1)$$

where:

$\sigma^o_s(\theta)$ = the backscattering coefficient of the ice surface.

$T(\theta)$ = the power transmission coefficient of the upper surface.

$\sigma^o_v(\theta')$ = the volume backscattering coefficient of the ice layer.

$\sigma^o_g(\theta')$ = the backscattering coefficient of the lower interface.

$L(\theta')$ = $\exp(k_e d \sec\theta')$, which represents one-way loss factor through the layer with extinction coefficient k_e and thickness d (see Section 4.2.1).

θ' = the angle of refraction in the ice medium.

This type of model has been used for snow [Stiles and Ulaby, 1980, 1981] and for a vegetation canopy [Attema and Ulaby, 1978]. Also, Karam and Fung [1982] reduced the general theoretical solution of the radiative transfer equation to the form of equation (5.1) under several simplifying conditions. The factors neglected in this formulation are the terms representing the volume-surface interaction which may be significant for cross-polarized scattering [Karam and Fung, 1982]. These are the terms scattered by the volume inhomogeneities and reflected by the lower interface. For the multiyear-ice problem, the backscattering coefficient of the lower interface, $\sigma^o_g(\theta')$ would be very

small because the interface is artificial and the dielectric discontinuity is very small. The average dielectric constant of the air bubble layer is about 2.5 to 2.7 while that of the next layer is about 3.1. With these figures, the power reflection coefficient is less than 0.0033 at normal incidence. Neglecting σ^0_g, equation (5.1) can be further simplified.

$$\sigma^0(\theta) = \sigma^0_s(\theta) + T^2(\theta)\sigma^0_v(\theta') \tag{5.2}$$

Here, the volume backscattering coefficient of the ice layer $\sigma^0_v(\theta')$ can be derived as follows, based on the model of Figure 5.1. Let the incident power density just below the upper surface of the volume scattering layer be S_i. Then the power density at the infinitesimal layer of distance z' from the top is $S_i e^{-Kez'}$, and the scattered power density dS_r due to the scatterers in the infinitesimal layer at a distance $R(>>z')$ from the ice layer is, approximately,

$$dS_r = \frac{S_i e^{-2Kez'}(n\sigma_b)}{4\pi R^2} \tag{5.3}$$

where:

A = Illuminated area.

N = Number of scatterers per unit volume (see (4.11)).

$Adz'\cos\theta'$ = Infinitesimal volume.

σ_b = Backscattering cross-section of individual scatterer.

n = number of identical scatterers in the infinitesimal layer.

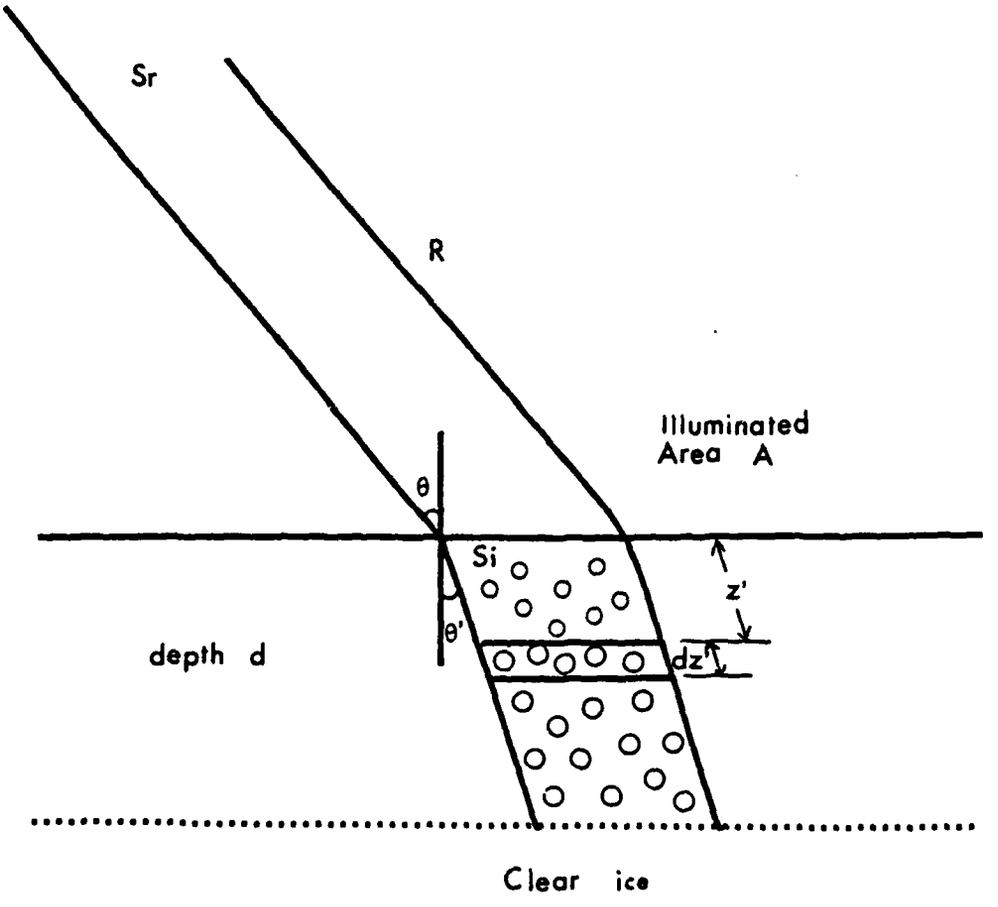

FIGURE 5.1: Multiyear Ice Model

$$= NAdz'\cos\theta' \tag{5.4}$$

For Rayleigh scatterers,

$$\sigma_b = 4\pi r_s^6 \, e_b'^2 \, ko^4 \left| \frac{n_1^2 - 1}{n_1^2 + 2} \right|^2 \tag{5.5}$$

where n_1 = index of refraction. Therefore, the total scattered power density, S_r, is

$$\begin{aligned} S_r = \int dS_r &= \int_o^{dsec\theta'} \frac{S_i NAdz'\cos\theta'\sigma_b e^{-2kez'}}{4\pi R^2} \\ &= \frac{S_i NA\cos\theta'\sigma_b}{4\pi R^2(2ke)}\left(1 - e^{-2kedsec\theta'}\right) \end{aligned} \tag{5.6}$$

From the definition of $\sigma^o{}_v(\theta')$,

$$\sigma_v^o(\theta') = \frac{4\pi R^2 S_r}{AS_i} = \frac{N\sigma_b\cos\theta'}{2ke}\left(1 - \frac{1}{L^2(\theta')}\right) \tag{5.7}$$

In the above derivation, all the scatterers are assumed to be the same size, and the multiple scattering is neglected. The transmission loss through the upper surface (interface) is included in the $T^2(\theta)$-term in

equation (5.2) and $T^2(\theta)\cdot\sigma^o_v(\theta')$ will be the effective volume scattering term in the final $\sigma^o(\theta)$ seen by the radar.

The volume scattering term, $\sigma^o_v(\theta) = T^2(\theta)\cdot\sigma^o_v(\theta')$ is calculated using equations (5.4) through (5.7) and the same physical parameters as used in the radiative transfer model given in the previous section. Figure 5.2 shows the comparison of the empirical model behavior with that of the radiative transfer model. The radiative transfer models include the effect of surface roughness, while the empirical model does not.

As can be seen in the figure, the empirical model prediction matches very well with that of the radiative transfer models for all the frequencies considered. This similar prediction might have resulted from the fact that the physical parameters (the diameter of scatterers and the physical depth of the scattering layer) used in the theoretical computation resulted in a small optical depth and small scattering albedo at the frequencies below about 10 GHz, so that the scattering process might actually approach single scattering which was assumed for the empirical model. As the frequency is increased from about 10 GHz, and therefore the scattering albedo and the optical depth is increased above certain values, the discrepancy between single scattering and multiple scattering (theoretical model) increases as can be seen in Figure 4.13 (see the theoretical curve for smooth surface and the curve for empirical model).

Figures 5.3 and 5.4 show the angular behavior of the empirical model at 13 GHz, HH-polarization. Again, similar results are found for the theoretical model and the empirical model when the scattering albedo is small. When the average air bubble diameter is 3 mm (albedo = 0.67,

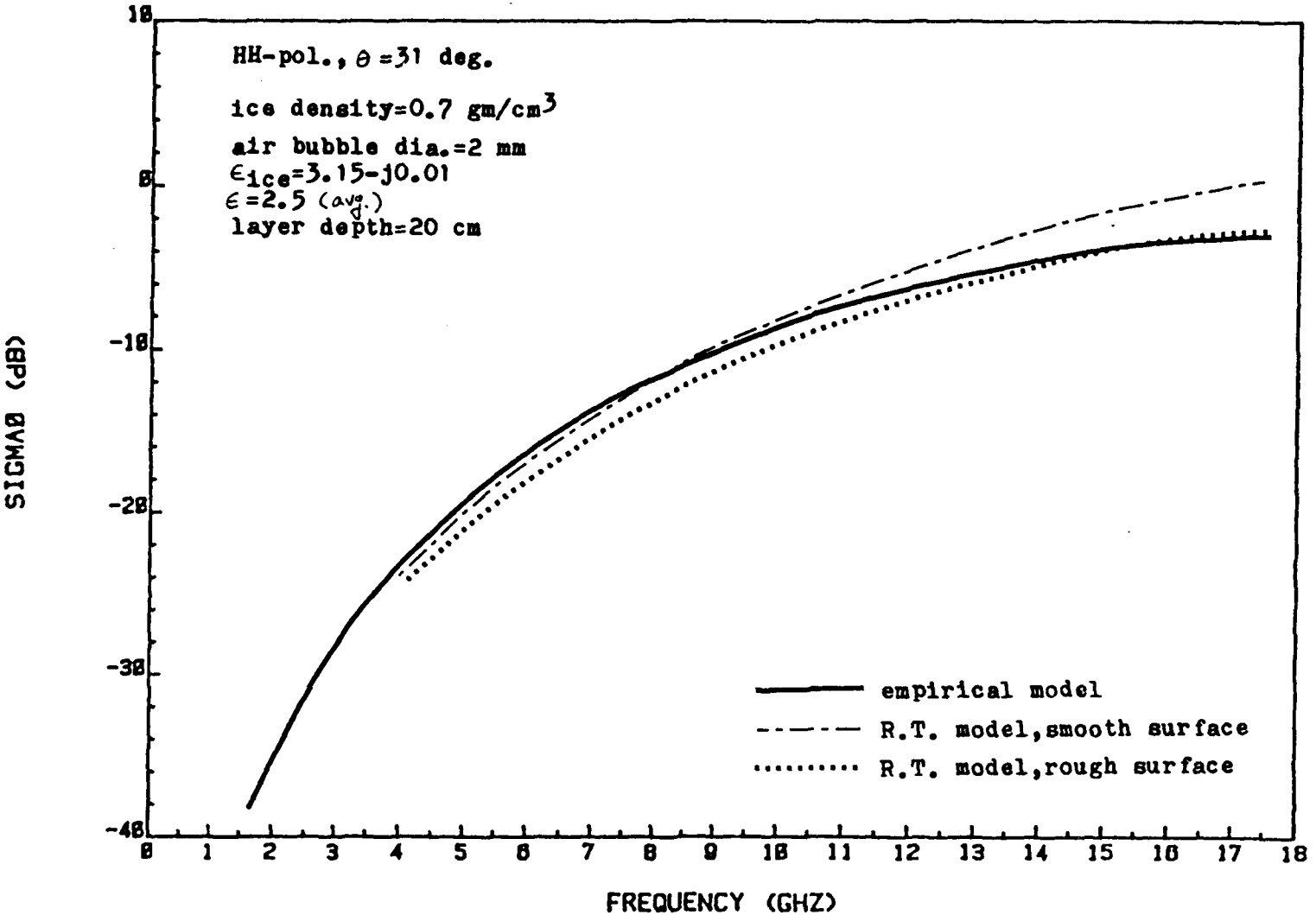

FIGURE 5.2: Comparison of Empirical Model Behavior with That of Radiative Transfer Model. Empirical model does not include the effect of surface roughness while the radiative transfer model does.

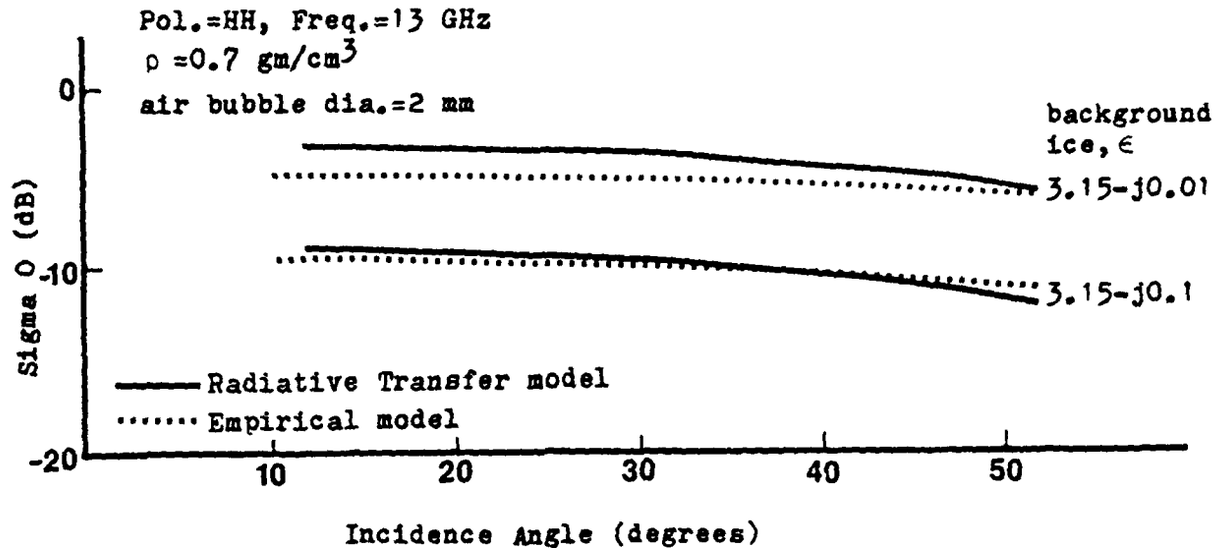

FIGURE 5.3: Comparison of Empirical Model Behavior with that of Radiative Transfer Model. Shown are the effects of the imaginary part of the dielectric constant of ice. Smooth surface is assumed (σ=0.15 cm, ℓ=8.9 cm)

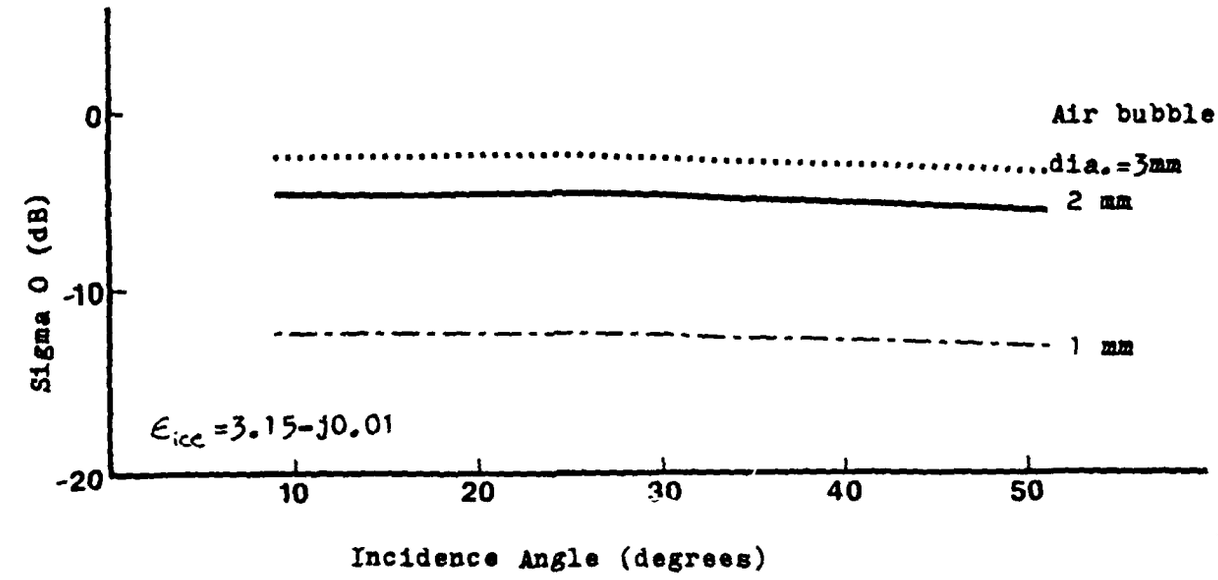

FIGURE 5.4: Effect of the Size of Air Bubbles Predicted by the Empirical Model. See also Fig. 4.7 for the radiative transfer model prediction. Freq. = 13 GHz, Pol. = HH.

optical depth = 1.8), the difference between theoretical and empirical model is about 3.5 dB (compare Figure 4.7 with Figure 5.4), but when the air bubble size is 2 mm (albedo = 0.67, optical depth = 0.69), the difference at 13 GHZ is on the order of 1 dB for smooth ice. When the surface becomes rougher, the difference reduces even further. Therefore, for all the practical values of physical parameters, the empirical model seems to be able to predict the volume scattering from multiyear ice.

In the above development, a uniform distribution of identical scatterers with constant density was assumed for the scattering layer. However, the thin section pictures of the ice cores show that the scatterers are actually distributed in size rather than being identical at a given depth. Moreover, the density profiles show variations with depth.

5.1.1 Scatterer Size Distribution

The effect of the distribution of the scatterer sizes can be treated as is done for the scattering due to rain or cloud. For these problems, numerous experiments have been done to find the drop size distribution; for the air-bubbles in the sea ice, only a limited data set is available [Poe et al., 1974; Onstott, 1980]. Therefore, only some simple cases will be considered. Equation (5.5) shows that the scattering cross-section of individual elements increases as $(\text{radius})^6$. However, to maintain the same density of ice, the number of scatterers has to decrease as $(\text{radius})^3$, as can be seen in Equation (4.11). Therefore, the term $N\sigma_b$ in equation (5.7) increases as

(radius)^3. However, as the scattering cross-section increases, the extinction coefficient increases as well. The relative amount of increase in K_e depends on the scattering albedo. Also as K_e increases, the loss L increases, thereby increasing the term $(1 - 1/L^2)$ in equation (5.7). When there are scatterers with various sizes, the problem gets more complicated; Table 5.1 summarizes the results for several cases of drop size distribution. The parameters used in preparing Table 5.1 are:

$\varepsilon_{ice} = 3.15\text{-}j0.01$

$\rho_{ice} = 0.7$ gn/cm^3

depth = 20 cm

f = 13 GHz

When the exact air-bubble size distribution is available, the same concept can be applied to calculate the empirical volume scattering coefficient, σ^0_v of the multiyear ice. If 10% of the air bubbles are larger (3 mm diameter) than the 2 mm air bubbles, the σ^0_v can be up to 1.3 dB higher.

TABLE 5.1
EFFECT OF SCATTERER SIZE DISTRIBUTION

	Case 1 100% 2mm-diameter air bubbles	Case 2 10% 1 mm 80% 2 mm 10% 3 mm	Case 3 33% 1 mm 33% 2 mm 33% 3 mm	Case 4 100% 3mm-diameter air bubbles
Total number of scatterers	N	0.87 N	0.67 N	0.30 N
$N\sigma_b$ term in eq.(4.19)	$N\sigma_b$	1.69 $N\sigma_b$	2.76 $N\sigma_b$	3.38 $N\sigma_b$
K_e	K_e	1.46 K_e	2.17 K_e	2.58 K_e
$1 - 1/L^2$	$1 - 1/L^2$	$1.16(1-1/L^2)$	$1.26(1-1/L^2)$	$1.29(1-1/L^2)$
$\sigma^\circ_v(\theta')$	$\sigma^\circ_v(\theta')$	σ°_v+1.3 dB	σ°_v+2.1 dB	σ°_v+2.3 dB

5.1.2 Density Variations

The density of multiyear ice usually increases with depth. This can either be modeled as: (1) the number of air bubbles decreases with depth, or (2) the size of the air bubbles decreases with depth. In this section, only case (1) is considered.

When the density profile is given as a function of depth, $\rho = \rho(z)$, the corresponding number of scatterers per unit volume can be estimated as a function of depth as follows.

$$N(z) = \left(1 - \frac{\rho(z)}{0.926}\right) / \frac{4}{3}\pi r^3 \tag{5.8}$$

where r is the scatterer radius.

The extinction coefficient, K_e, is also a function of depth because of changes in the density of scatterers which causes K_s and K_a to change. Therefore, the volume scattering coefficient, σ^o_v, given in equation (5.7) becomes

$$\begin{aligned}\sigma^o_v(\theta') &= \int_o^{d\sec\theta'} N(z)\cos\theta'\sigma_b e^{-K_e(z)z'}\, dz \\ &= \sigma_b \cos\theta' \int_o^{d\sec\theta'} N(z) e^{-K_e(z)z'}\, dz\end{aligned} \tag{5.9}$$

This equation could be evaluated numerically if $\rho(z)$ were given. Alternatively, the following simple approximation seems to be better when one considers the difficulties associated with the measurements of the density of the sea ice.

Let us assume that the measured density profiles show a linear increase with depth from 0.7 to 0.8 gm/cm^3. The average density is 0.75 gm/cm^3 and this layer can be divided into two layers of equal depth with densities of 0.7 and 0.8 gm/cm^3, respectively, maintaining the same average density. Let $\sigma^o{}_1$ be the volume scattering coefficient of the first layer and $\sigma^o{}_2$ be that of the second layer. Then the total volume scattering coefficient $\sigma^o{}_v$ is

$$\sigma_v^o = \sigma_1^o + \sigma_2^o/L^2 = \frac{N_1\sigma_b \cos\theta'}{2K_{e1}}\left(1 - \frac{1}{L_1^2}\right) + \frac{N_2\sigma_b\cos\theta'}{2K_{e2}}\left(1 - \frac{1}{L_2^2}\right)\left(\frac{1}{L_1^2}\right) \tag{5.10}$$

where L_1 is the loss through the first layer. This concept can be extended further to divide the layer into smaller sublayers, and

$$\begin{aligned}\sigma_v^o &= \sigma_1^o + \sigma_2^o/L_1^2 + \sigma_3^o/L_1^2L_2^2 + \sigma_4^o/L_1^2L_2^2L_3^2 + \ldots \\ &= \frac{\sigma_b\cos\theta'}{2}\left[\frac{N_1(1-1/L_1^2)}{K_{e1}} + \frac{N_2(1-1/L_2^2)}{K_{e2}L_1^2}\right. \\ &\left. + \frac{N_3(1-1/L_3^2)}{K_{e3}L_1^2L_2^2} + \frac{N_4(1-1/L_4^2)}{K_{e4}L_1^2L_2^2L_3^2} + \ldots\right]\end{aligned} \tag{5.11}$$

Table 5.2 summarizes the results for several approximations that all have the same average densities and same size scatterers. As can be

TABLE 5.2
EFFECT OF DENSITY VARIATIONS

	One Layer 20 cm	Two Layers 10 cm each	Three Layers 6.7 cm each	Four Layers 5 cm each
	ρ=0.75 gm/cm^3 scatterer dia.=2 mm	ρ_1=0.7 ρ_2=0.8	ρ_1=0.7 ρ_2=0.75 ρ_3=0.8	ρ_1=0.7 ρ_2=0.733 ρ_3=0.766 ρ_4=0.8
Number of scatterers per unit vol.	N	N_1=1.28 N N_2=0.72 N	N_1=1.28 N N_2=N N_3=0.72 N	N_1=1.28 N N_2=1.1 N N_3=0.9 N N_4=0.72 N
$\sigma^\circ_v(\theta')$	$\sigma^\circ_v(\theta')$	σ°_v+0.19(dB)	σ°_v+0.17(dB)	σ°_v+0.16(dB)

seen from the table, the approximation of assuming the same average density for the whole layer gives satisfactory results when compared to the results of decomposing the layer into multiple layers with varying densities.

5.1.3 Comments

The concept of adding the contributions of several layers to get the effective volume scattering coefficient can be used to see the effect of small air bubbles which are found throughout the multiyear ice below the main scattering layer (milky portion). In the clear ice region, the densities are usually higher (0.85 - 0.9 gm/cm^3), and the air bubble sizes are small (diameter < 1 mm). Moreover, the loss increases due to the slight increase in the salinity and therefore the imaginary part of the dielectric constant. At 13 GHz with HH-polarization the contribution of the secondary layer of 50 cm clear ice

with ρ = 0.85 gm/cm^3, and air bubbles of diameter = 1 mm to the total volume scattering coefficient is about 17 dB lower than that of the main 20-cm deep scattering layer with ρ = 0.75 gm/cm^3 and air bubbles of diameter = 2 mm. The effect of the secondary layer with small air bubbles seems negligible; therefore, the multiyear ice can be modeled as the single-scattering layer of air bubbles as shown in Figure 4.1.

The empirical model given in equation (5.2) does not give the cross-polarized scattering coefficient. If the scatterers can be assumed to be spherical in shape, and if the scatterer distribution in the layer does not show any particular directivity, the only difference between VV- and HH-polarization is in the transmissivity term due to the presence of the air-ice boundary. Therefore, with the empirical model, σ^o_{VV} is normally higher than σ^o_{HH} and the difference becomes larger as the incidence angle approaches the Brewster angle, which is about 60° for an air-ice boundary. At 13 GHz when the incidence angle is 50° the difference is about 1.2 dB.

The discussions so far considered only the volume scattering contribution. However, as discussed in Section 4.2, and depicted in equation (5.2), the surface scattering term is always present and may very well be the dominant factor at lower frequencies where the volume scattering term is small.

5.2 Volume Scattering Considerations for Snow-Free First-Year Ice

Although surface scattering is considered the dominant scattering mechanism for first-year ice, the semi-empirical volume scattering model presented so far was tested for possible volume-scattering contributions to radar return from snow-free first-year ice.

The possible volume scatterers are the air bubbles and the brine pockets. The air bubbles found in the first-year ice are smaller and the density of the ice is higher (see Figure 4.2) which implies that there are fewer air bubbles than for multiyear ice.

The brine pockets are approximately spherical in shape in the frazil-ice zone [Ramseier et al., 1974] and the average diameter is far less than 1 mm (0.025 mm [Pounder, 1965]; 0.092 mm [Anderson, 1960]), although this is highly variable depending on salinity and temperature. The brine pockets found in the columnar-ice zone are reported to be elongated in the vertical direction with average length of 3 to 5 mm [Poe et al., 1974]. However, due to the high loss of the frazil-ice zone, the columnar ice with elongated brine pockets is not expected to be seen with microwave frequencies. Figure 5.5 shows the calculated penetration depth through the first-year ice as a function of frequency at several temperatures and salinities. In the calculations, the empirical dielectric constant model by Vant [1978] was used (equations (2.4) and (2.5)). However, as was noted in Section 2.2, the empirical equations seem to estimate too low values of ϵ'' compared to the measured values of frazil ice (see Table 2.1). The penetration depths are less than about 15 cm for the frequencies above C-band, and can be as much as 45 cm at 1 GHz, although these values might be exaggerated.

Figure 5.6 shows the calculated volume scattering term due to air bubbles and brine pockets in the first-year ice compared to the surface scattering term calculated using the physical-optics model. When the surface is smooth, and when the density of the first-year ice is low (about 0.85 gm/cm^3), the air bubbles of 1 mm in diameter [Poe et al.,

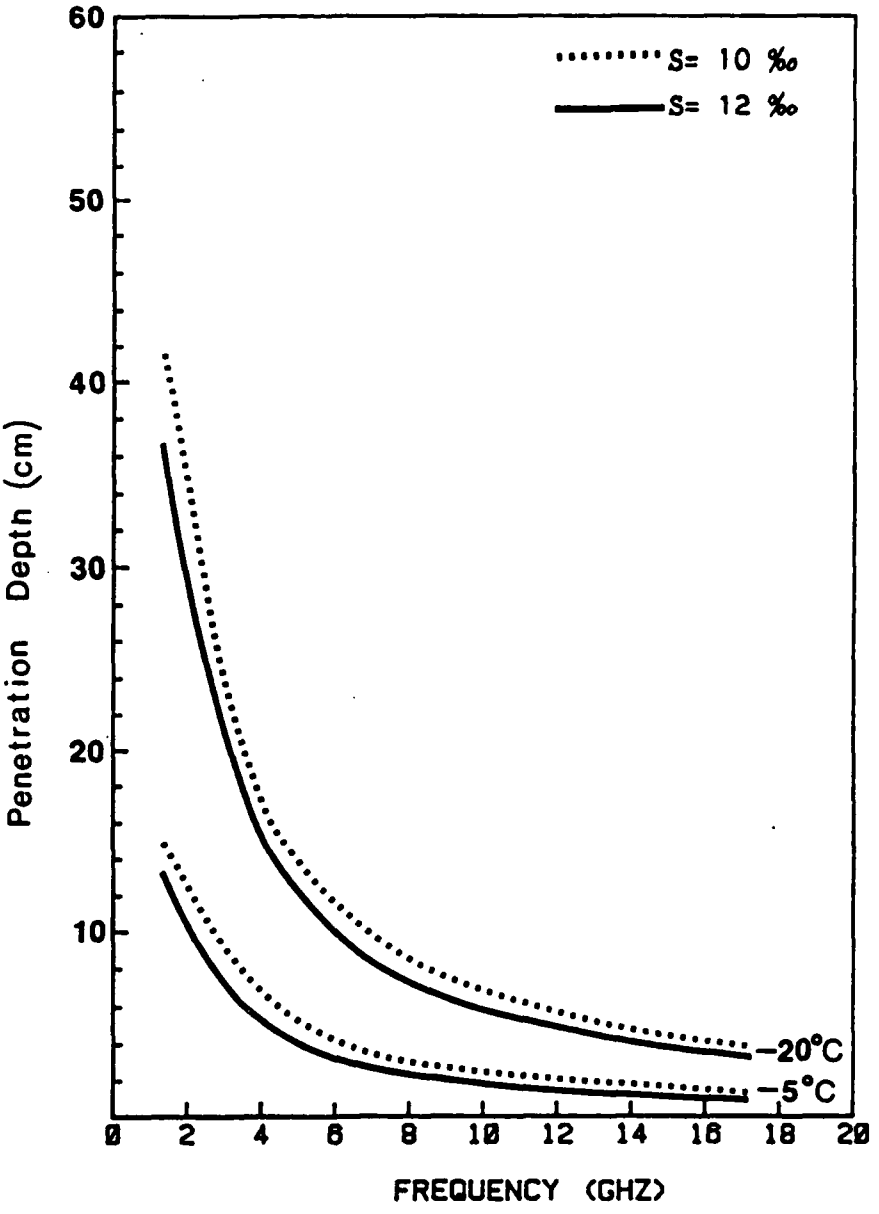

FIGURE 5.5: Penetration Depth through Frazil Ice Calculated Using the Dielectric Constant Model by Vant (1978). See Eqs. (2.4) and (2.5).

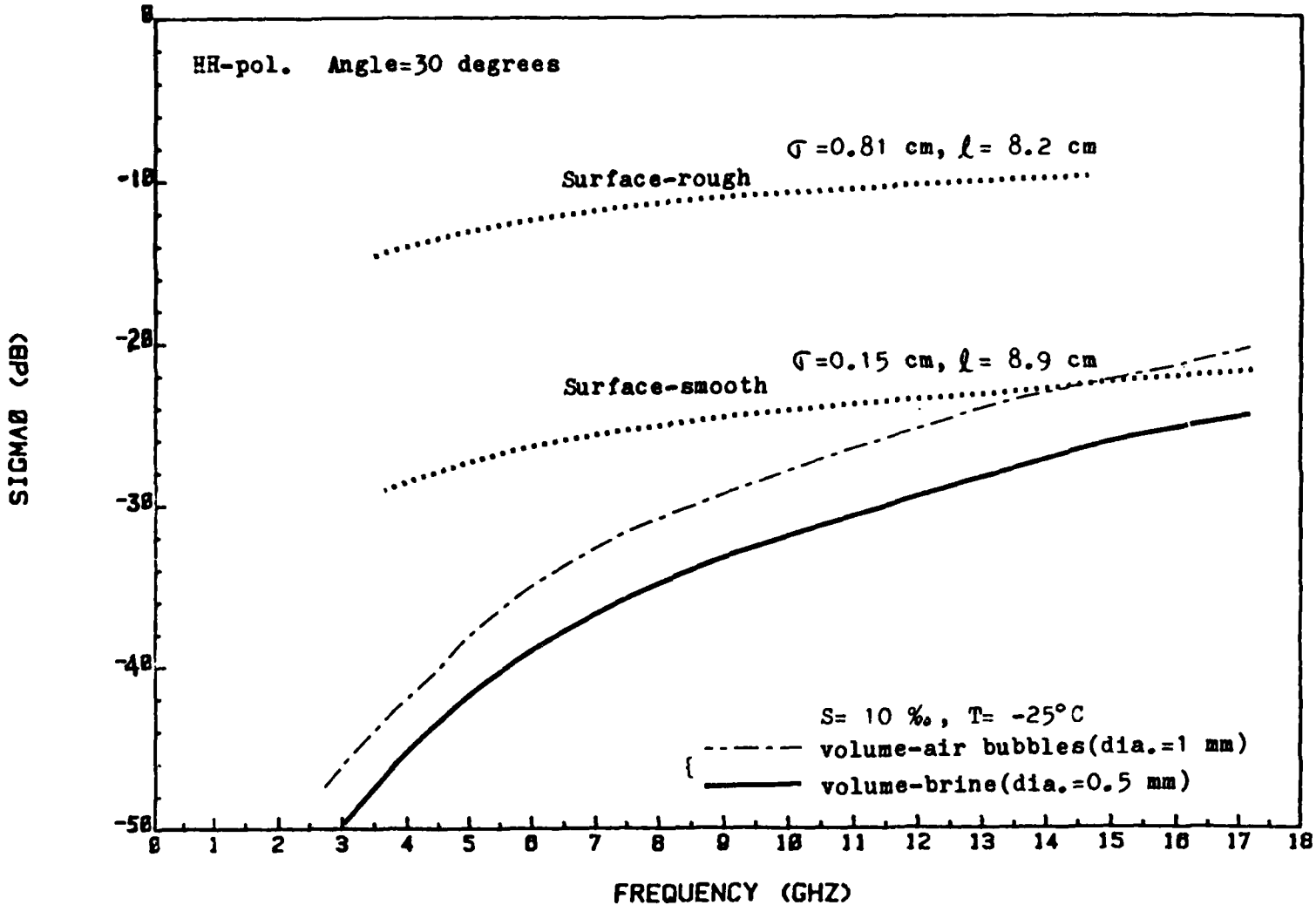

FIGURE 5.6(a): Volume Scattering Due to Air Bubbles and Brine Pockets in the First-Year Ice. Also shown is the surface scattering term using the physical-optics model.

1974] give a volume scattering contribution comparable to that of surface scattering at frequencies above X-band at angles away from nadir.

The spherical brine pockets in the frazil ice layer (having diameters less than 0.1 mm) have a negligible effect (see Figure 5.6(b)). Larger brine pockets (diameter = 0.5 mm) which might be found with warmer temperatures make some contributions at incidence angles greater than about 50° and high frequencies above Ku-band, when the surface is smooth.

5.3 The Effect of Snow Cover on Sea Ice

The snow cover on sea ice has variations with all spatial scales [Carsey, 1982]. The snow cover can have various effects on the backscattering from sea ice, although it generally is considered to be sufficiently transparent to the microwave frequencies when the snow layer is dry and shallow.

The thermal conductivity of snow is very low compared to that of sea ice, so the snow-covered ice surface is warmer; in turn, the whole temperature profile of sea ice is warmer than that of snow-free sea ice. The warmer sea ice has higher average dielectric constant, especially the imaginary part. The higher loss in the ice layer means smaller scattering albedo of any inclusions, thereby reducing the volume scattering contributions of the ice layer (see Section 4.2.1).

The addition of a snow layer causes refraction of the incident waves, therefore effectively changing the incidence angle to the ice surface. The new air-snow boundary may have to be considered as a source for surface scattering and also the volume scattering

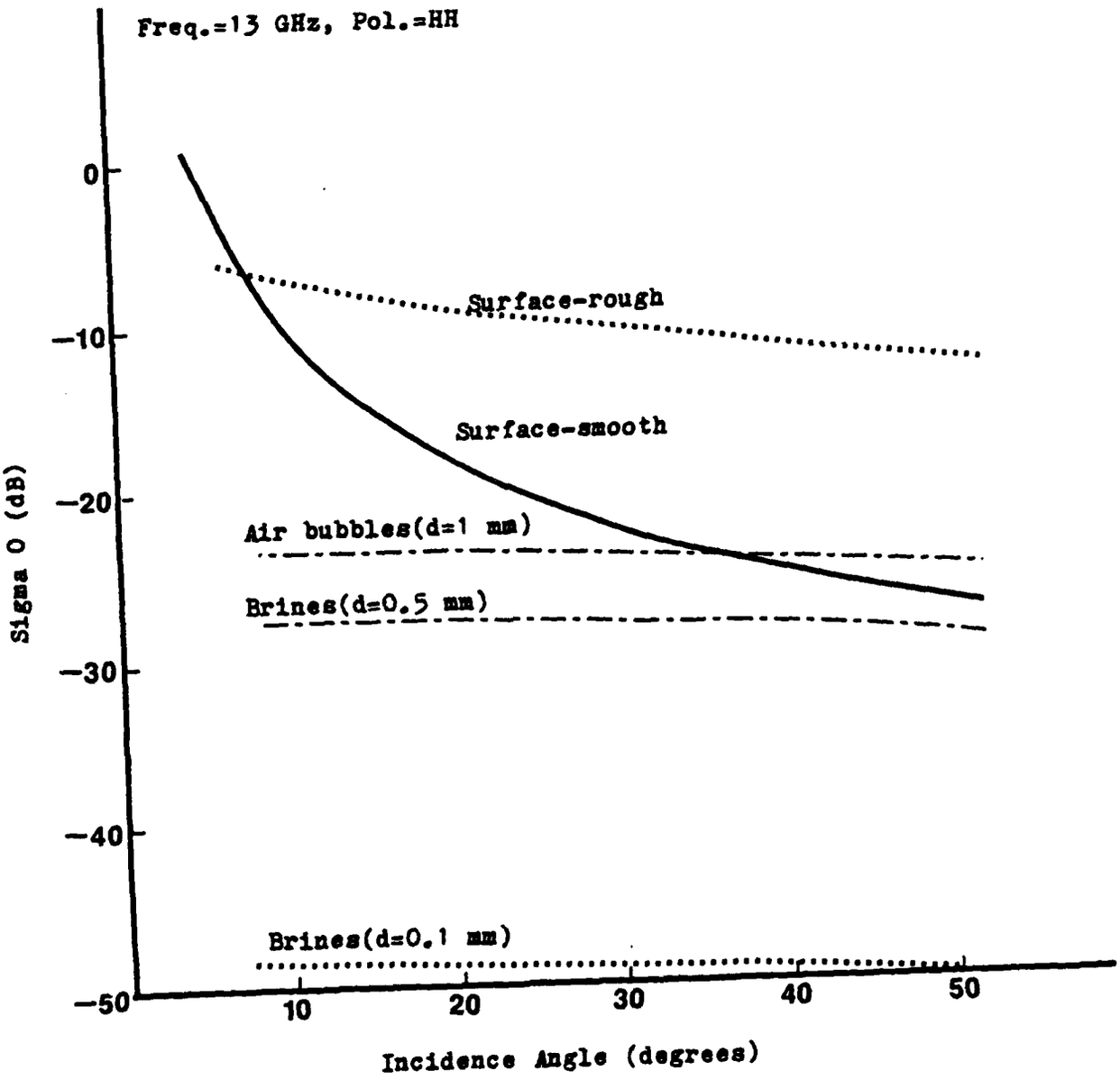

FIGURE 5.6(b): Angular Behavior at 13 GHz. The effect of air bubbles and brine pockets in first-year ice are shown. All the parameters are same as shown in (a).

contribution of the snow layer must be considered. Furthermore the backscattered signal from sea ice is affected by the two-way loss through the snow layer.

Thinner sea ice types often are topped by wet snow layers, but in general the snow cover on the thick first-year ice and multiyear ice can be considered to be dry during most of the year, and the effect of dry snow cover will be considered first.

5.3.1 Average Snow Depths

Although the Arctic is generally a dry place, sea ice very often has a snow cover with depths on the order of 10 centimeters. Figure 5.7 shows spatial variations of snow depths on several types of ice studied during the 1981 Mould Bay experiment. The average snow depths were about 5 cm in October. Figure 5.8 shows variations of average snow depths and density during the winter of 1977-78 in Baffin Island, Canada [Nawako and Sinha, 1981]. The average snow depth for the whole winter was 11.4 ± 4.2 cm, and the average snow density was 0.35 ± 0.04 gm/cm^3. Table 5.3 summarizes several available ice characteristics together with snow depths. In this section, the effect of snow cover is treated for snow depths of up to 20 centimeters.

5.3.2 The Effect of Snow Cover on Ice Surface Temperature

The thermal conductivity of snow is about 1/8 that of sea ice, although these are variables depending on temperature, density, and salinity [Schwerdtfeger, 1963; Nawako and Sinha, 1981]. The temperature of the snow surface is close to ambient air temperature. By assuming linear temperature gradients in both the snow and ice layers, Nawako and

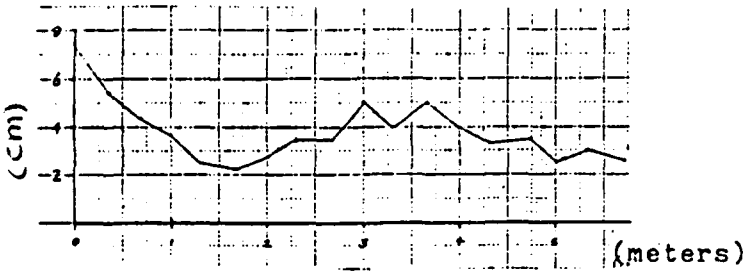

(a) Multiyear Ice- Hummock Area

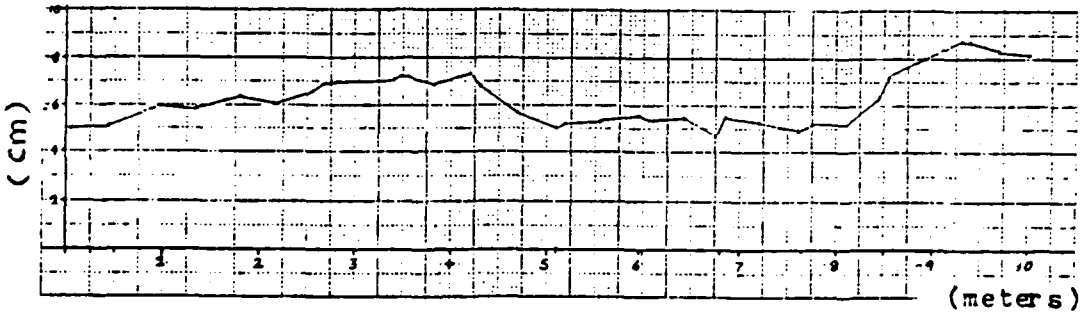

(b) First-year Ice

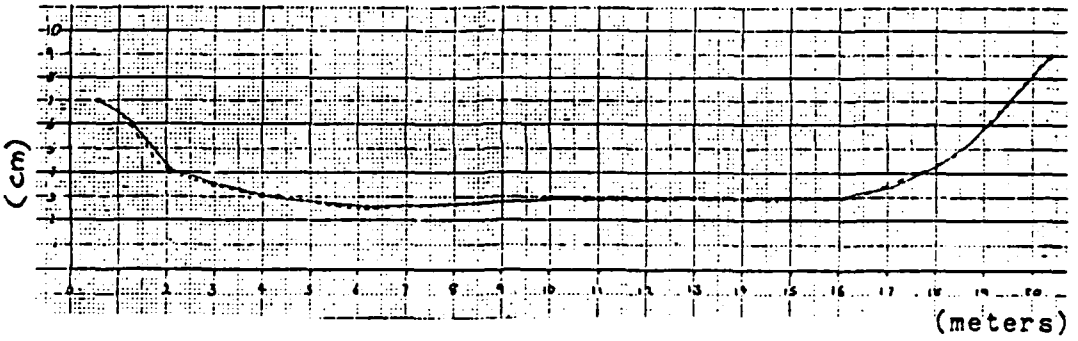

(c) Multiyear Ice- Meltpond Area

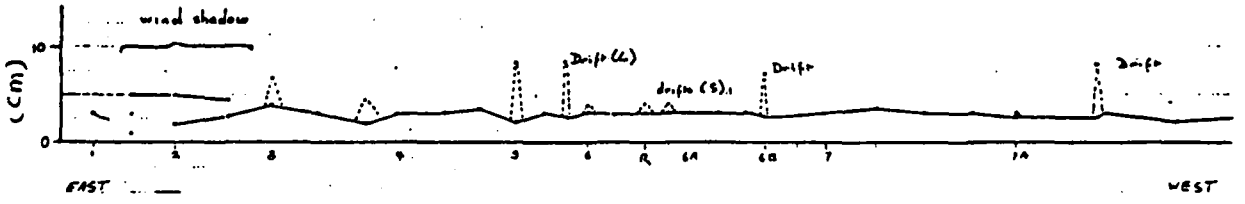

(d) First-year Ice; Large Scale Variation, 8 Km line

FIGURE 5.7: Snow Depth Variations on Sea Ice. (a), (b), (c) - Small-Scale Variations. (d) - Large-Scale Variation Across Mould Bay, N.W.T. Vertical scales are snow depths in centimeters.

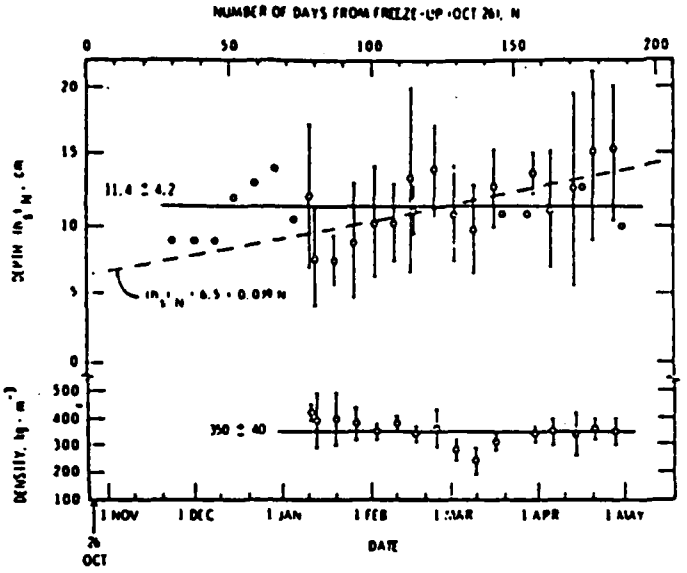

FIGURE 5.8: Variation of Snow Depth and Density During Winter of 1977-1978 (from Nawako and Sinha, 1981).

TABLE 5.3
SEA ICE CHARACTERISTICS

ice type	ice thickness	snow cover	ice surface characteristics	source
thin first year	0.3-0.35 m	5-8 cm	vertical roughness scale 0.5-1.5 cm	Oct. 81, Mould Bay (RADARSAT)
thick first year shore	1.65 m	6-14 cm	surface composed of 2-3 m diameter pans. Topography was flat except for 4 cm high vertical steps at pancake edges	May 77, Point Barrow (Onstott, 1980)
multi-year melt hummock	> 3 m	1-19 cm	small scale roughness 4 mm occasional 1 cm roughness. Hummock was 50 cm high with diameter of 3 m.	same
thick first year	1.37 m	2 cm	very smooth, uniform, unrafted	same
first year pressure ridge	2.3 m	0-43 cm	composed of ice blocks of 10 cm thick. The total width of ridge was 2 m.	same
multi-year fragment	> 3 m	0	flat on large scale with pronounced small scale melt-produced roughness of 0.5-1.0 cm high	same
lake	2.06 m	0	flat on both scale	same
lake	0.74	18 cm	very smooth	same
thick first year	~ 1 m	2-5 cm	roughness elements 2.5 - 3.7 cm	June 82, Mould Bay

Sinha [1981] developed the following equation for the ice surface temperature.

$$T_s = \frac{k_i d_s T_m + k_s d_i T_a}{k_i d_s + k_s d_i} \qquad (5.12)$$

where:

k_i = thermal conductivity of sea ice = 5×10^{-3} cal cm^{-1} s^{-1} deg^{-1} (S = 6°/oo)

k_s = thermal conductivity of snow = 6×10^{-4} cal cm^{-1} s^{-1} deg^{-1}

d_i = ice thickness

d_s = snow depth

T_m = melting point of sea ice

T_a = air temperature

Using equation (5.12), ice surface temperatures under the snow cover are calculated for several cases of ice- and snow-depths and air temperatures (see Table 5.4).

As can be seen from equation (5.12) and Table 5.4, the surface temperature of the multiyear ice (d = 3 m) under 10 cm of snow cover is not much different from the air temperature, while 20 cm of snow cover can change the ice surface temperature as much as 10° C. The thinner types of ice will be more affected by the snow cover as far as the ice surface temperature is concerned. These are approximate results, but Nawako and Sinha [1981] found a good fit with the experimental results (see Figure 5.9), and similar effects of snow cover have been reported [Hallikainen, 1977; Digby, 1982].

The effect of the changing temperature of the ice surface may play an important role in passive measurements; in active microwave

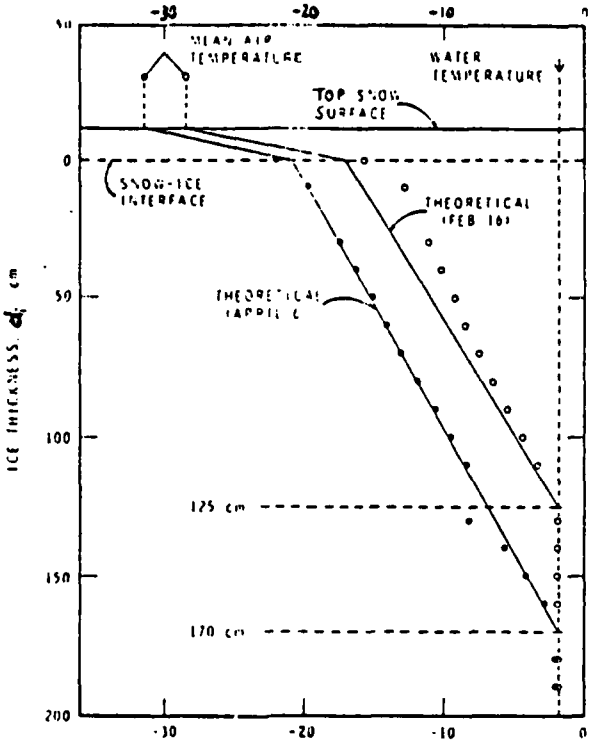

FIGURE 5.9: Calculated and Measured Temperature Profile of Sea Ice. The effect of snow cover (11 cm) can be seen (Nawako and Sinha, 1981).

TABLE 5.4
ESTIMATED ICE SURFACE TEMPERATURE

Ice Depths	Snow Depths	Air Temperatures -30°C	-20°C	-10°C
3 m	10 cm	-24.1	-16.2	-8.3
	20 cm	-20.2	-13.7	-7.1
1 m	10 cm	-17.5	-11.9	-6.3
	20 cm	-12.6	- 8.8	-5.0

measurements the effect, in most cases, seems to be secondary. Consider a first-year ice floe 1 m thick with 10 cm of snow cover. When the air temperature is -30° C, the ice surface temperature is -17.5° C and the dielectric constant of the snow-covered ice surface is 3.29 compared to 3.21 for the snow-free ice surface (calculated using equation (2.4)) (ice salinity = $10^{o}/oo$; see Section 2.2). The resultant Fresnel reflection coefficient changes from 0.289 to 0.284 at vertical incidence, while at angles off-vertical the Fresnel reflection coefficient has to be evaluated at smaller angles due to refraction in the snow medium. The effect seems to be minor at very low temperatures, but when the air temperature is above -20° C, the dielectric constant experiences a greater temperature variation and the effect may not be negligible.

When the near-surface layer of the multiyear ice (> 3 m) is completely free of brine (salinity = $0^{o}/oo$), the scattering albedo of the air bubbles is approximately independent of temperature, and therefore of the snow cover.

When the surface layer is somewhat saline ($S < 0.7^{o}/oo$), the imaginary part of the dielectric constant changes with temperature and therefore the scattering albedo is affected by the snow cover. The exact temperature behavior of the dielectric constant of multiyear ice is not established, but the empirical equations given in Section 2.2 can be used to show the relative effect due to snow cover. At frequencies lower than about X-band, the scattering albedo, for the layer with 2-mm-diameter air bubbles, is very small. Therefore the effect of snow cover is summarized only at 13 GHz in Table 5.5. The density of multiyear ice was assumed to be 0.75 gm/cm^3 and the depth of the air-bubble layer was set to be 20 cm for the calculation of the optical depth.

TABLE 5.5
THE EFFECT OF SNOW COVER ON THE VOLUME SCATTERING CHARACTERISTICS OF THE MULTIYEAR ICE (13 GHz)

	Ice Thickness = 3 m						5 m	
	Air Temperatures							
	-30°C		-20°C		-10°C		-10°C	
	ω	τ	ω	τ	ω	τ	ω	τ
10 cm-snow	0.403	0.893	0.347	1.042	0.244	1.474	0.254	1.415
no-snow	0.432	0.832	0.377	0.955	0.272	1.321	0.272	1.321

ω = scattering albedo
τ = optical depth
ice salinity = $0.6^{o}/oo$

The scattering albedo decreases and the optical depth increases due to the increase in the absorption loss of the air bubble layer when the ice is covered with snow. The overall effect on the volume scattering coefficient of the multiyear ice is to lower the σ^{o} by about 0.3 dB when the 3-m ice is covered with 10-cm snow when the air temperature is -20° C. This was calculated using the radiative-transfer model. When

the ice is thicker or the snow cover is shallower, the effect seems to be negligible.

5.3.3 Backscattering Contribution of the Snow Layer on Sea Ice

When snow covers the ice, the empirical model for the scattering given in equation (5.2) should be modified to include the effect of snow surface and the volume. The new empirical model is as follows.

$$\sigma^0(\theta) = \sigma^0_{ss}(\theta) + T_s^2(\theta)\left[\sigma^0_{sv}(\theta') + \frac{1}{L^2(\theta')}\right.$$
$$\left.\{\sigma^0_{is}(\theta') + T_i(\theta')\,\sigma^0_{iv}(\theta'')\}\right] \qquad (5.13)$$

where:

$\sigma^0_{ss}(\theta)$ = σ^0 for snow surface.

$\sigma^0_{sv}(\theta')$ = σ^0 for snow volume.

$\sigma^0_{is}(\theta')$ = σ^0 for ice surface.

$\sigma^0_{iv}(\theta'')$ = σ^0 for ice volume.

$T_s(\theta)$ = power transmission coefficient of air-snow boundary.

$T_i(\theta')$ = power transmission coefficient of snow-ice boundary.

$L(\theta')$ = one-way loss through the snow layer.

θ' = angle of refraction in the snow.

θ'' = angle of refraction in the ice.

For first-year ice, the last term including σ^0_{iv} becomes negligible and can usually be omitted (see Section 5.2).

5.3.3.1 Dry Snow

Ulaby et al. [1982] derived a set of empirical equations to describe the effect of the snow cover on several natural surfaces (concrete, asphalt, grass and packed ground). Their model behavior has been tested for snow cover on sea ice. When the snow is dry, the scattering contribution from the snow surface σ^o_{ss} can be neglected. This is based on experimental observations which indicate that σ^o is almost independent of snow surface roughness [Stiles and Ulaby, 1980]. Additionally, T_s^2 is close to unity for dry snow because the real part of the dielectric constant of dry snow is only about 1.6 to 1.7 ($T_s^2 = 0.97$) when the density of snow is 0.35 gm/cm^3. This is based on the model given by Hallikainen et al. [1982].

$$\varepsilon'_{dry\ snow} = 1 + 1.91\ \rho_{snow} \tag{5.14}$$

where ρ is the density in gm/cm^3. Now the model given by equation (5.13) reduces to

$$\sigma^o(\theta) = \sigma^o_{sv}(\theta') + 1/L^2\ \sigma^o_{is}(\theta') \tag{5.15}$$

Also from the point of view of equation (5.7), the volume scattering contribution of snow can be viewed as

$$\sigma^o_{sv}(\theta') = \sigma^o_{sv\infty}\ (1 - 1/L^2) \tag{5.16}$$

where $\sigma^o_{sv\infty}$ is the volume scattering coefficient for snow of infinite depth. Therefore equation (5.15) becomes

$$\sigma^0(\theta) = \sigma^0_{sv\infty} - 1/L^2(\sigma^0_{sv\infty} - \sigma^0_{is}) \tag{5.17}$$

which is the form of the empirical equations given by Ulaby et al. [1982]:

$$\sigma^0 = 0.63 - (0.36 - \sigma^0_{is}) \exp(-0.0344\rho_s d_s \sec\theta'), \quad \text{at 8.6 GHz, } \theta = 20^\circ \tag{5.18}$$

$$\sigma^0 = 0.20 - (0.20 - \sigma^0_{is}) \exp(-0.0198\rho_s d_s \sec\theta'), \quad \text{at 8.6 GHz, } \theta = 50^\circ \tag{5.19}$$

$$\sigma^0 = 1.26 - (1.26 - \sigma^0_{is}) \exp(-0.0273\rho_s d_s \sec\theta'), \quad \text{at 17 GHz, } \theta = 20^\circ \tag{5.20}$$

$$\sigma^0 = 0.63 - (0.63 - \sigma^0_{is}) \exp(-0.0373\rho_s d_s \sec\theta'), \quad \text{at 17 GHz, } \theta = 50^\circ \tag{5.21}$$

where:

ρ_s = density of snow, in gm/cm^2

d_s = depth of snow in cm.

Equation (5.17) implies that the effect of snow cover depends on the relative magnitude of σ^0_{snow} and σ^0_{ice} for infinite depths as well as the depth of snow.

The backscattering coefficient of the snow of infinite depth is usually reported to be larger than that of sea ice, and the effect of snow cover on sea ice will be to increase the σ^0 of sea ice ($\Delta\sigma^0 > 0$). Figure 5.10 shows the prediction of the empirical model given by

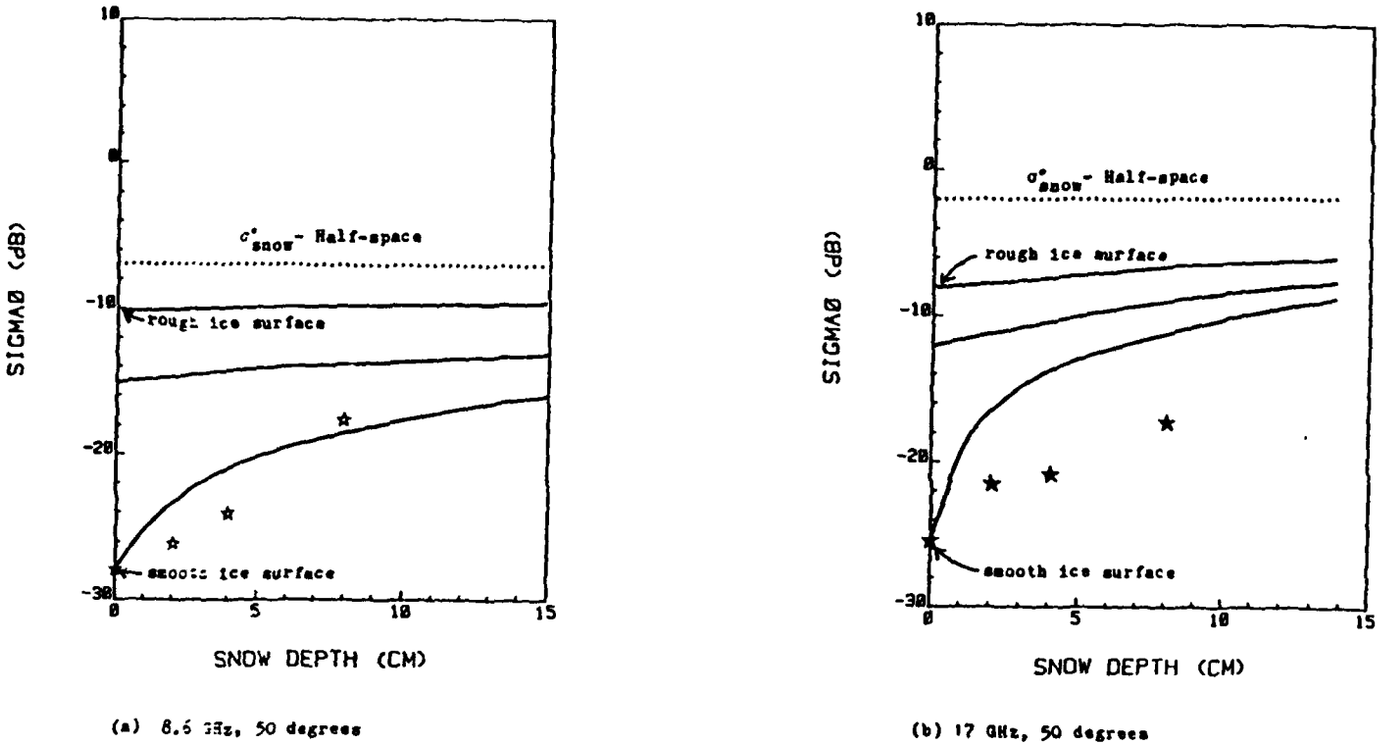

FIGURE 5.10: Effect of Snow Cover on Sea Ice as a Function of Snow Depth. The solid lines are predicted σ^0 of snow-covered ice surfaces whose σ^0 without snow cover can be very low (smooth ice) or close to that of dry snow (rough ice). The data shown were reported by Onstott (1980) and were the average values for the incidence angles of 42°, 51°, 60°, and 70°.

equations (5.18) to (5.21). As expected from equation (5.18), when the backscattering coefficient of the snow-free sea ice is very low compared to that of infinite snow, the effect of snow cover can be severe (5 cm of snow cover causes 8 dB increase in the backscattering coefficient for the case shown in Figure 5.10(a)). Actually, 4-cm-thick snow cover on lake ice was reported to give as much as 8 dB higher σ^0 than snow-free lake ice whose σ^0 is on the order of -30 dB [Delker et al., 1980].

When the σ^0 of bare ice (i.e., rough ice) is close to that of infinitely deep snow, the effect of snow cover becomes negligible (see Figure 5.10).

First-year ice measurements show large variations, and the effect of snow cover can vary from major to minor. Multiyear ice normally shows higher scattering cross-section than first-year ice, and therefore the effect of snow cover will be smaller for multiyear ice than for first-year ice with the same depth of snow cover.

Figure 5.10 also shows the measured effect of snow cover on thick first-year ice [Onstott, 1980]. The agreement is fair at 8 6 GHz and poor for 17 GHz. This can be viewed from two aspects: (1) the empirical model is based on the data with relatively larger depth of snow, and it may not be able to predict the snow cover effect for a small amount of snow; (2) the data points shown in Figure 5.10 may not show the real effect of snow cover because the underlying ice surfaces might have had different roughnesses and therefore different σ^0. Only when the measurements were made continuously as the snow started to fall on the bare ice surface can the effect of snow cover be determined exactly.

On the average, thick first-year ice with snow cover up to 8 cm was reported to have 1 to 4 dB higher backscattering coefficient than the snow-free thick first-year ice. The effect was negligible at L-band, and increased with frequency up to 17 GHz. This is illustrated in Figure 5.11.

5.3.3.2 Wet Snow

When the snow contains liquid (free) water, as found on thinner ice types, the average dielectric constant (both the real part and the imaginary part) increases drastically, and it is no longer valid to neglect the snow surface scattering contribution. Therefore the empirical model given by equation (5.17) has been modified as follows [Ulaby et al., 1982].

$$\sigma^0(d_s m_v) = \sigma^0_{ss} + \sigma^0_{sv'\infty} - 1/L'^2(\sigma^0_{sv'\infty} - \sigma^0_{is}) \qquad (5.22)$$

where:

σ^0_{ss} = σ^0 for snow surface.

$\sigma^0_{sv'\infty}$ = σ^0 for wet snow volume (infinitely thick).

$$= \sigma^0_{sv\,\infty} \exp(-\alpha m_v) \qquad (5.23)$$

σ^0_{is} = σ^0 for ice surface

$$L'^2 = L^2 \exp(\beta m_v) = \exp[(c_0 + \beta m_v)\rho_s d_s \sec\theta'] \qquad (5.24)$$

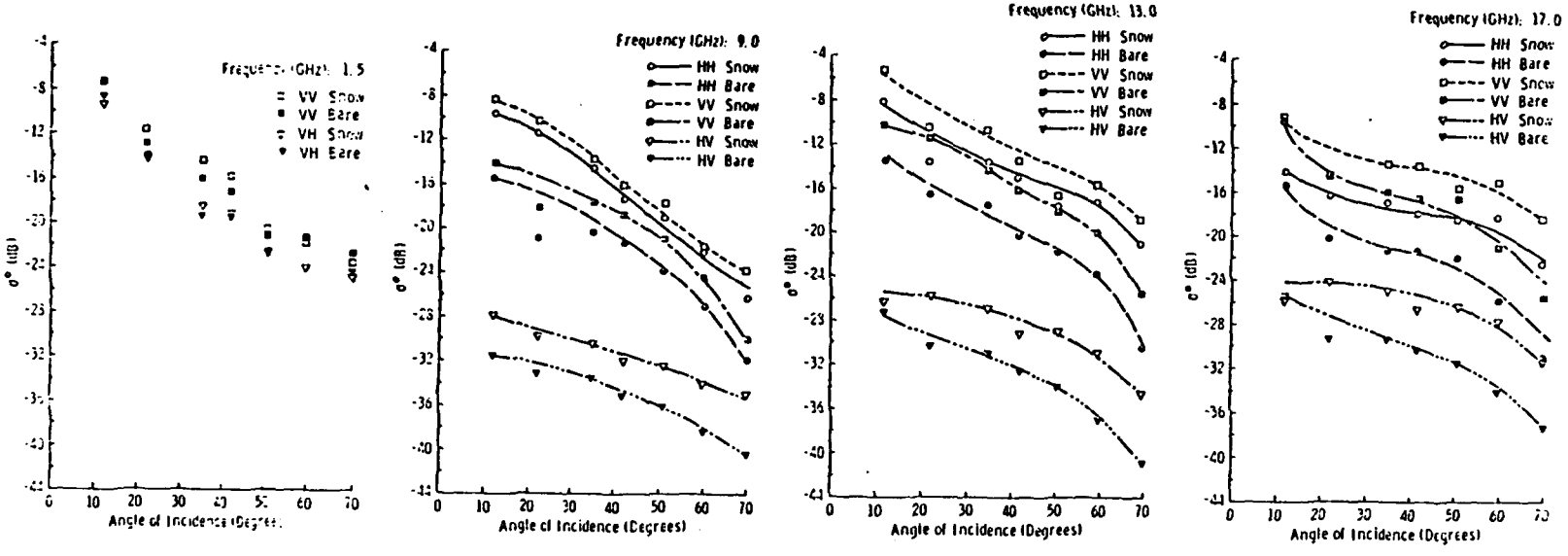

FIGURE 5.11: Average Backscattering Coefficient of Snow-Free and Snow-Covered Thick First-Year Ice at Several Frequencies (Onstott, 1980).

ρ_s = snow density in gm/cm^3

d_s = snow depth in cm

m_v = liquid water content in percent

α, β = parameters determining the dependence of $\sigma^0_{sv\infty}$ and L^2 to m_v.

All the model constants have been found from experimental data on several target classes, and summarized in Table 5.6.

TABLE 5.6
EMPIRICAL MODEL CONSTANTS [Ulaby et al., 1982]

	8.6 GHZ, 20°	8.6 GHz, 50°	17 GHz, 20°	17 GHz, 50°
σ°_{ss}	0.02	0.003	0.02	0.005
$\sigma^\circ_{sv\infty}$	0.63	0.2	1.26	0.63
α	0.802	0.910	1.387	1.372
c_0	0.0344	0.0198	0.0273	0.0373
β	0.143	0.0932	0.872	0.0522

The liquid water content in snow increases the loss through the snow layer and in general makes the backscattered power less sensitive to the underlying ice, as can be expected. Even a small depth of very wet snow can saturate the return.

The model behavior is shown in Figure 5.12 for small moisture contents in snow (m_v = 1% and 3%). The σ^0 values for bare ice were chosen to be the same as those used in dry-snow case (Figure 5.10) to see the difference between dry- and wet-snow cover. For wet-snow cover, it can be seen that σ^0 approaches the value of infinite wet snow (dotted

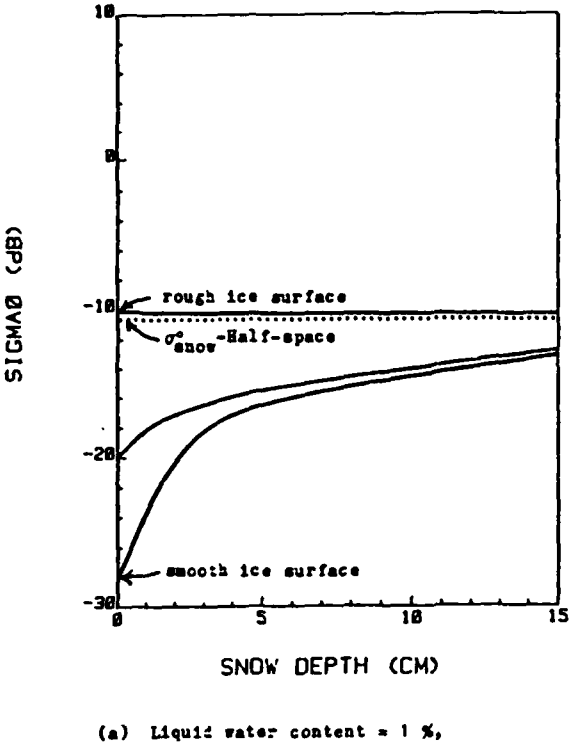

(a) Liquid water content = 1 %, 8.6 GHz, 50 degrees

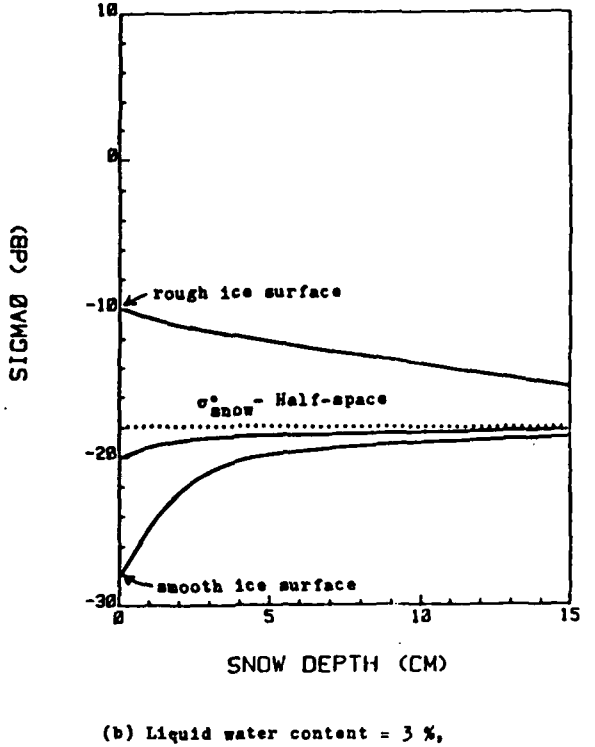

(b) Liquid water content = 3 %, 8.6 GHz, 50 degrees

FIGURE 5.12: Effect of Wet Snow Cover on Sea Ice as a Function of Snow Depth. The dotted lines are the σ^0 of wet snow of infinitely thick. The solid lines are predicted σ^0 of snow-covered ice surfaces whose σ^0 without snow cover can be very low or high depending on the surface roughness.

lines in Figure 5.12) fairly rapidly even with the small moisture content. Because the σ^0 for infinite wet snow decreases with moisture [Stiles and Ulaby, 1980], it is possible that the bare ice (especially multiyear ice) can have higher σ^0 than thick wet snow. In this case, the effect of wet-snow cover will be to block the high return from underlying ice, and therefore decrease the measured σ^0 (see Figure 5.12(b)).

The σ^0 for multiyear ice decreases during summer conditions (see Figure 3.5), and the wet snow cover may be one of the main reasons. When it is warm enough and the surface contains a water film or layer, the effect on the return from multiyear ice will be more severe.

As stated in the previous section, this model is based on the data from a relatively large depth of snow, and the exact behavior for a small amount of snow may be somewhat different.

On thinner types of sea ice, moisture often occurs in the bottom of the snow layer, forming a slush layer (or snow-ice-water mixture) just above the ice surface. The model given by Ulaby et al. [1982] is generally based on the data from snow-covered ground where the wetness is caused by the solar radiation and found in the upper part of the snow; so it may not be adequate for the wet-snow cover on sea ice. Figure 5.13 shows the effect of wet-snow removal from thin first-year ice. The snow was 5 to 8 cm deep and a slush layer was found at the bottom. It was possible that the ice surface characteristics might have changed during the snow removal process. In general, removing the wet snow layer caused σ^0 to drop up to 3 dB, and the effect was generally smaller at higher Ku-band frequencies. Detailed study of the moisture condition of the snow was not made, and the model could not be

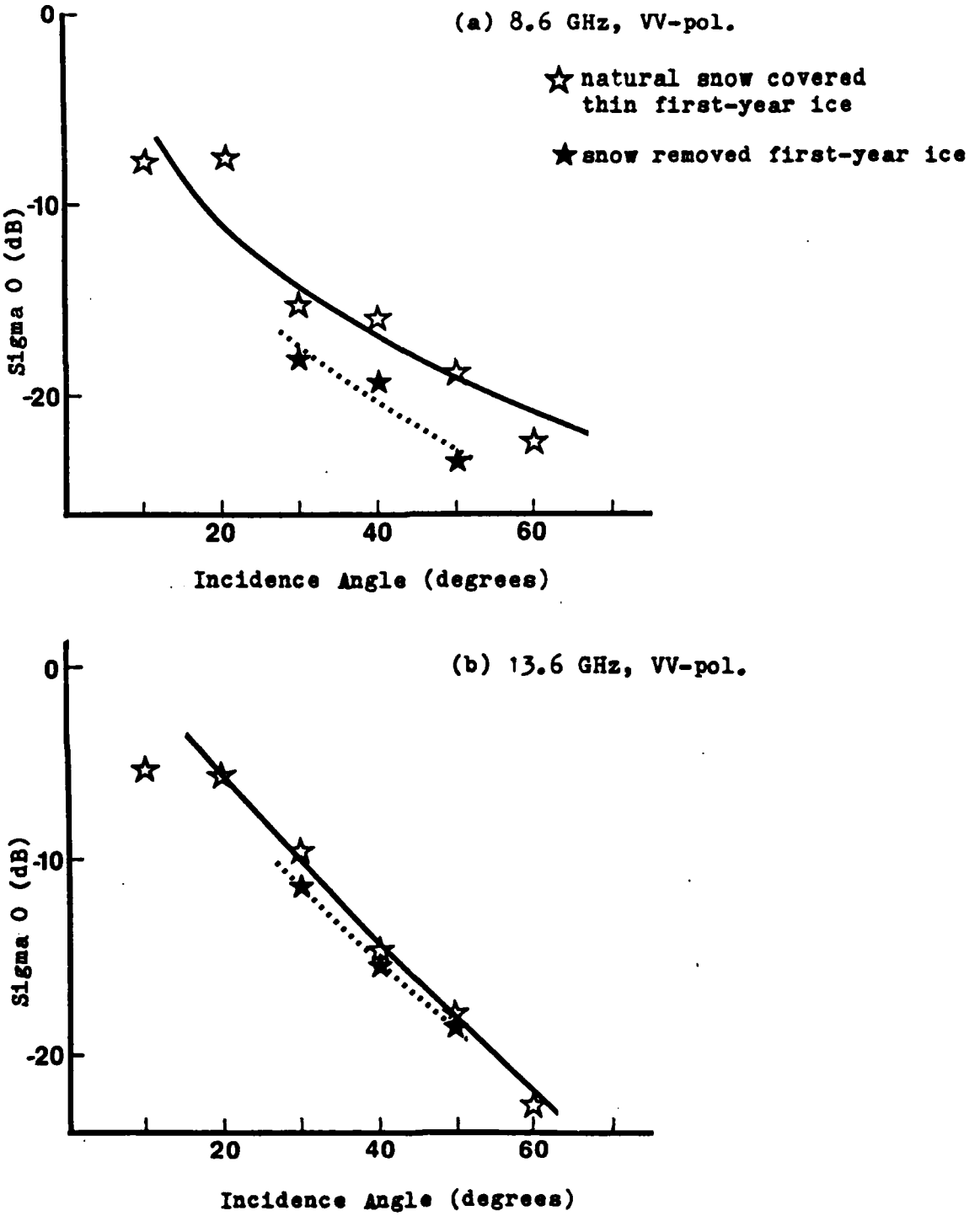

FIGURE 5.13: Effect of Wet Snow Removal from Thin First-Year Ice. The ice surface may have been disturbed. (Oct. 1981, Mould Bay, N.W.T.).

depend on specific requirements of different applications, and are not considered in this study.

6.1 Summary of Experimental Findings

In this section, a careful summary is presented of experimental findings reported so far in terms of better radar parameters for differentiating multiyear ice from first-year ice. There are two kinds of active-microwave data available. One is images taken using SLAR (real- or synthetic-aperture) and the other is the backscattering coefficient data taken using scatterometers. Both of these are reviewed.

6.1.1 Frequency

From the point of view of the image interpreter, X-band or higher freuencies are reported to be much better than L-band frequencies in differentiating different ice types in cold conditions [Luther et al., 1982; SURSAT Workshop Report, 1980; Gray, 1980]. L-band frequencies normally show almost no distinction between first-year and multiyear ice; radars at these frequencies are believed to be responding only to gross surface features. C-band imagery appears more like X-band than L-band imagery [Luther et al., 1982]. 13.3 GHz was observed to be better than 400 MHz in detecting multiyear ice from thinner types of sea ice [Parashar, 1974].

Multifrequency scatterometer data reported by Onstott et al. [1979] also show that L-band frequencies do not have the capability to discriminate multiyear ice from first-year ice under cold conditions. Their result showed that 9 GHz is the best among the frequencies between

8 and 18 GHz and 1.5 GHz. In a recent experiment in Mould Bay, N.W.T., Canada, it was found that X- and Ku-band frequencies have similar capability in differentiating multiyear ice from grey ice and are a little better than C-band frequencies. Also, the Ku-band frequencies showed largest separation between multiyear and first-year ice among the frequencies between 4 and 17 GHz. (See Section 7.0 for the Mould Bay experiment results).

A simple conclusion so far is that X-band or higher frequencies are better than L-band or C-band frequencies in differentiating multiyear ice from younger ice types, and due to the hardware complexities and atmospheric attenuation problem at Ku-band, X-band was recommended [Luther, 1982].

6.1.2 Incidence Angle

In general, incidence angles greater than 20° (SEASAT incidence angle) are recommended to minimize the ambiguity between open water and the ice [Gray, 1980]. Also, incidence angles smaller than 80° are suggested because topography may dominate the backscatter at shallow depression angles [Gray et al., 1977; SURSAT Workshop Report, 1980].

The difference in σ^0 between multiyear ice and first-year ice was reported to increase up to about 30° and remain constant beyond that angle [Gray et al., 1977]. Onstott, et al. [1979] reported that 20° to 40° are best for VV-polarization, and it was found that 40° to 60° were better in discriminating multiyear ice from grey ice and first-year ice [Onstott et al., 1983]. When there is no open water, all the scatterometer angles between 8° and 55° were reported to give the same classification accuracy [Guindon et al., 1982]. Parashar's result

[1974] showed that the incidence angles greater than 25° give better discrimination than smaller angles at 13.3 GHz.

In summary, incidence angles between 20° and 80° are usually recommended, while some measurements show 30° to 60° are better.

6.1.3 Polarization

Cross-polarization usually gives more grey-scale information in the imagery, but new ice forms are harder to identify [Gray et al., 1977]. In σ^0 the differences between multiyear ice and first-year ice are usually larger for cross-polarization than like-polarization at X- and Ku-band frequencies [Gray et al., 1977, 1982; Onstott et al., 1979; Hawkins, 1980], although Guindon, et al. [1982] reported that there was no evidence to favor any particular polarization in classification accuracy. Parashar [1974] noted that the cross-polarization gives more separation between thick-first-year and thin-first-year ice at 0.4 GHz.

It is usually said that, although cross-polarization has a little better capability than like-polarization, it does not justify the added cost and complexity [Gray, 1980].

6.2 Theoretical Model Behavior

In this section, the surface-scattering model for first-year ice (see Section 3.0) and the volume-scattering model for multiyear ice (see Sections 4.0 and 5.0) are considered together in an attempt to find an optimum set of radar parameters in distinguishing multiyear ice from first-year ice. The possible ranges of σ^0 for multiyear ice and first-year ice as all the model parameters are varied within reasonable values

are calculated and the optimum set of radar parameters is selected from these ranges of values.

6.2.1 Frequency

Figure 3.8 shows that the physical-optics model using an exponential correlation function can predict the frequency behavior of σ^0 for first-year ice with proper choice of surface-roughness parameters. Figure 4.13 shows that the radiative-transfer model combined with the physical-optics model gives a good match with the data taken from the multiyear ice. The volume-scattering calculation was simplified by using the semi-empirical model described in Section 5.1 (see Figure 5.2).

In Figure 6.1, typical frequency and angular behaviors of σ^0 for multiyear ice and first-year ice predicted by the physical optics model for the surface scattering and by the empirical model for the volume scattering are shown. The model parameters were adjusted to match the data shown [Onstott et al., 1983]. Note that the curve for multiyear ice includes both the rough-surface scattering and the volume-scattering contributions, while the curve for first-year ice includes only the surface-scattering term. From the figure, it can be seen that the difference in σ^0 between multiyear ice and first-year ice increses as the frequency is increased. The difference is about 5 dB at 4 GHz and about 11 dB at 18 GHz. One should note that this is for just one case of the physical parameters of first-year ice and multiyear ice, which are all variables depending on temperature history, temperature, salinity, etc.

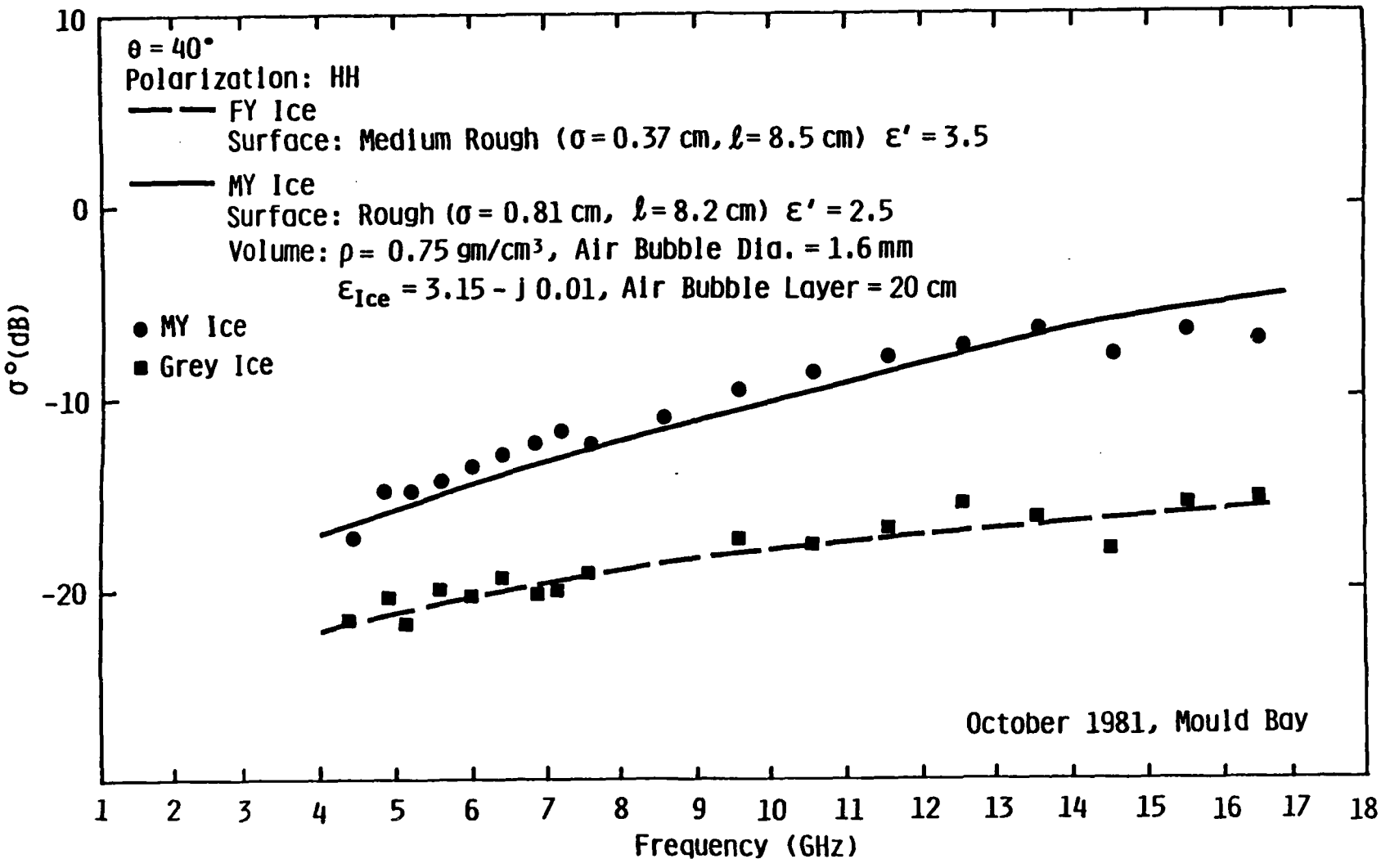

FIGURE 6.1(a): Typical Frequency Behaviors of Multiyear Ice and First-Year Ice Predicted by Theoretical Models. The model parameters are adjusted to match the data shown.

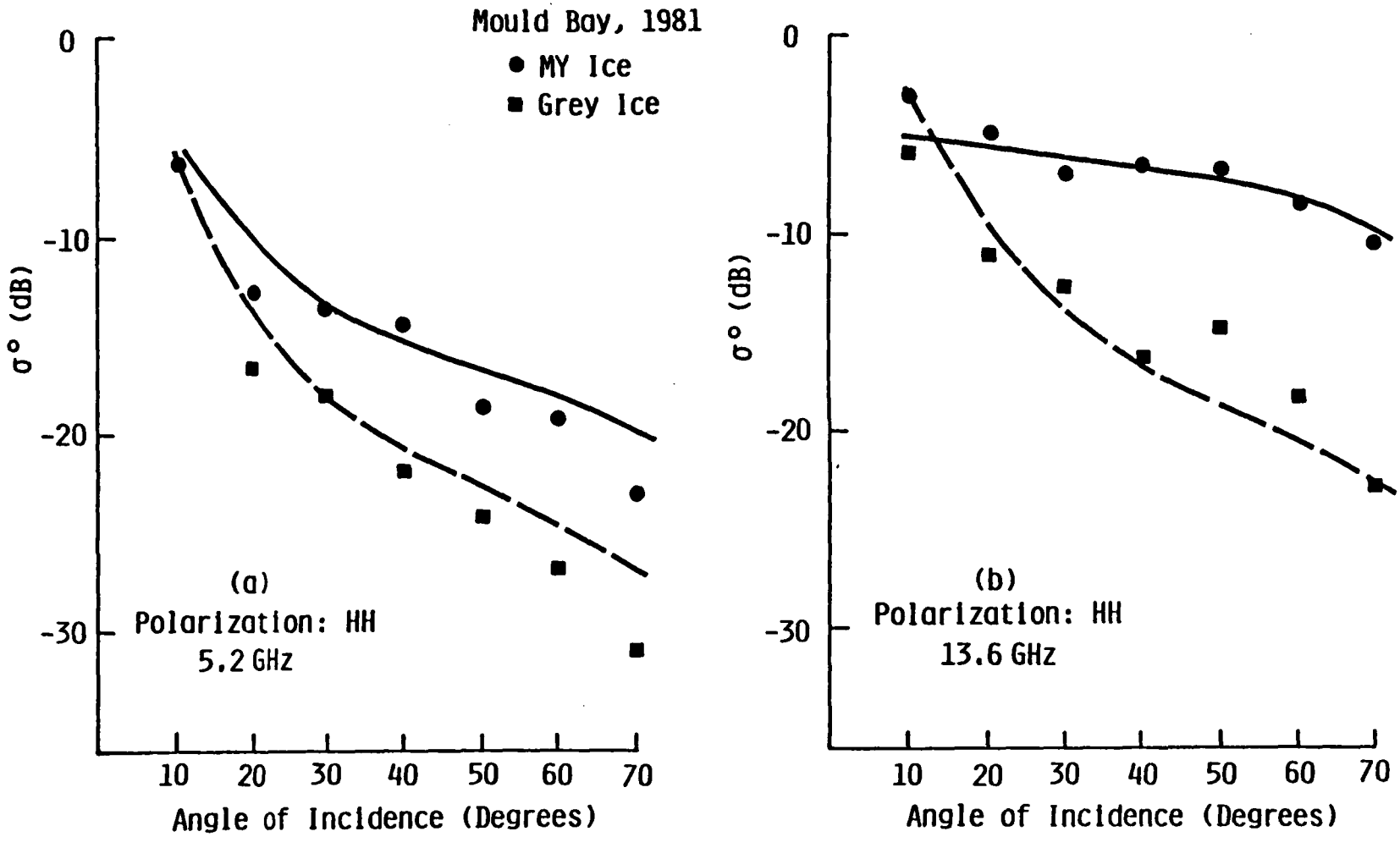

FIGURE 6.1(b): Theoretical Angular Variations of σ^0 of Multiyear Ice and First-Year Ice. The model parameters are the same as those used in (a). The same data set shown in Figure 6.1(a) are shown together.

The surface roughness plays an important role in determining the σ^0 of first-year ice (see Figures 3.6(b), 3.10 and 3.11) as well as that of multiyear ice (see Figure 4.12).

As temperature changes, the dielectric constant of the ice changes, as discussed in Section 2.2, although the expressions given by equations (2.4) through (2.7) are approximate and the exact dependence of the dielectric constant of sea ice on temperature has yet to be determined. The change in the dielectric constant of sea ice causes a change in the Fresnel reflection coefficient, resulting in a variation of σ^0 up to about 2 to 3 dB for first-year ice (see Section 3.1). The change in ε'' due to temperature change causes a change in the volume scattering characteristics of the multiyear ice, and the σ^0 of the multiyear ice can have variations of as much as 6 dB (see Section 4.2.3) under different temperature conditions.

The average air-bubble size in the multiyear ice has significant impact (up to 10 dB) on σ^0, and so does the density of the multiyear ice (2 to 3 dB).

Figure 6.2 shows the ranges of theoretical σ^0 for multiyear ice and first-year ice as the model parameters are varied. The lowest curve (1) is for first-year ice with a smooth surface when the salinity and temperature are very low. As the salinity or temperature is lowered, the dielectric constant decreases. The next lowest curve (2) is for first-year ice with a medium-rough surface and increased salinity and temperature. The next curve (3) is for multiyear ice with medium-rough surface and small air bubbles when the temperature is low. The highest curve (4) is for multiyear ice with rough surface, larger air bubbles, and zero salinity, which causes a larger volume-scattering contribution

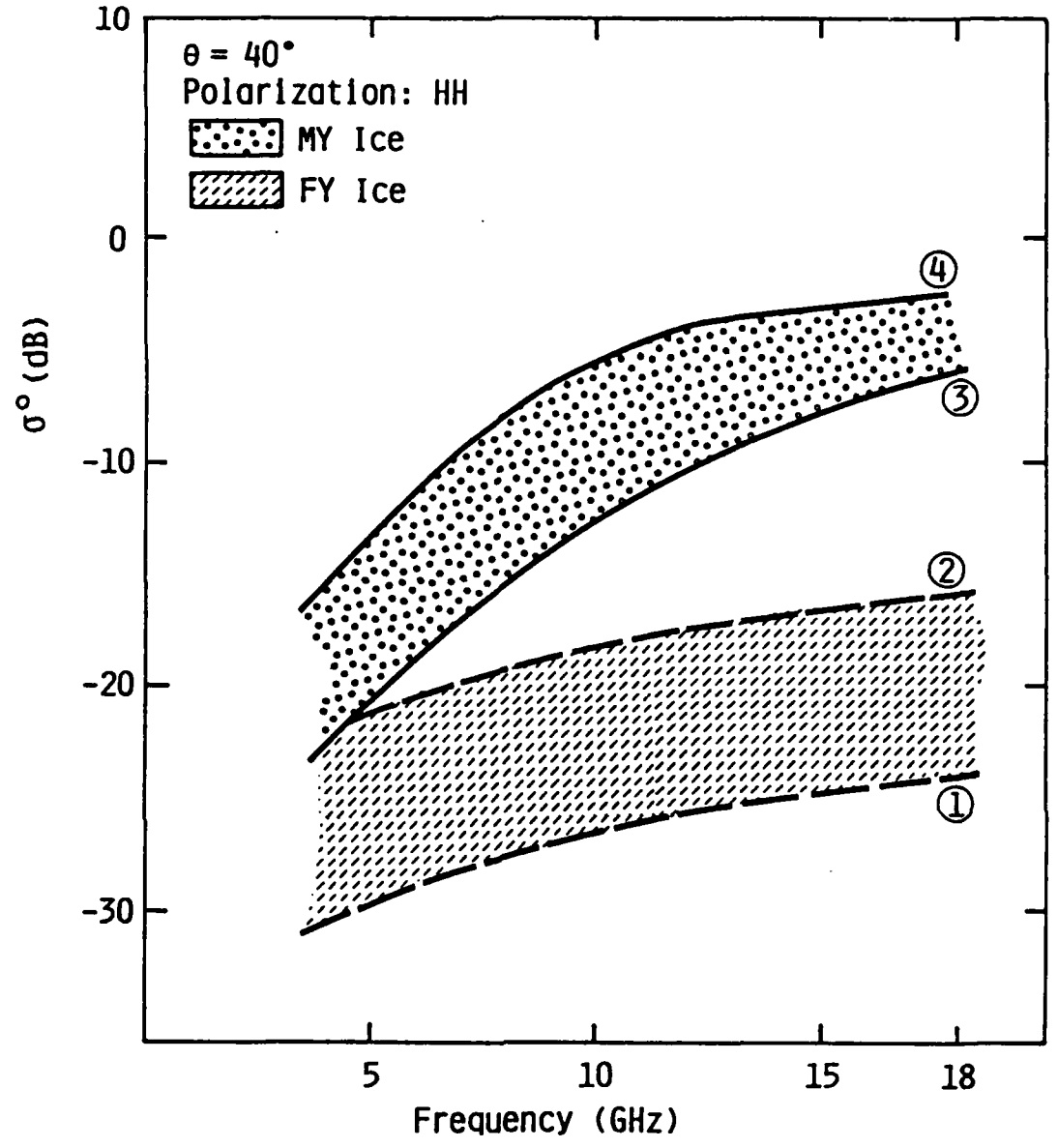

FIGURE 6.2: Theoretical σ^0 for multiyear ice and first-year ice. The ranges of values are illustrated as several model parameters are varied. (1) smooth first-year ice (σ=0.15, ℓ=8.9 cm), S=8°/oo, T=-25°C; (2) medium rough FY ice (σ=0.37, ℓ=8.5 cm), S=10°/oo, T=-15°C; (3),(4) Multiyear ice: (3) medium rough surface (σ=0.37, ℓ=8.5 cm), S=0.6°/oo, T=-20°C, ρ=0.75 gm/cm^3, air bubble dia.=1.6 mm, bubble layer=20 cm; (4) rough surface (σ=0.81, ℓ=8.2 cm) S=0°/oo, T=-15°C, ρ=0.7 gm/cm^3, air bubble dia.=2 mm, bubble layer =50 cm.

due to decreased absorption loss. Note that the effect of higher temperature is to increase the σ^0 of first-year ice (mainly due to the surface scattering) and to decrease the σ^0 of multiyear ice (mainly due to volume scattering for frequencies higher than about X-band (see Figure 4.12)). Therefore at higher temperatures the difference between signals of first-year and multiyear ice decreases. In Figure 6.2 it can be seen that the difference between multiyear and first-year ice still exists for the cases considered for nearly all the frequency range considered. It can also be seen that higher frequencies give better discrimination.

In Figure 6.3, the model parameters are varied further to include the case of very rough first-year ice with high salinity and temperature (curve (2)). Lossier multiyear ice with medium-rough surface and higher salinity and temperature than curve (3) of Figure 6.2 is considered (curve (3)), and multiyear ice with a rough surface and larger air bubbles and zero salinity is plotted (curve (4)). In these cases, a large overlap between the σ^0 for first-year ice and multiyear ice can be seen except above 17 GHz.

The surface roughness is the major factor in determining the σ^0 of first-year ice, and the first-year ice with a very rough surface can be confused as smoother multiyear ice with smaller air bubbles unless the frequency is high enough.

The ranges shown in Figure 6.3 are in no sense the absolute ranges of σ^0 for multiyear ice and first-year ice. Only the small-scale surface roughness is considered, and the effect of ridging (larger scale variation) is neglected. The range of surface roughness for multiyear ice and first-year ice have never been determined. Also the maximum or

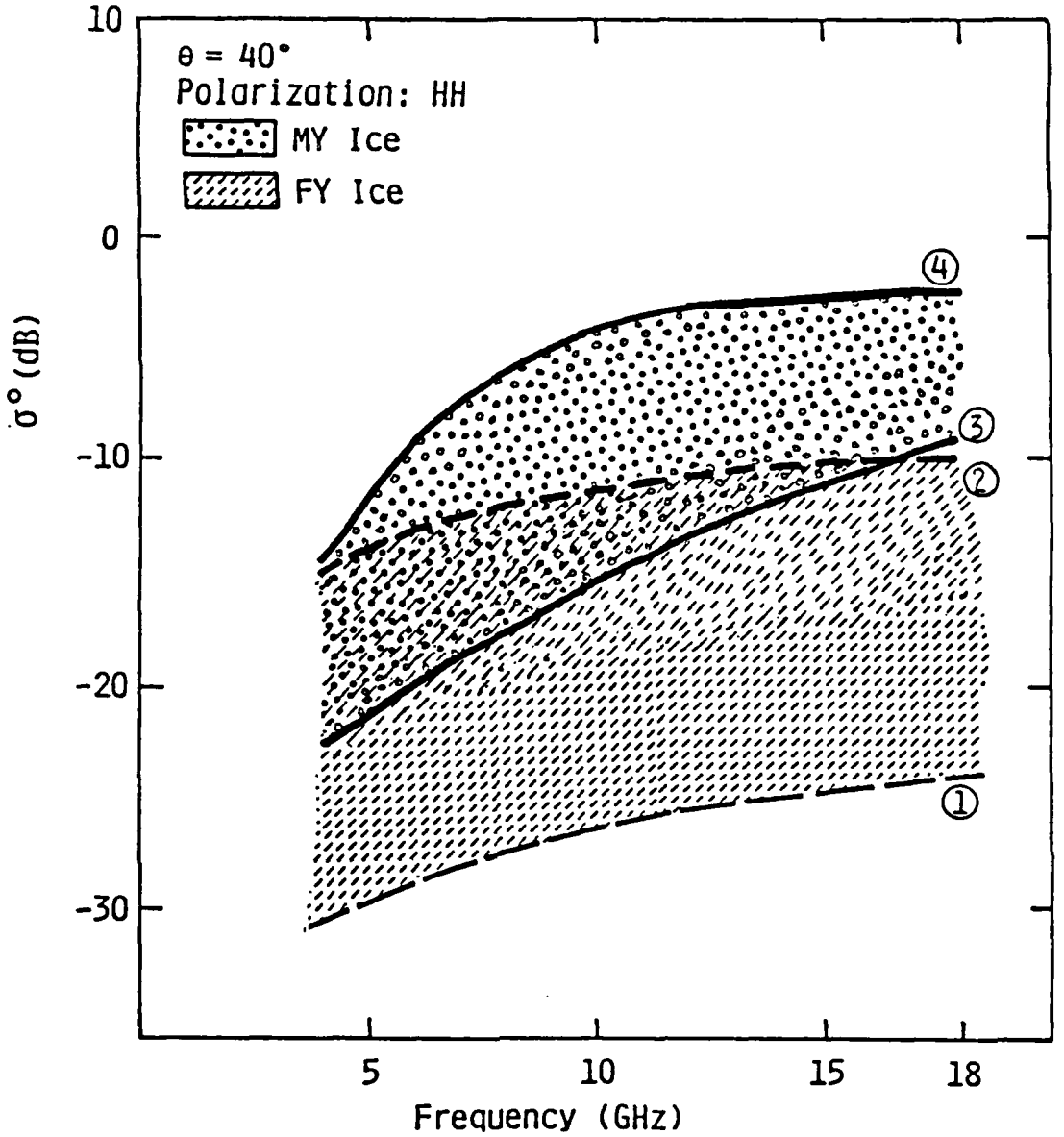

FIGURE 6.3: Theoretical σ^0 for Multiyear Ice and First-Year Ice. The ranges of values are illustrated as several model parameters are varied. (1) Smooth first-year ice (σ=0.15, ℓ=8.9 cm), S=8°/oo, T=-25°C; (2) Rough FY ice (σ=0.81, ℓ=8.2 cm), S=12°/oo, T=-5°C; (3),(4) Multiyear ice: (3) medium rough surface (σ=0.37, ℓ=8.5 cm), S=0.7°/oo, T=-5°C, ρ=0.75 gm/cm^3, air bubble dia.=1.6 mm, bubble layer=20 cm; (4) rough surface (σ=0.81, ℓ=8.2 cm), S=0°/oo, T=-25°C, ρ=0.7 gm/cm^3, air bubble dia.=2.5 mm, bubble layer=50 cm.

minimum average diameters, or the distribution of sizes of air bubbles, is in question. The temperatures above -5° C where the dielectric constant of sea ice is very sensitive (see Figure 2.5) are not considered.

The effect of snow cover is most severe for first-year ice with a smooth surface (see Section 5.3.1) whose σ^0 is very low, and the result is to raise the overall level of the curves (1) in Figures 6.2 and 6.3. In terms of frequency, higher frequency seems to be more easily affected (see Figures 5.10 and 5.11), but the exact frequency behavior has not been established.

With all these limitations in mind, one can generally say that higher frequency is better in discriminating multiyear ice from first-year ice.

6.2.2 Incidence Angle

In Figures 3.10, 4.10 and 6.1(b), the ability of theoretical models to predict the σ^0 of first-year ice and multiyear ice was shown. In Figure 6.4, the ranges of theoretical angular response of σ^0 of multiyear ice and first-year ice at 5 GHz and 13 GHz are shown. The model parameters are the same as those used in Figure 6.2.

Due to the volume scattering contribution at higher frequencies than about X-band, the σ^0 of multiyear ice decays slowly as the incidence angle increases, while σ^0 of first-year ice decays faster. Therefore in terms of discrimination capability, larger incidence angles (greater than 30° to 40°) seem to be better.

As the model parameters are varied further to include very rough first-year ice and more lossy multiyear ice, the overlap between

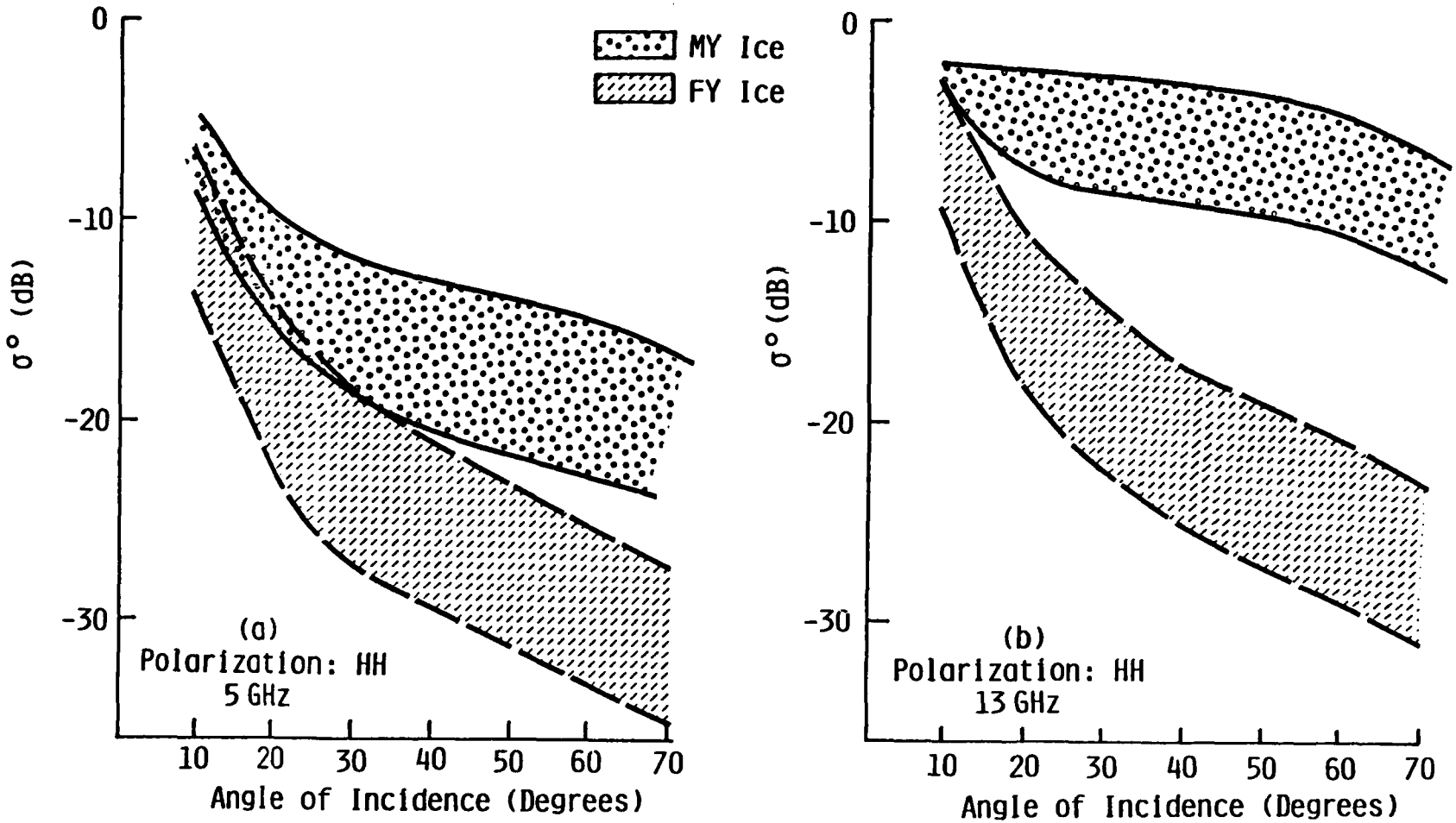

FIGURE 6.4: Theoretical Angular Variations of σ^0 of Multiyear Ice and First-Year Ice. The model parameters are the same as those used in Figure 6.2.

multiyear ice and first-year ice occurs in all the incidence angles as shown in Figure 6.5. Several reported measurements are shown together in the figure, and it can be seen that the theoretical model can bound all the measurements except one case. As mentioned in the previous section, the boundaries are not the absolute limits, and further study is needed.

6.2.3 Polarization

In Sections 3.3.3 and 4.2.5, polarization considerations are given for first-year ice and multiyear ice, respectively.

The radiative transfer model predicts higher σ^0_{VV} than σ^0_{HH} for multiyear ice (volume scattering), while the physical-optics model predicts lower σ^0_{VV} than σ^0_{HH} for first-year ice (surface scattering), mainly due to the Brewster angle effect. Therefore, in terms of discrimination capability, VV-polarization should be better than HH-polarization according to these models (see Figure 6.6). However, the measurements do not always show that kind of behavior (see Figures 3.9 and 4.14), and the limitations of these theoretical models can be seen. Additional terms (i.e., volume scattering) may have to be included to properly explain the behavior with VV-polarization.

σ^0_{HV} is zero for the physical-optics model unless the multiple scattering is considered. Therefore a quantitative comparison of the capabilities of the like-polarization and cross-polarization is not made. Since the cross-polarized component in surface scattering (first-year ice) is a second-order term, cross-polarization should be better in distinguishing multiyear ice from first-year ice.

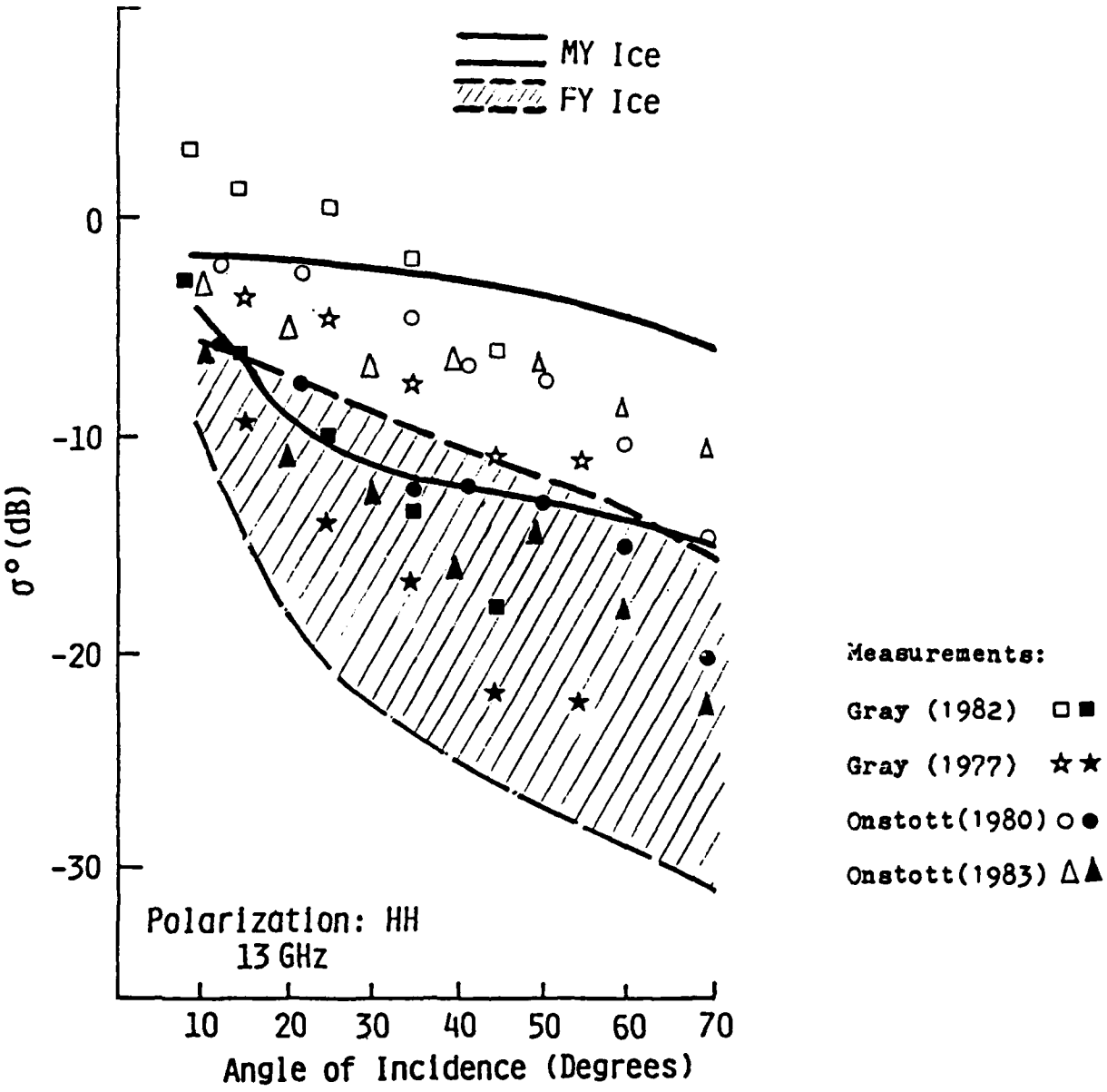

FIGURE 6.5 Theoretical Boundaries of σ^0 of Multiyear Ice and First-Year Ice. The model parameters are the same as those used in Fig. 6.3. Several reported measurements are shown together. Except for one case, all lie within the boundaries. Dark points are first-year ice.

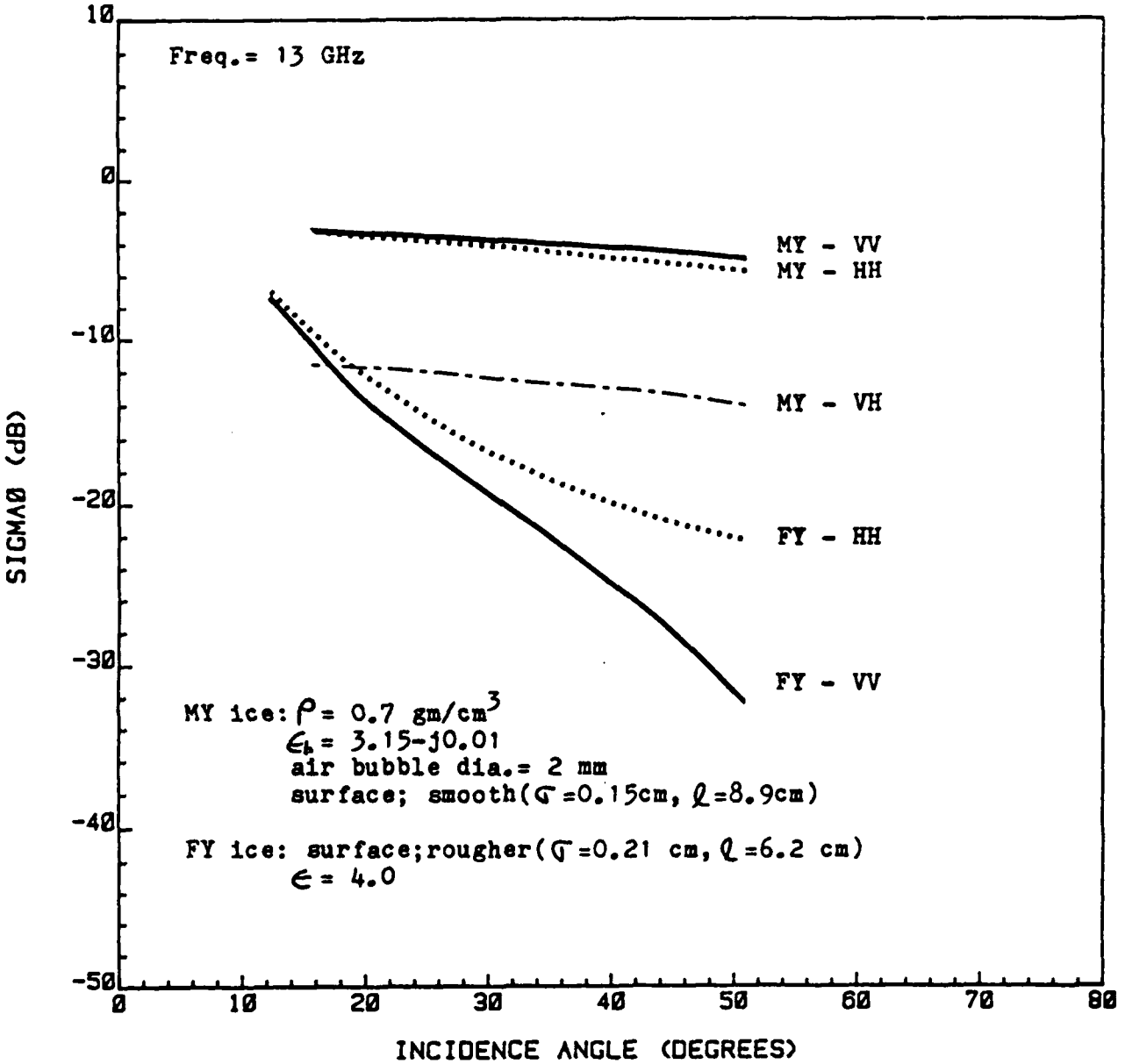

FIGURE 6.6 Theoretical Polarization-Dependence of a Smooth Multiyear Ice and a Rougher First-Year Ice at 13 GHz. Radiative transfer model and the physical-optics model are used. Note that the cross-polarized term is zero for first-year ice.

6.3 Summary

The theoretical model behavior seems to confirm the experimental findings about better radar parameters to be used in sea ice monitoring, although the theoretical considerations are of first-order and preliminary. Higher frequencies than about X-band, and incidence angles larger than about 30° to 40° seem to be best suited for sea-ice monitoring. No specific resonances have been found to suggest any particular frequency or incidence angle, either in the measurements or in theoretical model behavior.

7.0 RADAR BACKSCATTER STUDY OF SEA ICE IN THE FALL

Measurements of the radar backscatter properties of sea ice under fall conditions were made during October 1981 as part of the FIREX/ RADARSAT Project.

The measurements used the helicopter-borne University of Kansas microwave active spectrometer (HELOSCAT), operating over a frequency range of 4 to 17 GHz and an incidence-angle range of 10° to 70°. A detailed system specification can be found in Onstott, et al. [1982]. Initially the helicopter was not available due to weather conditions, and a surface-based system was assembled and used to make similar measurements with more carefully controlled ground truth.

Multiyear ice, a very large multiyear pressure-ridge, first-year ice with varying degrees of small-scale surface roughness, grey ice with varying degrees of deformation, fast ice and lake ice were investigated with the airborne system. A multiyear meltpond, a multiyear hummock, and a smooth area of first-year ice were investigated with the surface-based system.

The complete σ^0 data base is reported in Onstott, et al. [1983], and the ground truth is summarized in Digby [1982]. In this section, a brief summary of measurement results is given. Also, by using the theoretical and empirical models given in Sections 3.0 through 5.0, an attempt is made to correlate the available ground-truth with the σ^0 data.

7.1 Helicopter-Borne Experiment Results

Most of the backscatter data were obtained using the helicopter-borne system (HELOSCAT). The measurements are recorded as a function of

time to traverse the flight line. From these profiles, average σ^0 for each ice type is derived as a function of frequency, incidence angle and polarization.

7.1.1 Multiyear/Grey Ice

Multiyear ice frozen in grey ice was easily detectable due to its higher (5 dB or more) σ^0 than that of grey ice, for almost all the frequencies from 4 to 17 GHz at incidence angles of 20° to 70°. Figures 7.1(a) and (b) show typical profiles for the composite ice floe, together with the histograms which show the distribution of σ^0 in 1 dB intervals. In the profiles, one can see the large variation inside the multiyear ice which included a pressure-ridge and a hummock. The variations inside the grey ice are due to varying degrees of deformation; also, a piece of multiyear ice can be seen embedded in the grey ice.

The multiyear pressure-ridge and the hummock did not show up clearly in the profiles, and the separate flight along the pressure-ridge showed that the average σ^0 for this pressure-ridge was slightly lower than that for multiyear ice with VV-polarization.

Typical angular behaviors of average σ^0 of multiyear ice and grey ice are shown in Figure 7.2, together with that of first-year ice. Figure 7.3 shows the difference in average σ^0 between multiyear ice and grey ice as a function of frequency with HH-polarization. Except for 10° incidence, multiyear ice always showed 5 to 10 dB higher σ^0 than grey ice. Ku-X-band frequencies had slightly better discrimination capability than lower C-band frequencies, and the incidence angles larger than about 30° to 40° seem to be better.

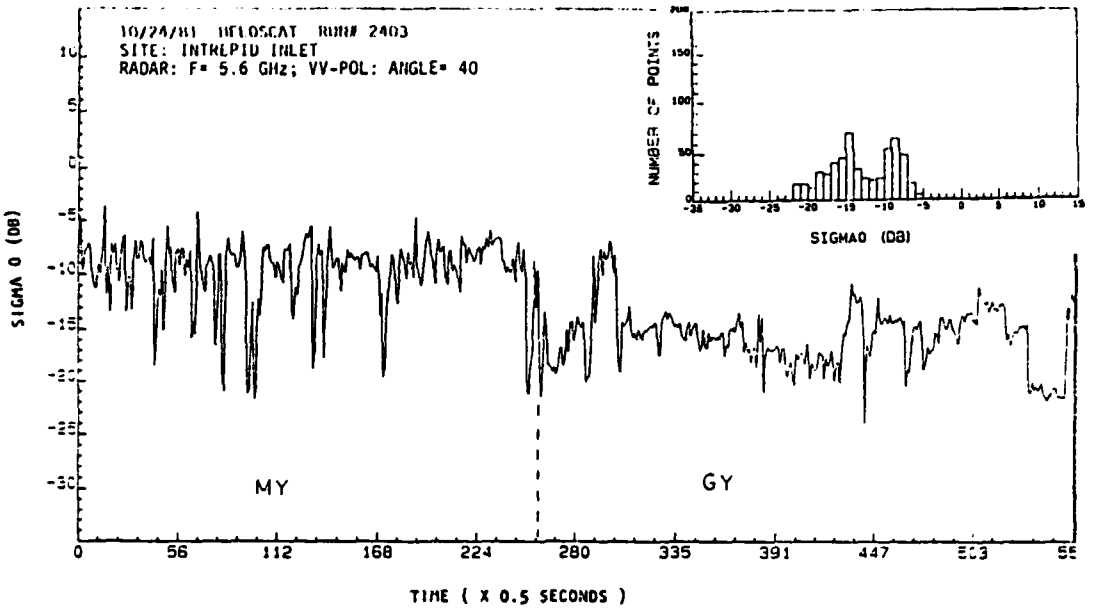

(a): 5.6 GHz

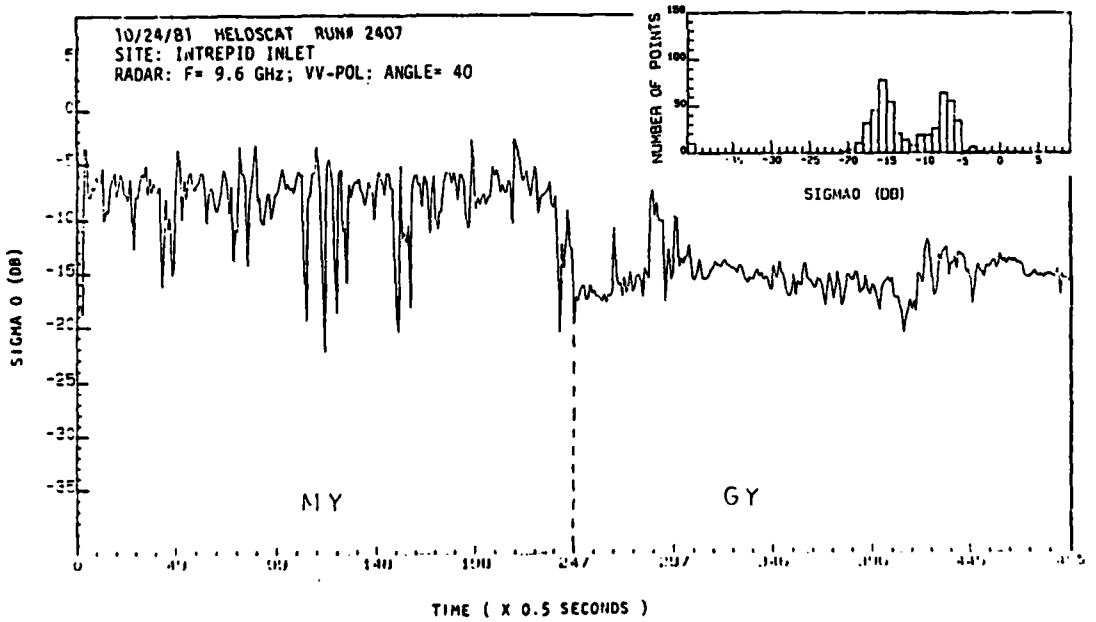

(b): 9.6 GHz

FIGURE 7.1: Profile of a Composite Multiyear Ice Floe

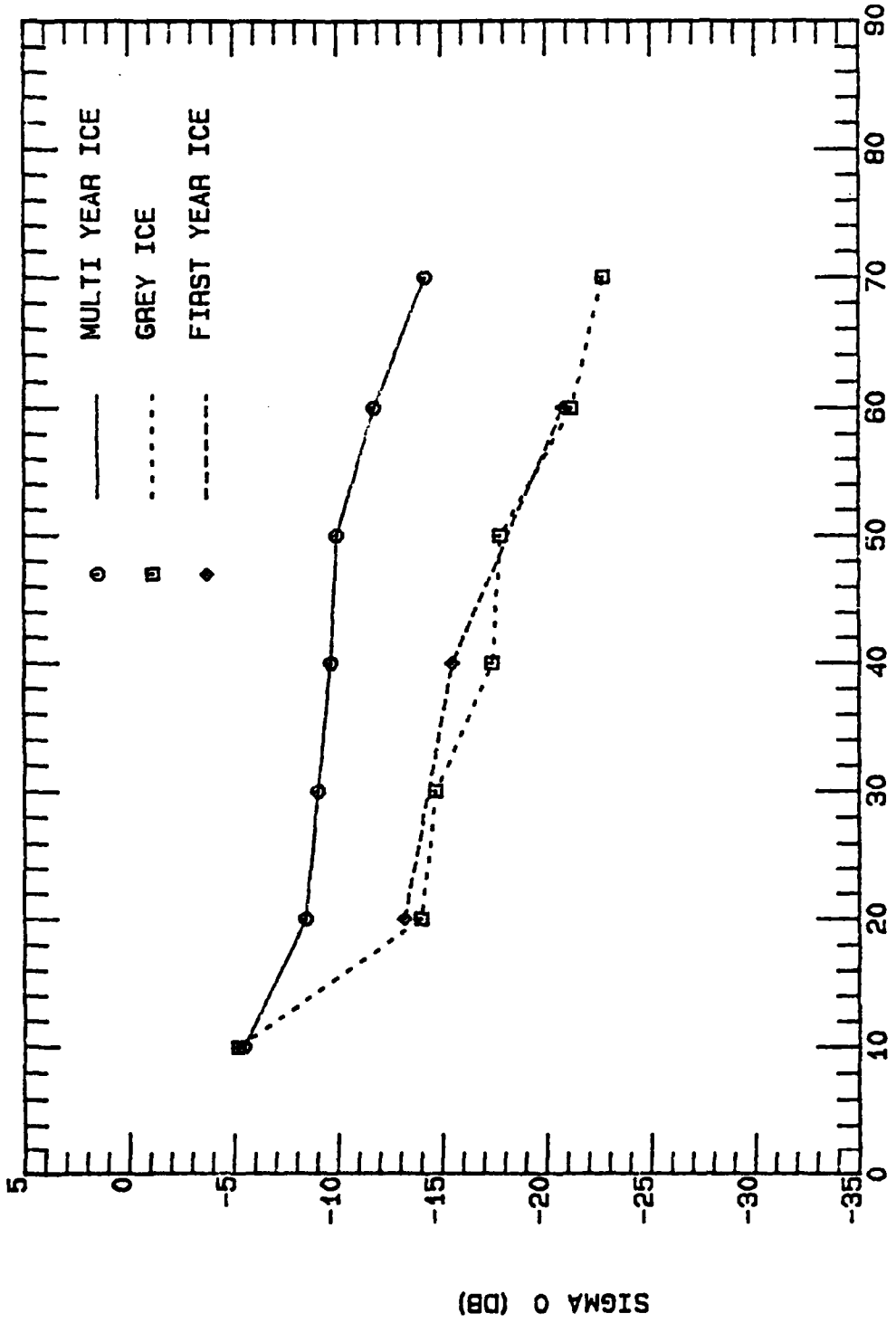

FIGURE 7.2: Typical Angular Behavior of Average σ^0.

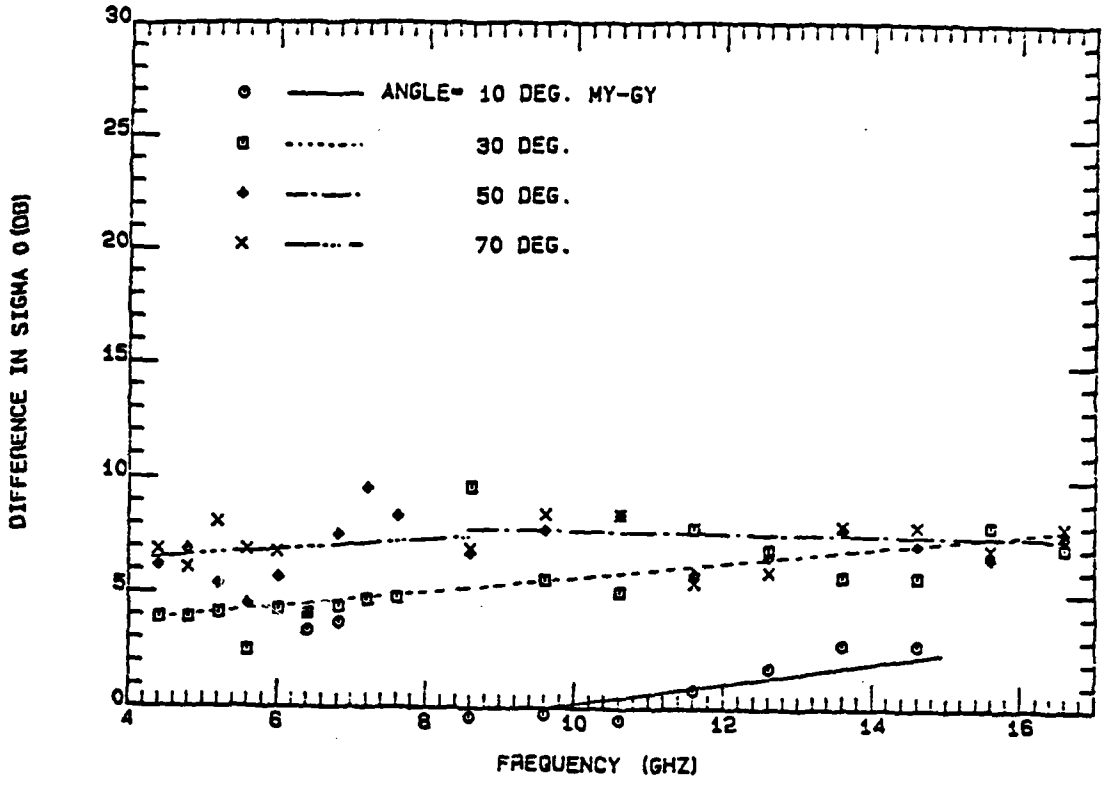

(a)

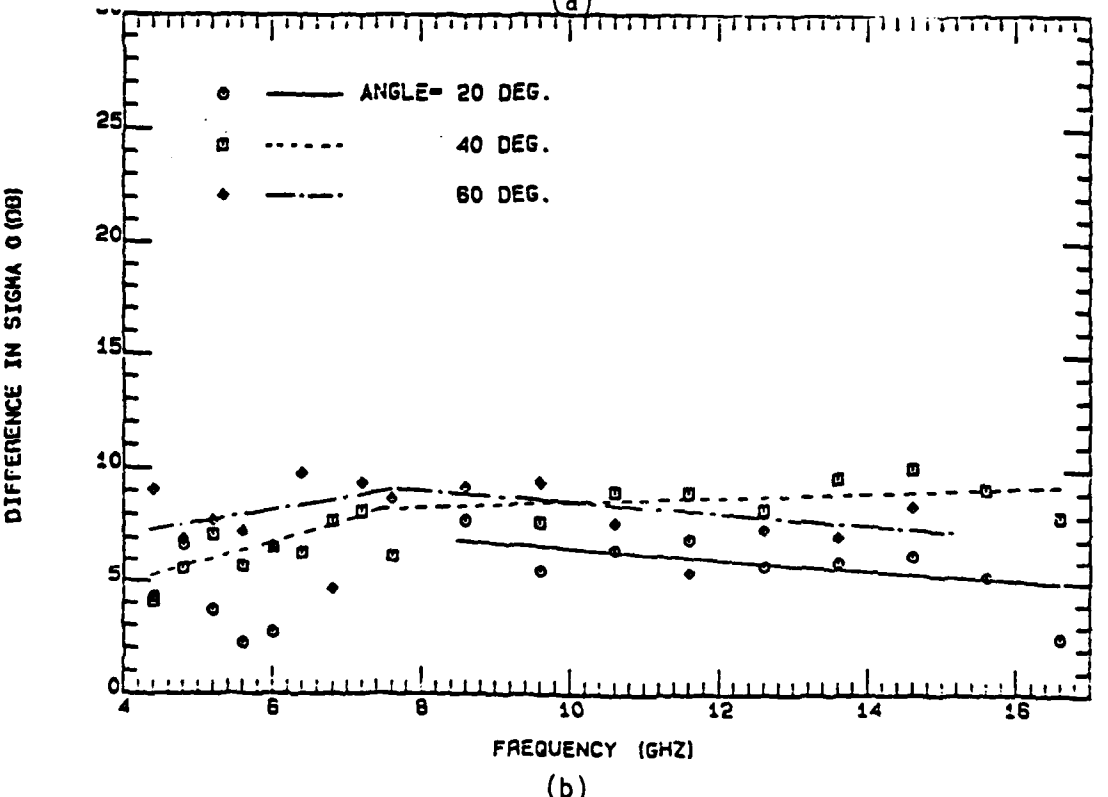

(b)

FIGURE 7.3: Difference between Ice Types. Pol.=HH, Oct. 1981

In Sections 3.0 to 5.0, the physical-optics model for surface scattering and the radiative-transfer model (or semi-empirical model) for volume scattering are shown able to predict the backscattering data from sea ice. These models are tested here against the average σ^0 of multiyear ice.

No ground truth is available for the ice floe, and the model parameters are selected arbitrarily within typical reported values to match the data at the incidence angle of 40°. In Figures 7.4(a) and (b), the frequency behavior at several incidence angles and the angular behavior at several frequencies predicted by the model and measured multiyear ice data are shown. Even though the model parameters are not optimized in any sense, a good general agreement can be seen in both the frequency and angular behavior.

More scatter in the data at low frequencies (C-band) might be due to the variations in the surface roughness, since at low frequencies surface scattering may be the dominant backscattering mechanism for multiyear ice even at large incidence angles (see Section 4.2 and Figure 4.12). The volume scattering is characterized by a very slow angular drop-off (see Figure 7.4(b)).

In Section 3.0, it was shown that the physical-optics model, using the exponential correlation function, may be able to explain the data from thick first-year ice. The model is tested for the data taken from the grey ice (about 15 cm thick). The air temperature was about -20° C, and the salinity data was not available, although it is usually high for thin types of sea ice. Therefore, the dielectric constant was set to be 3.5 (see Figure 2.7). The small scale roughness was not measured, so it was adjusted to match theoretical scatter and data at 40° incidence

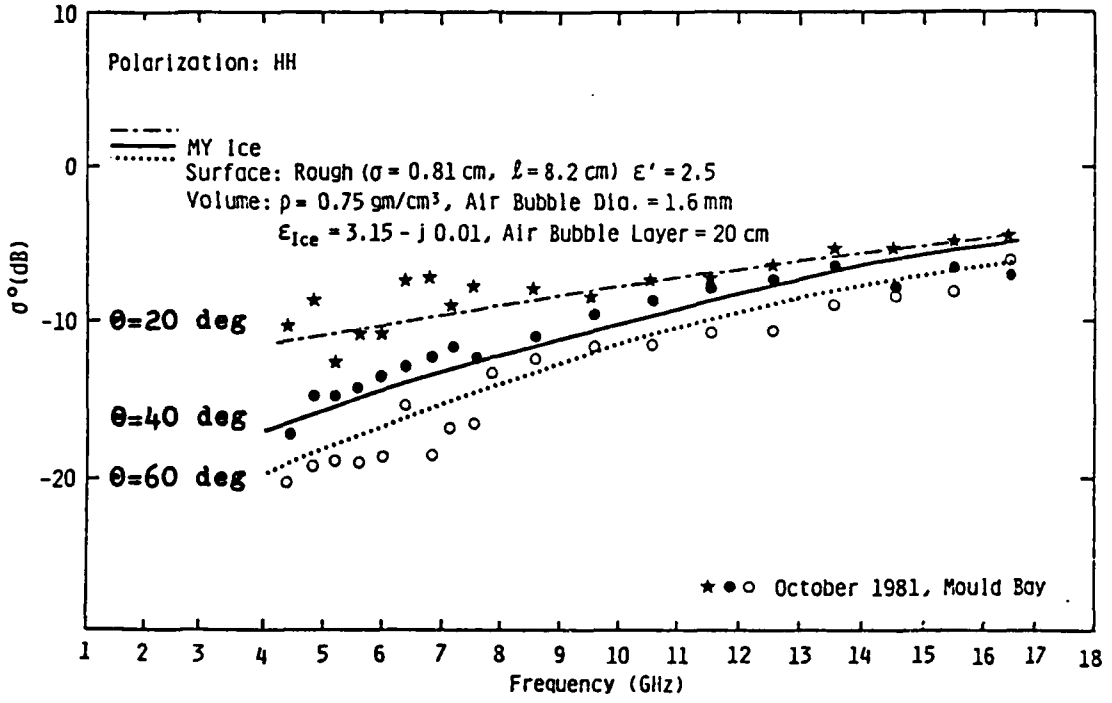

FIGURE 7.4(a): Measured and Predicted Average σ^0 of Multiyear Ice. The model parameters are chosen to match the data at 40°. At low frequencies (C-band), the surface scattering is dominant and therefore more scatter in the data can be seen.

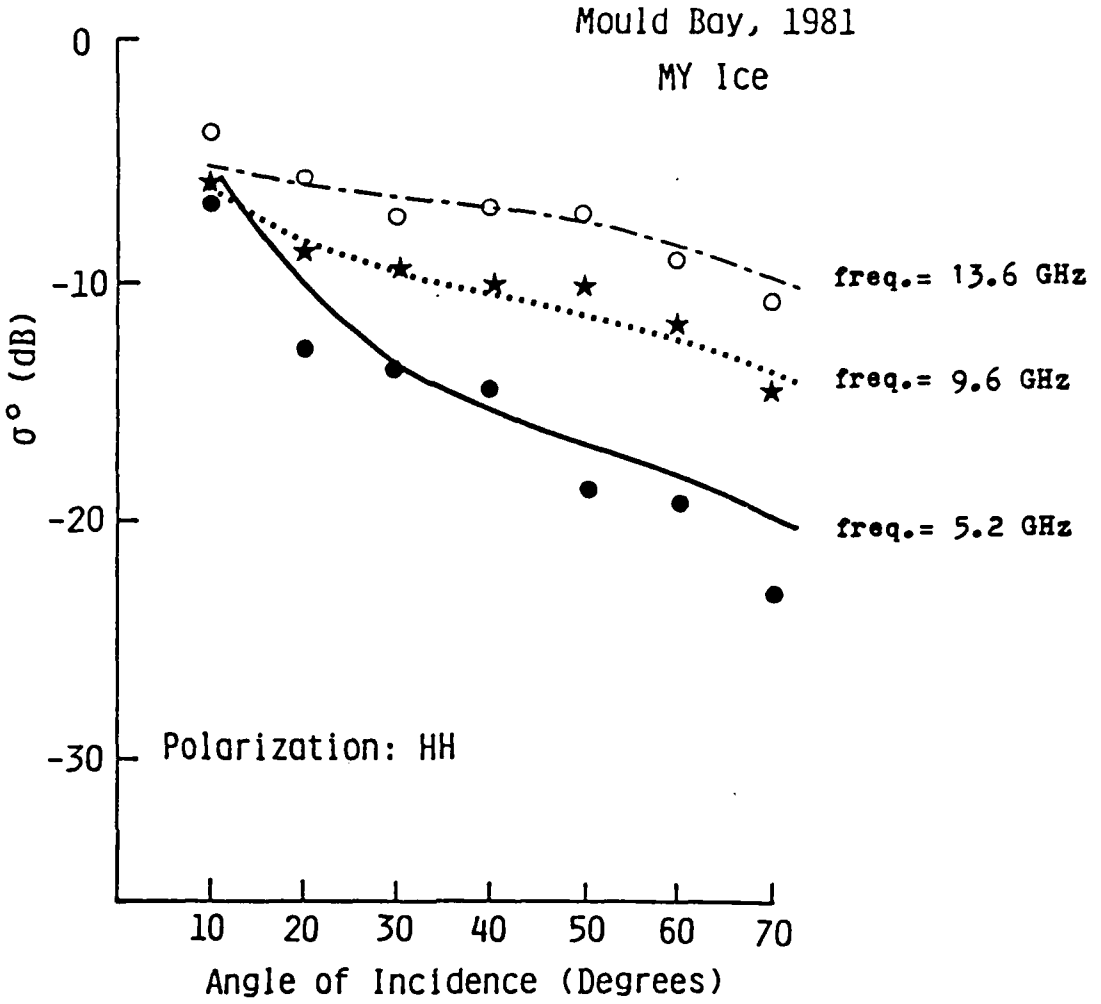

FIGURE 7.4(b): Measured and Predicted Average σ^0 of Multiyear Ice. The model parameters are the same as shown in (a). At 13.6 GHz, the main contribution is from the volume, while at 5.2 GHz, the surface scattering is dominant.

angle. In Figures 7.5(a) and (b), the measured and predicted frequency and angular behavior of σ^0 of grey ice are shown. The match is not as good as was the case with multiyear ice. Most of the multifrequency data were taken using the frequency-stepping scheme while flying over an ice floe with varying degrees of deformation, so this is not surprising. Also, at low frequencies, it is possible that the irregular ice bottom might have been reached with the waves (see Figure 5.5), while the model does not include the effect of ice bottom. Even so, the shape of the model prediction matches that of the data reasonably well.

In Figures 6.1(a) and (b), predicted and measured σ^0 of the multiyear ice and grey ice were shown together.

7.1.2 First-Year Ice

The first-year ice in Mould Bay was about 30 to 35 cm thick at the time of measurement and the surface was covered with 3 to 10 cm of snow. The ice surface had varying degrees of roughness, primarily due to rafting. Figure 7.6 shows two of the profiles across Mould Bay. The flight line across Mould Bay was divided into 10 intervals. The first and last are the heavily rafted areas near the shore and they usually show higher σ^0 than the rest of the intervals.

The average σ^0 values for these intervals show up to 4 to 5 dB differences. Quantitative surface roughness information is not available, but according to the descriptive surface information the ice had widely varying (from smooth to very rough) surfaces; so the differences in average σ^0 between the intervals are not surprising (see Figure 6.5). The flight line had varying thickness of snow cover and sometimes large snow drifts were included. Actually, the snow cover

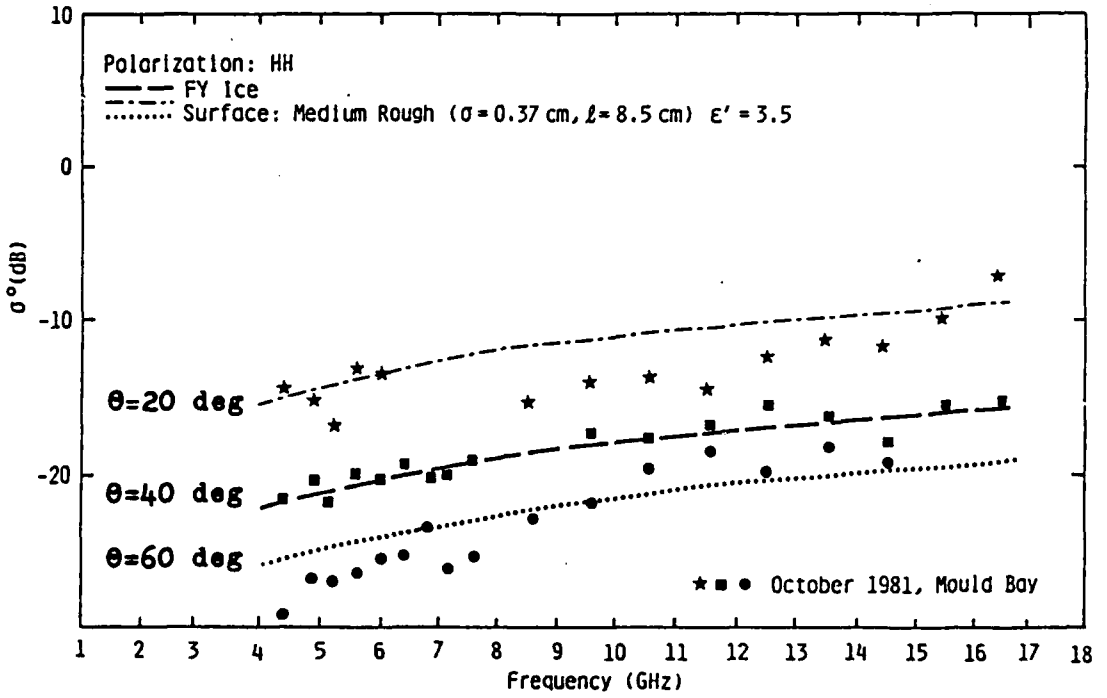

FIGURE 7.5(a): Measured and Predicted σ^0 of Grey ice. The model parameters are chosen to match the data at 40°.

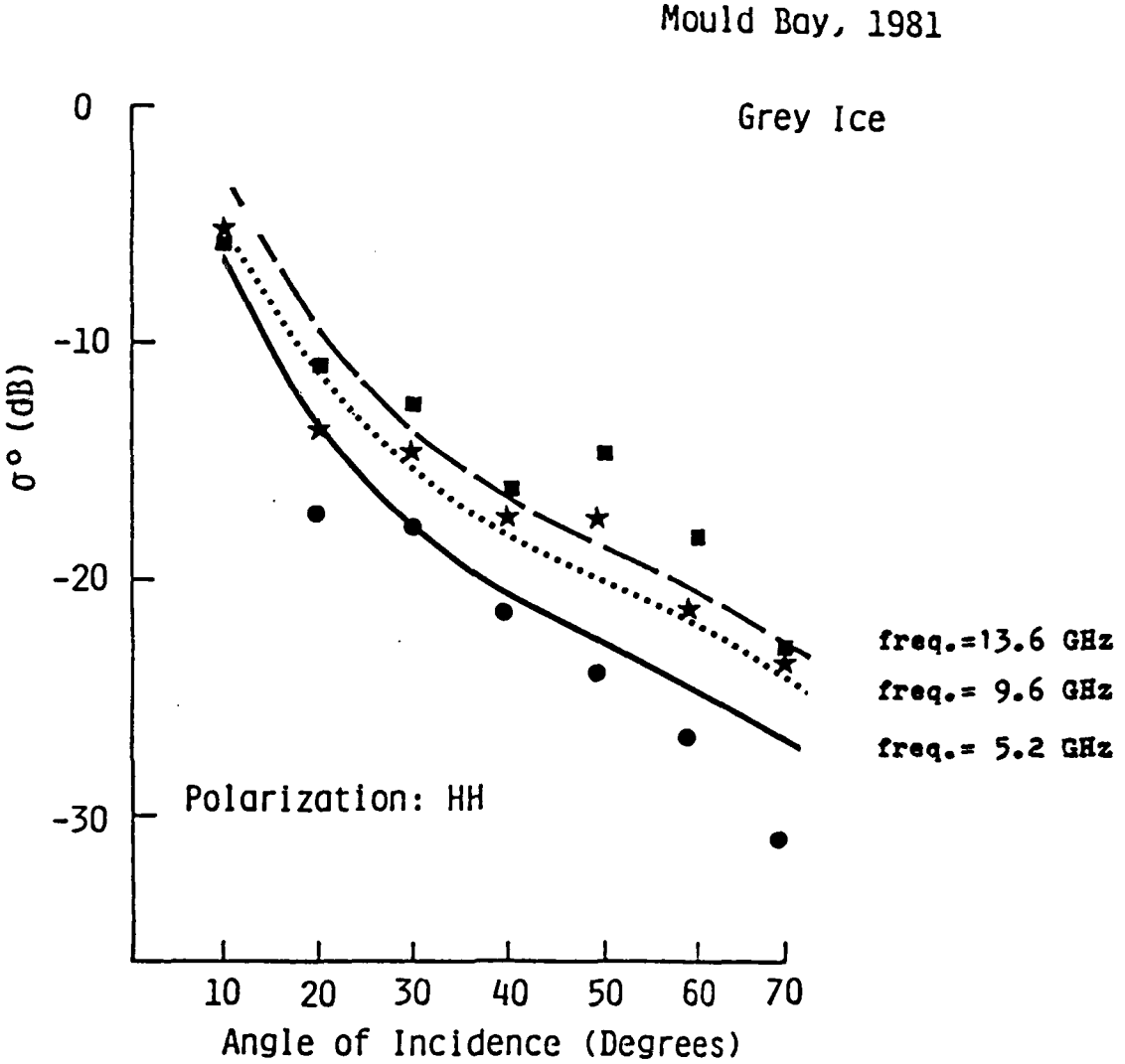

FIGURE 7.5(b): Measured and Predicted Average σ^0 of Grey Ice. The model parameters are the same as shown in (a).

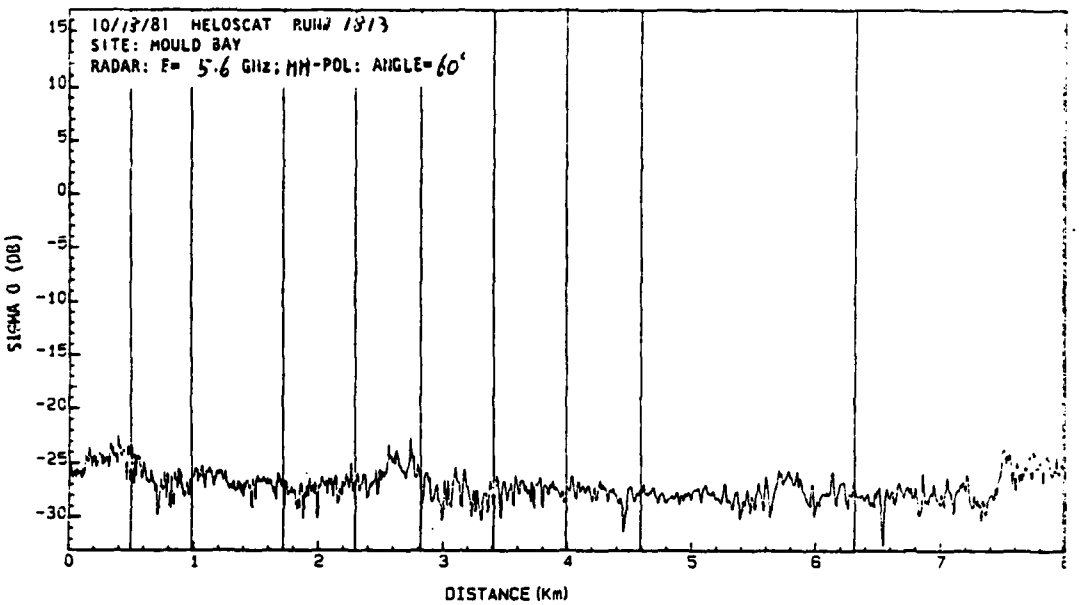

(a): 5.6 GHz

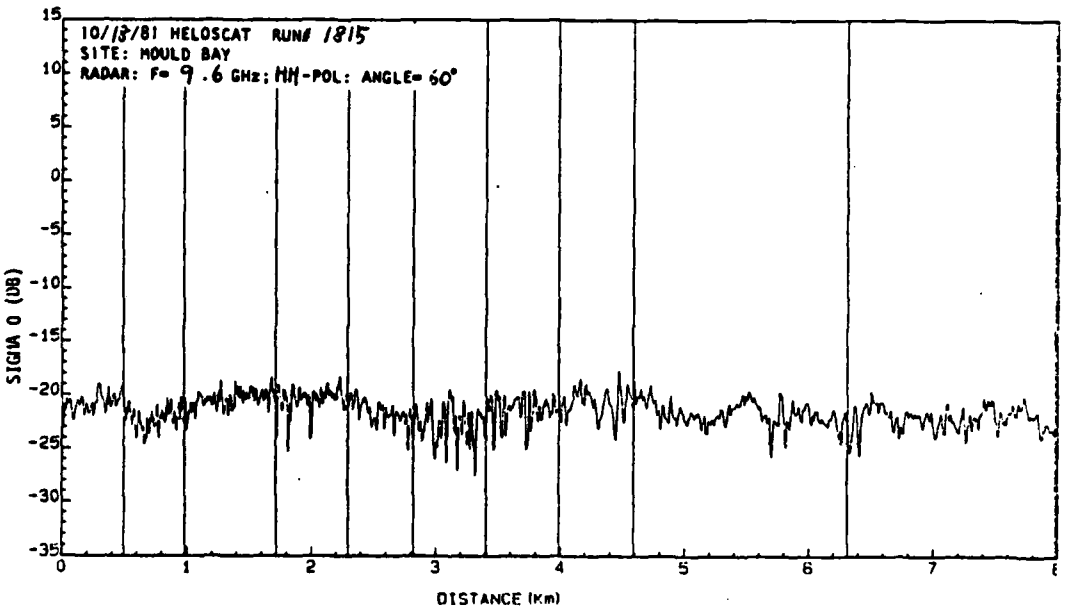

(b): 9.6 GHz

FIGURE 7.6: Profile of Mould Bay First-Year Ice

might have reduced the variation in measured σ^0 in the sense that snow cover on smooth ice with low σ^0 contributes more than the snow cover on rough ice with high σ^0 (see Section 5.3.3.1 and Figure 5.10).

Sample snow and ice thicknesses, and also salinity profiles are available for each interval, but this sparse information is not expected to correlate directly with the measured σ^0 because the surface roughness is expected to be the dominant factor determining the response from first-year ice.

On the average, first-year ice showed σ^0 similar to that of grey ice with HH-polarization (see Figure 7.2), while σ^0 of grey ice was higher than that of first-year ice with VV-polarization as shown in Figure 7.7. In Figure 7.8, the difference in average σ^0 between multiyear ice and first-year ice with VV-polarization is shown. X-Ku-band frequencies seem to be better than C-band frequencies in discriminating multiyear ice from first-year ice.

7.1.3 Shore-Fast Ice

Heavily deformed shore-fast ice at Hardinge Bay was also investigated. A river-like flat area was running through the fast ice, but due to the malfunction of the target encoder switch, this was hard to separate. A very high ridge (6 to 10 m tall) gave about 20 dB higher return than the flat area with 4.4 GHz, and various ridges had 5 to 10 dB higher σ^0 than uniform shore-fast ice. On the average, the whole floe of shore-fast ice showed similar or 2 to 3 dB lower σ^0 than multiyear ice with Vv-polarization (see Figure 7.7). The X-band SLAR imagery of this area showed many dark spots, and the average σ^0

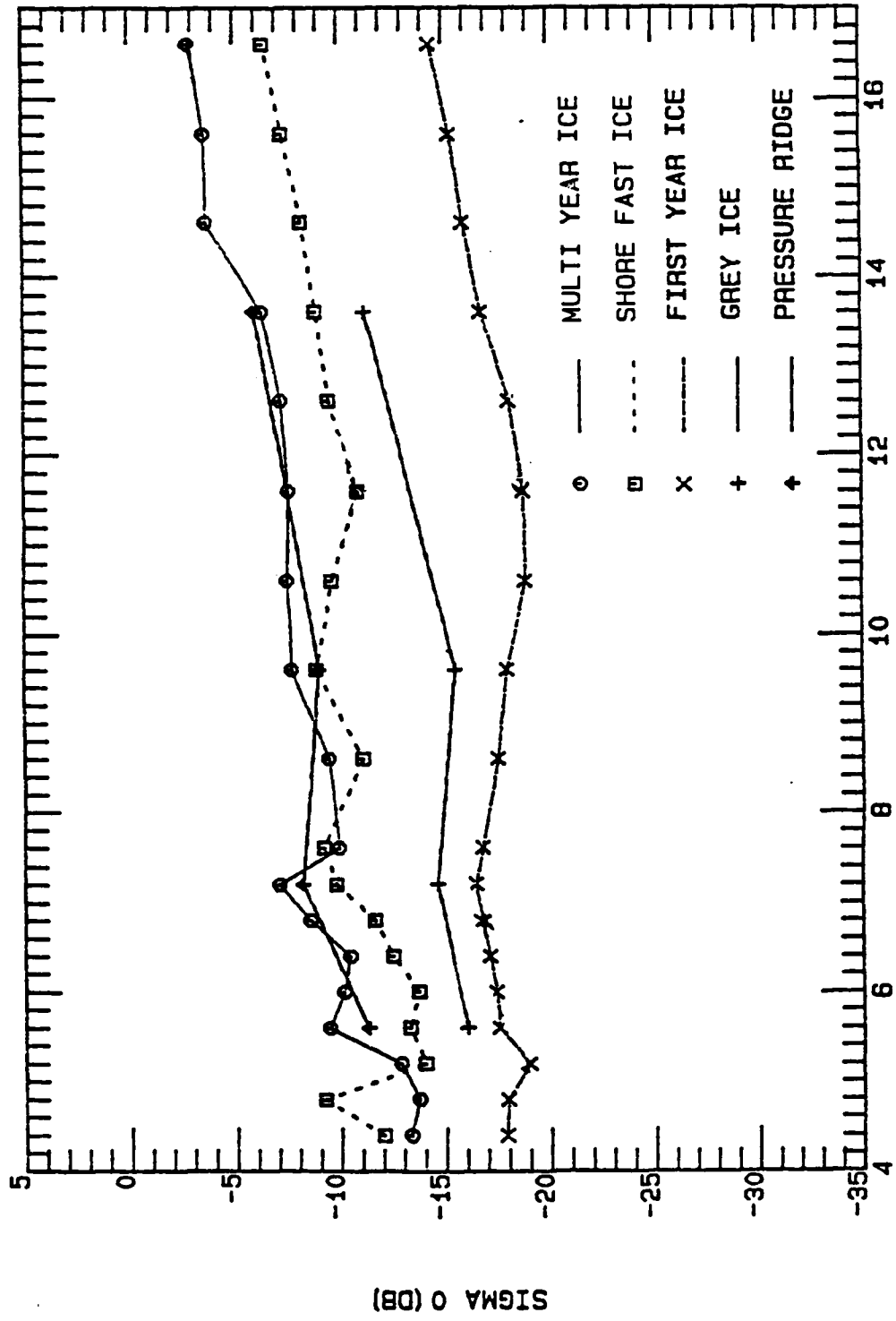

FIGURE 7.7: Frequency Response of σ^0 for Several Types of Ice with VV-Polarization.

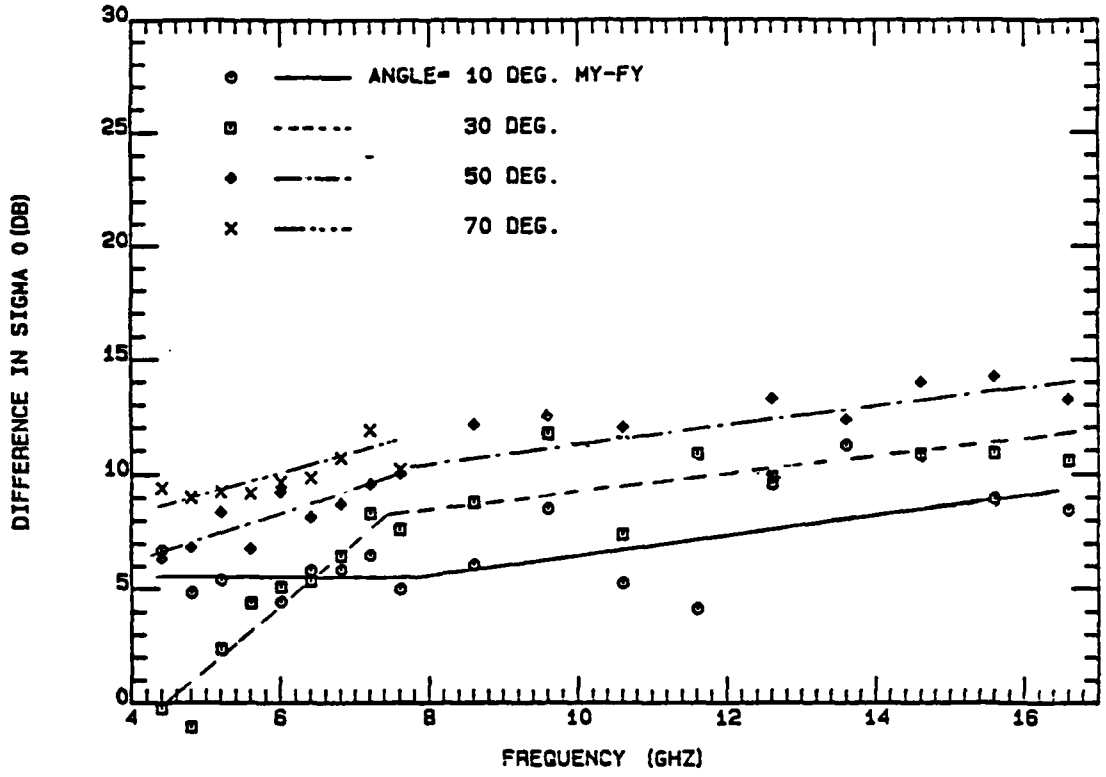

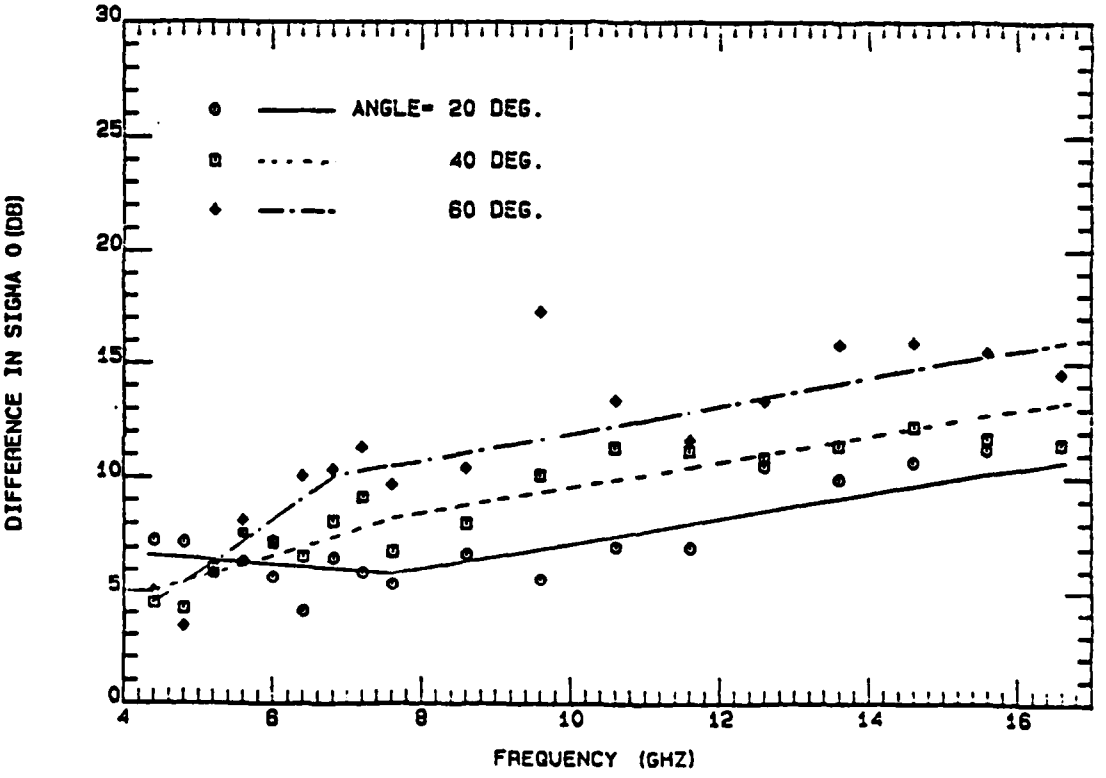

FIGURE 7.8: Difference Between Multiyear Ice and First-Year Ice with VV-Polarization.

calculated may be a little too low because the averaging process averaged the whole flight lines, including all these flat areas (river).

7.1.4 Lake Ice

Fresh-water lake ice showed average σ^0 similar to the first-year ice at C-band frequencies as shown in Figure 7.9. Above X-band frequencies the lake ice had higher σ^0 than first-year ice. Detailed ground truth is not available, but it may be possible that the lake ice contained a large enough amount of air bubbles to show a significant volume scattering effect at high frequencies.

7.2 Surface-Based Experiment Results

A smooth area of thin first-year ice in Mould Bay and a large, mobile multiyear ice floe were investigated with the surface-based system. Unusually warm weather (-4° C) when the first-year ice was investigated caused a part of the snow layer (about 0.5 to 1.2 cm) to be water-saturated, and it provided a unique data set. The multiyear ice exhibited very uniform hummock and meltpond formation, and a large hummock and a large meltpond were picked for separate investigations, which are not usually possible with airborne systems.

7.2.1 Thin First-Year Ice Under Warm Temperature

A representative area (10 meters by 20 meters) of first-year ice in Mould Bay was chosen for a detailed study. The ice was covered with 5 to 9 cm of snow (see Figure 5.7(b) for a profile), and the snow was composed of 3 main layers; the top was a fine-grained, low-density drifted snow 2.6 to 4.8 cm deep; the second layer was a wet layer 0.4 to

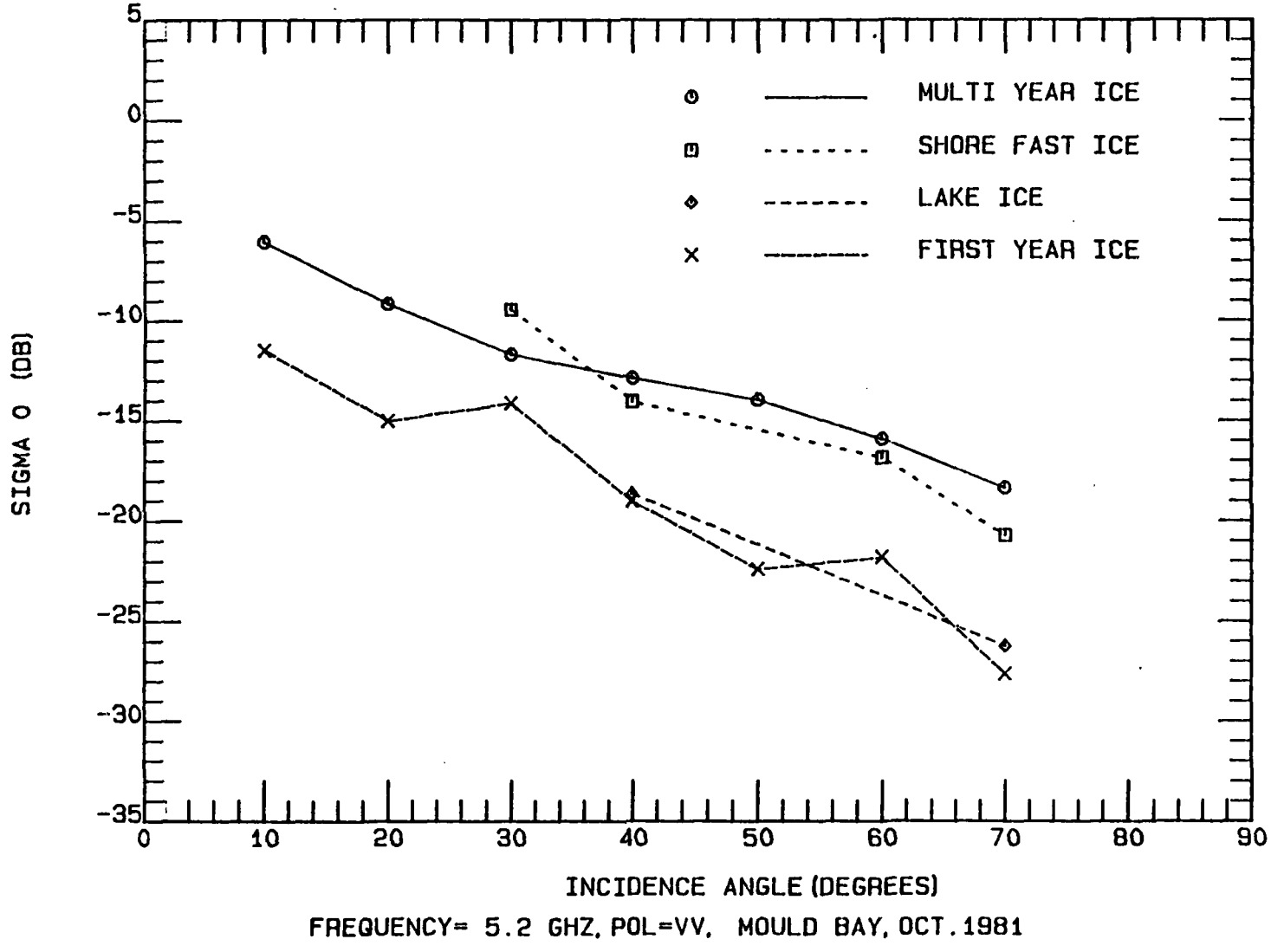

FIGURE 7.9: Typical Angular Behavior of σ^0.

1.2 cm thick with very high salinity (15% to 20%); the bottom snow layer was the old frost-flower zone of 0.6 to 1 cm (often filled with water).

This type of 4-layer (3 snow layers and ice) situation is beyond the scope of this study from the points of view both of the backscattering theories and of the available works on the dielectric properties of wet snow layer saturated with saline water. Also the dielectric properties of a water-filled frost-flower zone or the sea ice at high temperature (-2° C) have never been well established.

The scatterometer was moved 20 times within the studied area to get spatially independent samples, and some detailed ground truth is available for selected sites. The situation seems to be very complicated, and no simple relations between the backscattered power and the ground truth were found.

The average σ^0 of thin first-year ice (about 30 cm thick) under wet snow cover is shown in Figure 7.10, together with that of multiyear ice. The multiyear ice was studied at a colder temperature (-15° C), and direct comparison may not be very meaningful. Figure 7.10 shows that the average σ^0 of thin first-year ice at a warm temperature is quite comparable to that of multiyear ice at a colder temperature.

7.2.2 Multiyear Ice

The area chosen for the surface-based study was in the center of a large, mobile multiyear ice floe. Two sites were selected; one was a representative hummock area, and the other was a refrozen meltpond. Both are integral parts of the multiyear ice.

The hummock area was covered with 2 to 5 cm of hard, crystalling snow (see Figure 5.7(a) for a snow profile of the studied area) and a

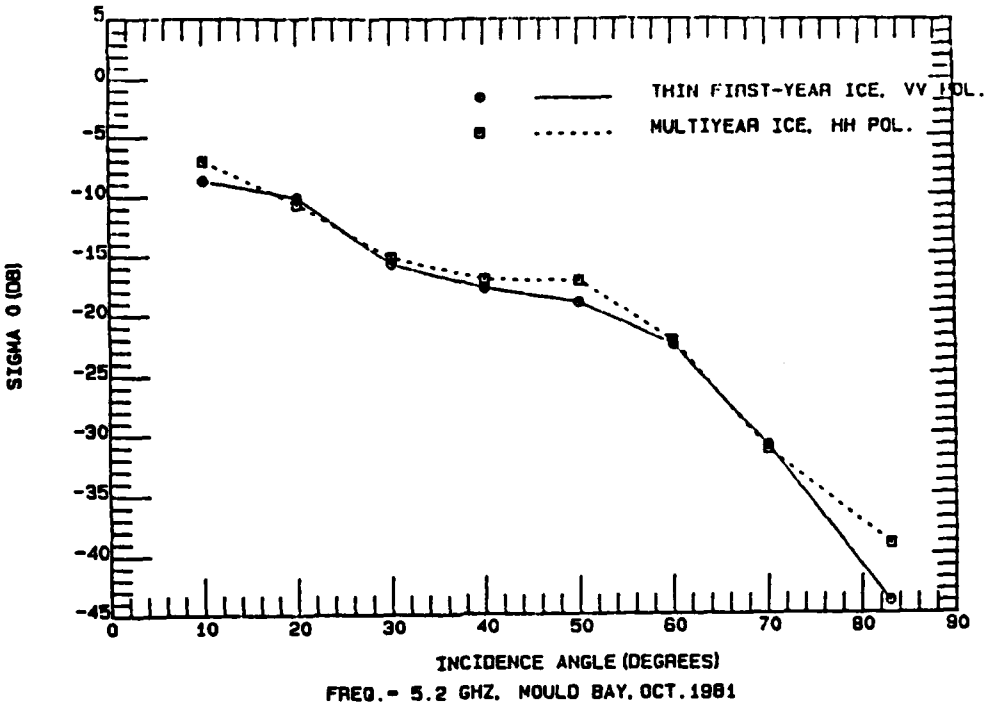

(a)

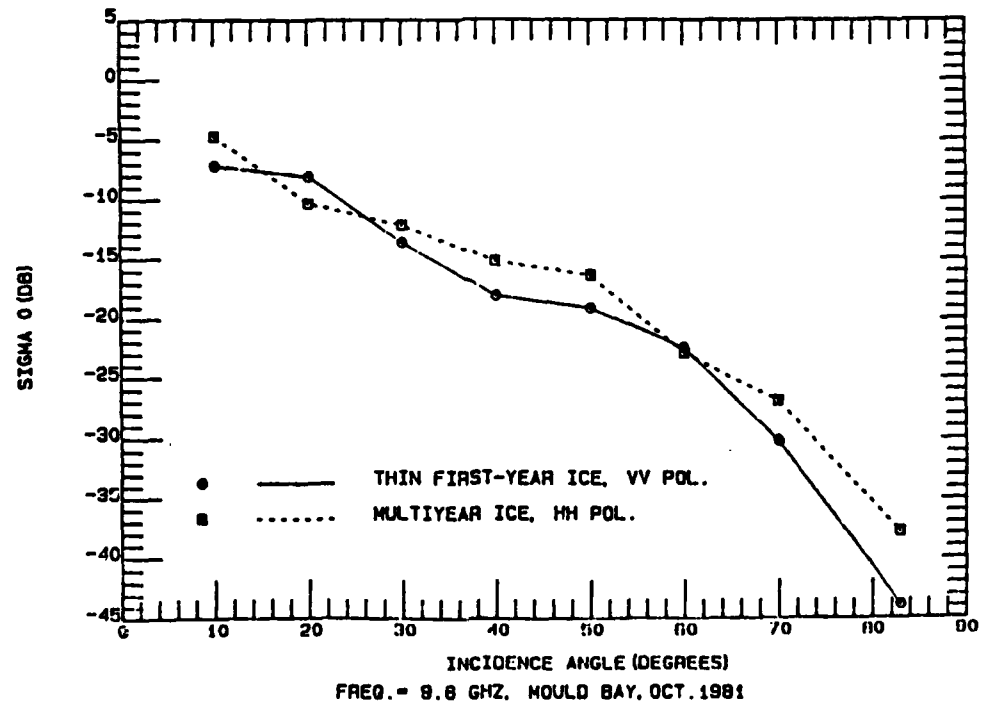

(b)

FIGURE 7.10: Average σ^0 of Thin First-Year Ice and Multiyear Ice--Surface-Based Results.

gradual snow-ice interface (about 1 cm) was found on top of the milky, opaque ice layer. Several ice samples were collected from the hummock area to measure the density and salinity profiles of the multiyear ice. The ice cores showed typical multiyear ice characteristics, having a milky layer on top followed by the clear ice layer. The milky ice layer with air bubbles was 10 to 20 cm thick, and the density of the top layer was low, from 0.62 to 0.8 gm/cm^3. However, some of the salinities of the top layer were unreasonably high, from 0.8 to as high as $8.9^{o}/oo$. This means that the loss through the air-bubble layer is very high, and therefore the volume-scattering contribution of the air bubbles could have been reduced significantly (see Figure 4.6(a)).

The shape of the angular behavior of σ^{o} of multiyear ice shown in Figure 7.10 is very similar to that of first-year ice, and one possible reason may be the high salinity of the multiyear ice which reduced the volume-scattering contribution of the multiyear ice.

The absolute calibration of the surface-based system was in question, and therefore the theoretical model fit discussed in previous sections was not attempted for the surface-based results.

The refrozen meltpond was about 40-cm thick and had 3 to 9 cm of fine-grained snow cover on top (see Figure 5.7(c) for the snow profile of the studied area). The meltpool formed during the summer was not completely refrozen to the bottom by October, and beneath the refrozen ice layer, there was about 30 cm of water pool above the main multiyear ice floe which was suspected to be more than 3 m thick.

The salinity profiles provided an interesting contrast with that of the multiyear hummock ice. The shape of the profile resembled more that of first-year ice than that of hummock, having high values of salinity

at top and bottom. The salinity of the top 1 to 2 cm was 3.3 to 6.8°/oo. The density was generally higher than that of the multiyear hummock, suggesting that there were fewer air bubbles in the meltpond ice. Due to the high salinity and high density, the volume-scattering contribution of the ice layer is not expected to be very much. The thicker layer of snow on the meltpool might have contributed more volume scattering at higher frequencies than about 13 GHz as suggested in Figure 7.11(a).

Unlike the helicopter-borne data set, the surface-based results always show higher σ^0 at low C-band frequencies and at high Ku-band frequencies. Some of the differences are suspected to result from the calibration error.

In Figure 7.11(b), the frequency behavior of σ^0 of thin first-year ice is compared to that of the weighted average of multiyear ice. The exact relative percentage of meltpond or hummock was not determined, but 70% hummock and 30% meltpond was assumed in the calculation. The difference between thin first-year ice under warm temperature and the average multiyear ice seemed to be approximately constant (about 1 to 3 dB) up to 10 GHz, with an increase above 13 GHz. The lines drawn in Figure 7.11 are eye-fit curves to show approximate behaviors.

The smaller contrast between the two major types of ice compared to that of helicopter-borne results (see Figure 7.8) might have resulted either from the higher σ^0 of thin first-year ice under warm temperature or lower σ^0 of multiyear ice with high salinity (loss) or both. Also, in the surface-based experiment, two different like-polarizations were used; VV for first-year ice, and HH for multiyear ice.

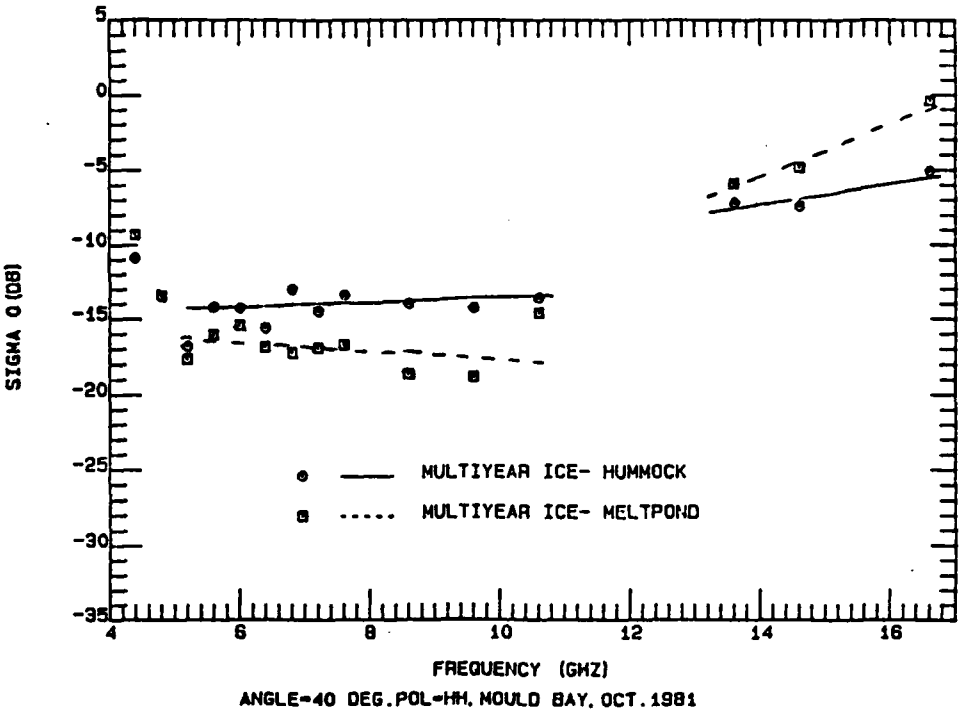

(a): Multiyear ice hummock and meltpond

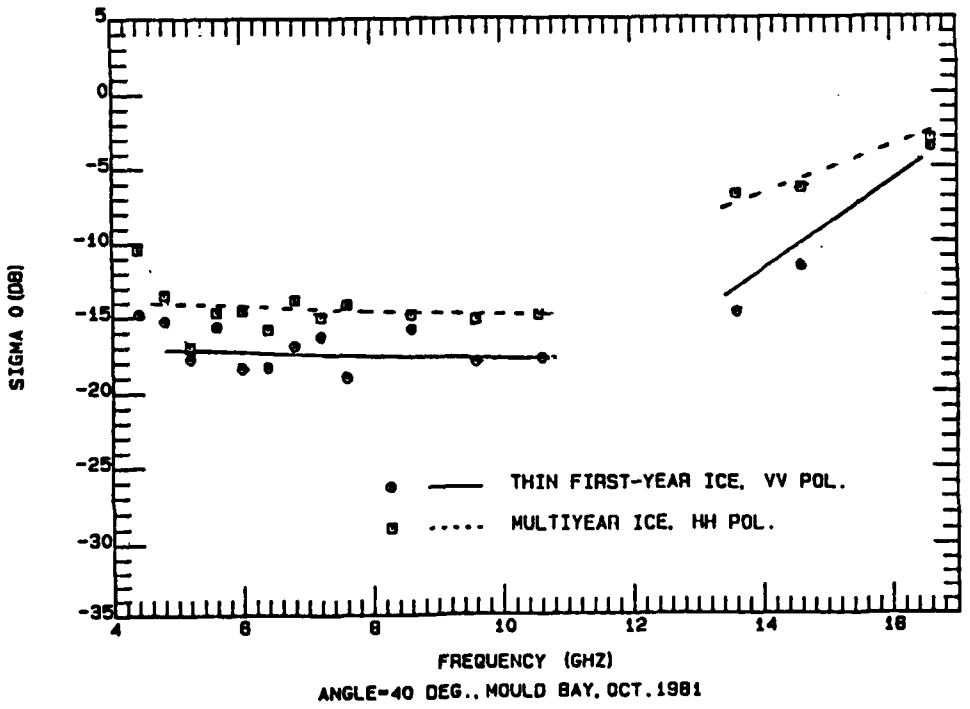

(b): Thin first-year ice and average multiyear ice

FIGURE 7.11: Frequency Behavior of σ^0 of Multiyear Ice and First-Year Ice--Surface-Based Results

7.3 Summary

The measurement results of sea ice under fall conditions are summarized in this section. At late October, it was shown that large contrast exists in σ^0 between multiyear ice and grey ice or first-year ice. In early October, when it was warm, the thin first-year ice and the multiyear ice gave similar signatures.

An attempt was made to fit the observations with the theoretical models presented in Sections 3.0 to 5.0. With appropriate choice of model parameters within reported ranges of values, the model prediction matches the multiyear ice data very well, and the grey ice data to some degree.

Most of the data were collected using the helicopter-borne system, but the ground-truth support was limited to first-year ice due to logistics problems. The available ground truth shows large variations of snow and ice characteristics even within a 1-m by 1-m area, and raises a question about the oversimplified models. The snow cover on sea ice has several layers with different characteristics (moisture condition, salinity, etc.), and the gradual snow-ice interface layer suggests that it may not be valid to treat a snow layer just as an additional scattering layer on top of ice. A further experimental and theoretical study is needed.

8.0 SUMMARY, CONCLUSIONS AND RECOMMENDATIONS

8.1 Summary and Conclusions

The main objectives of this research were to:

(1) develop a better understanding, theoretically and experimentally, of radar backscatter from sea ice; and

(2) identify optimum radar parameters (frequency, incidence angle, and polarization) for discriminating different ice types.

To fulfill these objectives, the following studies were conducted. First, an extensive literature search was done to gather all the available physical and electrical characteristics of sea ice considered to be relevant to microwave remote sensing.

Many measurements of the dielectric properties of sea ice have been reported, and they show large variations depending on temperature, salinity, ice types, and also on the measurement or sampling schemes. A dielectric constant model using a complicated dielectric mixture theory was reported, but to minimize the model parameters in further development of a backscatter model for sea ice, it was concluded that the simple empirical equations relating the dielectric constant of sea ice to estimated brine volume of sea ice would suffice. In this study, the empirical equations given by Vant [1974, 1978] and Hallikainen [1982] were used and summarized in Section 2.0. Other characteristics of sea ice were stated in appropriate sections where they were needed.

Next, the assumption was tested that surface scattering is the dominant backscattering mechanism for first-year ice, and that the volume scattering is dominant for multiyear ice.

The surface scattering theories were reviewed, and the signatures of first-year ice were tested against the predictions of surface scattering models. The measurements of small-scale surface roughness [Onstott, 1983] satisfy the requirements of the Kirchhoff model for the frequencies between 4 and 18 GHz, and it was shown that the physical-optics model using an exponential correlation function provides a good fit to measured angular and frequency behaviors of the backscattering coefficient of first-year ice. This was summarized in Section 3.0.

Section 4.0 treats the volume-scattering model for multiyear ice. A scattering volume can be modeled either as a continuous random medium characterized with correlation lengths and variances, or as a discrete medium embedded with random scatterers characterized with scattering albedo and optical depth. In this study the latter approach was adapted using the radiative-transfer model.

The air bubbles in the recrystallized ice layer in the top portion of the multiyear ice were assumed to be the primary volume scatterers, and the effect of varying physical characteristics (air bubble size, density, loss of the ice, layer depth) was studied. The surface scattering is always present, and when the frequency is below about X-band, it was shown that the volume scattering contribution can be smaller than the surface scattering contribution. The backscattered power is the sum of these two; this sum provides a good general agreement to the measured frequency and angular behavior of σ^0 of multiyear ice.

The complicated theoretical solution of the radiative-transfer equation reduces to a simple analytical solution if the multiple scattering and the volume-surface interaction can be neglected. In

Section 5.0, the volume backscattering coefficient given by the sum of the backscattering coefficients of all the single scatterers was shown to be a good approximation to the value calculated with the radiative-transfer equation. Using the simple model, the volume scattering contribution of first-year ice was calculated and it was shown to be negligible for most of the cases.

The effect of snow cover on sea ice was also studied in Section 5.0. The low thermal conductivity of snow compared to that of sea ice effectively raises the temperature of ice surface and changes the Fresnel reflection coefficient of the surface and the volume scattering characteristics. However, for active remote sensing, it was shown that the temperature effect is small (less than 0.3 dB) when the air temperature is below -10° C.

The backscattering contribution of the snow cover was calculated using the empirical equations [Ulaby et al., 1982] describing the effect of snow cover on natural surfaces. The basic concept of the empirical model is that the effect of snow cover on some surfaces depends on the relative difference between the σ^0 of bare surface and that of snow of infinite depth.

The σ^0 of dry snow is far greater than that of a smooth ice surface, and the effect of snow cover can be severe (5 cm of snow cover can raise the σ^0 by 8 dB at 9 GHz). For a large floe of first-year ice with a varying surface roughness, the effect of snow cover would be to reduce the variation of σ^0 due to surface roughness variation of the ice surface. The presence of wet snow cover can block the volume scattering contribution of the multiyear ice.

In an attempt to identify a better set of radar parameters for sea ice classification, Section 6.0 provides a summary of experimental findings reported so far in terms of preferred radar parameters. Also, the theoretical models which seemed to be able to predict or match the data sets with a reasonable set of model parameters were selected. By adjusting the model parameters within reported ranges of values, the possible ranges of values of σ^0 for multiyear ice and first-year ice were calculated. From these ranges of values, it was shown that the best radar parameters for sea ice monitoring are (1) higher frequencies than about X-band, and (2) incidence angles larger than 30° or 40°. No specific resonances have been found that might favor any specific frequency or incidence angle, and the theoretical findings agree with the general experimental conclusions.

The optimum polarization could not be selected. This was partly due to the lack of reliable cross-polarized data for the whole frequency range, and partly due to the inability of scattering theories to properly explain the polarization dependence of the backscatter from sea ice. Because depolarization is a secondary effect for the surface scattering (first-year ice) while this is not true for volume scattering (multiyear ice), cross-polarization should be better than like-polarization in discriminating multiyear ice from first-year ice. Because the cross-polarized σ^0 is big enough for multiyear ice, it could be used to detect multiyear ice from all the surroundings without having to have a greater dynamic range.

Measurements were made during October 1981 of the radar backscatter properties of sea ice under fall conditions in Mould Bay, N.W.T., Canada, as part of the FIREX/RADARSAT project. Section 7.0 provides a

brief summary of the experimental findings. Late in October, a large contrast in σ^0 existed between multiyear ice and first-year ice or grey ice. However, in early October, with warmer temperatures, the thin first-year ice and multiyear ice can give similar signatures.

The theoretical models presented in Sections 3.0 to 5.0 were tested with the data taken during the expedition. With appropriate choice of model parameters, the model prediction matches the multiyear ice data very well, and the grey ice data to some extent.

8.2 Recommendations

The limitations of the present results, which can also be viewed as recommendations for future research, are:

(1) Although the small-scale surface roughness information given by Onstott [1983] provided general guidance on the ranges of values it may have, these may not be the absolute limits. There is a definite need to do similar measurements, and to tabulate the ranges of values of small-scale surface roughness of multiyear and thinner types of sea ice.

(2) The behavior of the dielectric constant, especially the imaginary part, needs to be studied further to accurately model the σ^0 of multiyear ice.

(3) For multiyear ice, the characteristics of the volume-scattering layer need to be established (average or the distribution of the diameter of air bubbles, density of multiyear ice). The reported values, or the values used in this research may not be representative of the characteristics of multiyear ice in all regions or under all conditions.

(4) The effect of snow cover needs to be studied further. The measurements of dielectric constant of saline-water-saturated snow has rarely been reported, and the snow-ice transition layer effect should be investigated.

(5) The polarization dependence of the backscatter from sea ice has to be studied further, both experimentally and theoretically.

(6) In summer conditions, when the melting starts, the surface conditions change drastically. The concepts presented in this reearch are not expected to be valid during summer, and only a continuous monitoring of sea ice would describe the change of the microwave signature properly.

REFERENCES

Anderson, D.L., "The Physical Constants of Sea Ice," Research, vol. 13(8), 1960, pp. 310-318.

Attema, E.P.W. and F.T. Ulaby, "Vegetation Model as a Water Cloud," Radio Science, vol. 13(2), 1975, pp. 357-364.

Bogorodsky, V.V. and G.P. Khoklov, "Microwave Refractive Index and Absorption of Sea Ice Cover and Newly Formed Ice," Sov. Phys. Tech. Phys., vol. 22(6). Translated by American Institute of Physics, 1977.

Bogorodsky, V.V., "Electromagnetic Characteristics of Sea Ice and Its Radio Sounding," 1978, unpublished.

Campbell, W.J., R.O. Ramseier, P. Gloersen, M.L. Bryan, et al., "Microwave Remote Sensing of Sea Ice in the AIDJEX Main Experiment," Boundary Layer Meteorology, 13, 1978, pp. 309-337.

Campbell, J.K. and A.S. Orange, "The Electrical Anisotropy of Sea Ice in the Horizontal Plane," J. Geophys. Res., vol. 79(33), 1974, pp. 5059-5063.

Carsey, F.D., "Remote Sensing as a Research Tool," Chapter 11 of Air-Sea-Ice Interaction, (N. Untersteiner, ed.), 1982.

Carsey, F.D., R.O. Ramseier and W.F. Weeks, "Sea Ice Mission Requirements for the U.S. FIREX and Canada RADARSAT Programs," Report of the Bilateral Ice Study Team Workshop, Cornell, Ontario, Canada, February 1981, NASA JPL Report, January 1982.

Chang, T.C., P. Gloersen, T. Schmugge, T.T. Wilheit and H.J. Zwally, "Microwave Emission from Snow and Glacier Ice," J. Glacio., vol. 16(74), 1976, pp. 23-39.

Cumming, W.A., "The Dielectric Properties of Ice and Snow at 3.2 cm Wavelength," J. Appl. Phy., vol. 23, no. 7, 1952, pp. 768-773.

Delker, C.V., R.G. Onstott and R.K. Moore, "Radar Scatterometer Measurement of Sea Ice: The SURSAT Experiment," Remote Sensing Laboratory Technical Report 331-17, University of Kansas Center for Research, Inc., Lawrence, Kansas, 1980.

Digby, S.A., "Mould Bay Sea Ice Experiment I, Experiment Summary and Surface Characteristics Report," 82-15, RADARSAT, 1982.

Eom, H.J., "Theoretical Scatter and Emission Models for Microwave Remote Sensing," Ph.D. Thesis, University of Kansas, Lawrence, Kansas, 1982.

Evans, S., "Dielectric Properties of Ice and Snow -- A Review," J. Glacio., vol. 5, 1965, p. 773.

Frankenstein, G. and R. Garner, "Equation for Determining the Brine Volume of Sea Ice from -0.5° to -22.9° C," J. Glacio., vol. 6(48), 1967, pp. 943-944.

Fung, A.K. and M.F. Chen, "Scattering from a Rayleigh Layer with an Irregular Interface," Radio Science, vol. 16(6), 1981, pp. 1337-1347.

Fung, A.K., "Scattering and Depolarization of Electromagnetic Waves by a Horizontally Weakly Inhomogeneous Medium," Appl. Sci. Res., 20, May 1969, pp. 368-380.

Fung, A.K. and H.J. Eom, "Transmitted Scattering Coefficients Across Gently Undulating Surface," Remote Sensing Laboratory Technical Report 369-3, University of Kansas Center for Research, Inc., Lawrence, Kansas, 1979.

_____, "Multiple Scattering and Depolarization by Randomly Rough Kirchhoff Surface," IEEE Trans., vol. AP-29(3), 1981, pp. 463-471.

_____, "A Theory of Wave Scattering from an Inhomogeneous Layer with an Irregular Interface," IEEE Trans., vol. AP-29(6), 1981, pp. 899-910.

_____, Application of a Combined Rough Surface and Volume Scattering Theory to Sea Ice and Snow Backscatter," IEEE Trans., vol. GE-20, no. 4, October 1982, pp. 528-536.

_____, "Coherent Scattering of a Spherical Wave from an Irregular Surface," IEEE Trans., vol. AP-31, no. 1, January 1983, pp. 68-72.

Golden, K.M. and S.F. Ackley, "Modeling of Anisotropic Electromagnetic Reflection from Sea Ice," J. Geophys. Res., vol. 86(C9), 1981, pp. 8107-8116.

Gray, A.L., Paper presented at Venice, 1980.

Gray, A.L., R.O. Ramseier and W.J.Campbell, "Scatterometer and SLAR Results Obtained over Arctic Sea Ice," Presented to the 4th Canadian Symposium on Remote Sensing, Quebec City, Canada, May 1977.

Gray, A.L., R.K. Hawkins, C.E. Livingstone, L.D. Arsenault and W.M. Johnstone, "Simultaneous Scatterometer and Radiometer Measurements of Sea Ice Microwave Signatures," IEEE J. Oceanic Engrg., vol. OE-7(1), January 1982, pp. 20-32.

Gray, L., J. Cihlar, S. Parashar and R. Worsfold, "Scatterometer Results from Shorefast and Floating Sea Ice," presented at the 11th International Symposium on Remote Sensing of Environment, Ann Arbor, Michigan, April 1977.

Guindon, B., R.K. Hawkins and G.D. Goodenough, "Spectral-Spatial Analysis of Microwave Sea Ice Data," IEEE IGARSS Digest, vol. 11, 1982.

Hallikainen, M., "Dielectric Properties of Sea Ice at Microwave Frequencies," Helsinki University of Technology, Radio Lab., Report s-94, 1977.

_____, "Dielectric Properties and Passive Remote Sensing of Low-Salinity Sea Ice at UHF Frequencies," ACTA Polytechnica Scandinavia, EE Series No. 45, Helsinki, 1980.

_____, "The Brightness Temperature of Sea Ice and Fresh-Water Ice in the Frequency Range 500 MHz to 37 GHz," IEEE International Geoscience and Remote Sensing Symposium Digest, vol. 11, 1982.

Hallikainen, M., F.T. Ulaby and M. Abdelrazik, "Measurements of the Dielectric Properties of Snow in the 4-18 GHz Frequency Range," Remote Sensing Laboratory Technical Report 527-3, University of Kansas Center for Research, Inc., Lawrence, Kansas, July 1982.

Harrington, R.F., C.T. Swift and J.C. Fedors, "Microwave Radiometric Aircraft Observations of Fabry-Perot Interference Fringes of an Ice-Water System," Paper presented in Venice, 1980.

Hoekstra, P. and P.Cappillino, "Dielectric Properties of Sea and Sodium Chloride Ice at UHF and Microwave Frequencies," J. Geophys. Res., 76(20), 1971, pp. 4922-4931.

Karam, M.A. and A.K. Fung, "Propagation and Scattering in Multi-Layered Random Media with Rough Interfaces," Electromagnetics 2, 1982, pp. 239-256.

Lee, K.K. and A.K. Fung, "Transmitted Scattering Coefficients Across a Slightly Rough Dielectric Boundary," Remote Sensing Laboratory Technical Report 369-2, University of Kansas Center for Research, Inc., Lawrence, Kansas, 1979.

Luther, C.A., J.D. Lyden, R.T. Lowry, C.E. Livingstone, et al., "SAR Studies of Sea Ice," IEEE IGARSS Digest, vol. 11, 1982.

Martin, S., "A Field Study of Brine Drainage and Oil Entrainment in First-Year Sea Ice," J. Glacio., vol. 22(88), 1979, pp. 473-502.

Nawako, M. and N.K. Sinha, "Growth Rate and Salinity Profile of First-Year Sea Ice in the High Arctic," J. Glacio., vol. 27(96), 1981, pp. 315-329.

Onstott, R.G., "Radar Backscatter Study of Sea Ice," Ph.D. Thesis, University of Kansas, Lawrence, Kansas, 1980.

_____, "Ice Surface Characteristics During Summer Conditions," Remote Sensing Laboratory Technical Report, University of Kansas Center for Research, Inc., Lawrence, Kansas, to be published, 1983.

Onstott, R.G., R.K. Moore and W.F. Weeks, "Surface-Based Scatterometer Results of Arctic Sea Ice," IEEE Trans., vol. GE-17(3), 1979, pp. 78-85.

Onstott, R.G., R.K. Moore, S. Gogineni and C. Delker, "Four Years of Low Altitude Sea Ice Broadband Backscatter Measurements," IEEE J. Oceanic Engrg., vol. OE-7, January 1982, pp. 44-50.

Onstott, R.G., R.K. Moore, S. Gogineni, Y.S. Kim and D.B. Bushnell, "Helicopter-Borne Scatterometer," Remote Sensing Laboratory Technical Report 331-24, University of Kansas Center for Research, Inc., Lawrence, Kansas, October 1982.

Onstott, R.G., Y.S. Kim and R.K. Moore, "Preliminary Report on Active Microwave Measurements of Sea Ice Under Fall Conditions," Remote Sensing Laboratory Technical Report 331-28/578-2, University of Kansas Center for Research, Inc., Lawrence, Kansas, August 1983.

Parashar, S.K., "Investigation of Radar Discrimination of Sea Ice," Ph.D. Thesis, University of Kansas, Lawrence, Kansas, 1974.

Poe, G.A., A. Stogryn, A.T. Edgerton and R.O. Ramseier, Aerojet Electrosystems Co. Final Report, No. 1804 FR-1, (Unpublished), 1974.

Polder, D. and J.H. Van Santen, "The Effective Permeability of Mixture of Solids," Physica, 12(5), 1946, pp. 257-271.

Pounder, E.R., The Physics of Ice, Pergamon Press, New York, 1965.

Ramseier, R.O., P. Gloersen and W.J. Campbell, "Variation in the Microwave Emissivity of Sea Ice in the Beaufort and Bering Sea," Proc. URSI Commission H, University of Bern, Switzerland, 1974, pp. 87-93.

Raney, R.K., "RADARSAT-Canada's National Radar Satellite Program," IEEE Geoscience and Remote Sensing Society Newsletter, March 1982, pp. 5-9.

Schwarz, J. and W.F. Weeks, "Engineering Properties of Sea Ice," J. Glacio., vol. 19(81), 1977, pp. 499-527.

Schwerdtfeger, P., "The Thermal Properties of Sea Ice," J. Glacio., vol. 4(36), October 1963, pp. 789-807.

_____, "The Effect of Finite Heat Content and Thermal Diffusion on the Growth of Sea-Ice Cover," J. Glacio., vol. 5(39), 1964, pp. 315-324.

Shin, R.T. and J.A. Kong, "Radiative Transfer Theory for Active Remote Sensing of a Homogeneous Layer Containing Spherical Scatterers," J. Appl. Phys., vol. 52(6), 1981, pp. 4221-4320.

Skou, N., "Airborne Multifrequency Radiometry of Sea Ice," Technical University of Denmark, Report LD42, 1980.

Stiles, W.H. and F.T. Ulaby, "Microwave Remote Sensing of Snow Packs," NASA Report NASA CR-3263, 1980.

Stiles, W.H. and F.T. Ulaby, "Dielectric Properties of Snow," NASA Report NASA CR 166764, 1981.

Stogryn, A., "Equations for Calculating the Dielectric Constant of Saline Water," IEEE Trans., vol. MTT-19, 1971, pp. 733-736.

SURSAT Project Workshop Report, 1980.

Taylor, L.S., "Dielectric Properties of Mixtures," IEEE Trans., vol. AP-13(6), 1965, pp. 943-947.

Timco, G.W., "An Analysis of the In-Situ Resistivity of Sea Ice in Terms of Its Microstructure," J. Glacio., vol. 22(88), 1979, pp. 461-471.

Tinga, W.R. and W.A.G. Voss, "General Approach to Multiphase Mixture Theory," J. Appl. Phys., vol. 44(9), 1973, pp. 3897-3902.

Tiuri, M., M. Hallikainen and A. Laaperi, "Microwave Radiometer Theory and Measurement of Sea Ice Characteristics," Helsinki University of Technology, Radio Laboratory, Report s-89, 1976.

Troy, B.E., J.P. Hollinger, R.M. Lerner and M.M. Wisler, "Measurement of the Microwave Properties of Sea Ice at 90 GHz and Lower Frequencies," J. Geophys. Res., vol. 86(C5), 1981, pp. 4283-4289.

Tsang, L. and J.A. Kong, "Theory for Thermal Microwave Emission from a Bounded Medium Containing Spherical Scatterers," J. Appl. Phys., vol. 48(8), 1977, pp. 3593-3599.

_____, "Radiative Transfer Theory for Active Remote Sensing of Half-Space Random Media," Radio Science, vol. 13(5), 1978, pp. 763-773.

Tsang, L., M.C. Kubacsi and J.A. Kong, "Radiative Transfer Theory for Active Remote Sensing of a Layer of Small Ellipsoidal Scatterers," Radio Science, vol. 16(3), May-June 1981, pp. 321-329.

Ulaby, F.T., M.C. Dobson, J.A. Stiles, R.K. Moore and J.C. Holtzman, "Evaluation of the Soil Moisture Prediction Accuracy of a Space Radar Using Simulation Techniques," Remote Sensing Laboratory Technical Report 429-1, University of Kansas Center for Research, Inc., Lawrence, Kansas, May 1981.

Ulaby, F.T., W.H. Stiles and M. Abdelrazik, "Snow Cover Influence on Backscatter from Terrain," Remote Sensing Laboratory Technical Report 527-2, University of Kansas Center for Research, Inc., Lawrence, Kansas, June 1982.

Ulaby, F.T., R.K. Moore and A.K. Fung, Microwave Remote Sensing, Vol. I: Fundamentals and Radiometry; Vol. II: Radar Remote Sensing and Surface Scattering and Emission Theory; Reading, Massachusetts: Addison-Wesley Publishing Company, 1981, 1982.

Ulaby, F.T. and W.H. Stiles, "The Active and Passive Microwave Response to Snow Parameters, 2: Water Equivalent of Dry Snow," J. Geophys. Res., vol. 85(C2), 1980, pp. 1045-1049.

Ulaby, F.T., W.H. Stiles, A.K. Fung, H.J. Eom and M. Abdelrazik, "Observations and Modeling of the Radar Backscatter from Snowpacks," Remote Sensing Laboratory Technical Report 527-4, University of Kansas Center for Research, Inc., Lawrence, Kansas, July 1982.

van de Hulst, H.D., Light Scattering by Small Particles, New York: John Wiley and Sons, Inc., 1957, p. 270.

Vant, M.R., Ph.D. Dissertation,. Carleton University, 1976, unpublished.

Vant, M.R., R.G. Gray, R.O. Ramseier and V. Makios, "Dielectric Properties of Fresh and Sea Ice at 10 and 35 GHz," J. Appl. Phys., vol. 45, no. 11, November 1974, pp. 4712-4717.

Vant, M.R., R.O. Ramseier and V. Makios, The Complex Dielectric Constant of Sea Ice at Frequencies in the Range 0.1 - 40 GHz," J. Appl. Phys., vol. 49(3), 1978, pp. 1264-1280.

Wadhams, P., "Sea Ice Topography of the Arctic Ocean in the Region 70 W to 25 E," Phil. Trans. of Royal Society, London, England, vol. 302, 1981, pp. 45-85.

Weeks, W.F. and N. Untersteiner, "Sea Ice," NASA Oceanic Processes Program Status Report, NASA Technical Memorandum 80233, 1980.